DØ note 6153
Version 2.0

Measurement of $R_b = \mathcal{B}(t \to Wb)/\mathcal{B}(t \to Wq)$ and of the $t\bar{t}$ Production Cross-Section in Dilepton Final State

M. Besançon[1], F. Déliot[1], C. Deterre[1], Y. Peters[2], E. Shabalina[3], V. Sharyy[1]

[1] Irfu/SPP, CEA-Saclay, France
[2] University of Manchester, UK
[3] II. Phys. Inst., Goettingen, Germany

(Dated: February 4, 2011)

We present the results of the simultaneous measurement of the $t\bar{t}$ cross section and the ratio $\mathcal{B}(t \to Wb)/\mathcal{B}(t \to Wq)$ in the dilepton channel, in $p\overline{p}$ collisions at $\sqrt{s} = 1.96$ TeV. The sample studied corresponds to the RunIIa, RunIIb1 and RunIIb2 data-taking periods, and to an integrated luminosity of 5.3 fb^{-1}. We obtain:

$$R_b = 0.861 \pm 0.046(\text{stat+syst})$$
$$\sigma_{t\bar{t}} \times \mathcal{B}(t \to Wb)^2 = 7.29^{+0.90}_{-0.79}(\text{stat+sys})\ pb.$$

We also set limits on R and $|V_{tb}|$ at the 95% CL: $0.739 < R_b < 0.952$ and $0.859 < |V_{tb}| < 0.976$.

Combining the dilepton channel results with the ℓ+jets ones gives:

$$R_b = 0.924^{+0.036}_{-0.035}(\text{stat+syst})$$
$$\sigma_{t\bar{t}} \times \mathcal{B}(t \to Wb)^2 = 7.55^{+0.64}_{-0.57}(\text{stat+syst})\ \text{pb}.$$

Contents

I Introduction 3

II Data set and Event Selection 3
A Global Strategy 3
B Selection Cuts 3

III Background Estimation 5

IV Event Yields 6

V Method for the Measurement of Rb 7
A Template method 7
B Choice of the discriminating variable 8

VI Systematics 13

VII Mass Dependence 22

VIII Final Cross Section Results 22
A Measurement of $\sigma_{t\bar{t}}$ 23
1 Separated channels 23
2 RunIIa and RunIIb combinations 23
3 Total combination 23
B Measurement of R_b 24
1 Separated channels 24
2 RunIIa and RunIIb combinations 25
3 Total combination 25
C Simultaneous measurement of R_b and σ 26

IX Combination with the ℓ+jets channel 26
A Cross section only fit 27
B R_b only fit 28
C Simultaneous measurement 28

References 30

A Systematic tables 32

B Sanity plots 36
1 Control plots for electron-muon channel in RunIIa 36
2 Control plots for electron-muon channel in RunIIb 41
3 Control plots for di-electron channel RunIIa 46
4 Control plots for di-electron channel RunIIb 51
5 Control plots for di-muon channel in RunIIa 56
6 Control plots for di-muon channel in RunIIb 61

I. INTRODUCTION

The top quark belongs to the third generation of quarks, and its probability to decay to a W boson and a b quark is expected to be very close to one. In this analysis, we use a template method to measure

$$R_b = \frac{\mathcal{B}(t \to Wb)}{\mathcal{B}(t \to Wq)}$$

where $\mathcal{B}(t \to Wb)$ is the branching fraction from t to Wb and $\mathcal{B}(t \to Wq)$ is the branching fraction from t to Wq where q can be a b, s or d quark. Considering the elements of the Cabibbo-Kobayashi-Maskawa (CKM) mixing matrix, this ratio can be written as:

$$R_b = \frac{|V_{tb}|^2}{|V_{td}|^2 + |V_{ts}|^2 + |V_{tb}|^2}. \tag{1}$$

Assuming the CKM unitarity, $|V_{td}|^2 + |V_{ts}|^2 + |V_{tb}|^2 = 1$, and thus $R_b = |V_{tb}|^2$. The measured values of V_{td} and V_{ts} are very close to zero and assuming the CKM unitarity we have the constraint: $|V_{tb}| = 0.999152^{+0.000030}_{-0.000045}$. Any observed deviation from one would be the sign of new physics.

The selection and setup for this analysis are very close to the ones used to obtain the cross section measurement in the dilepton channel presented at Moriond 2010. The method used to extract R_b is based on templates built with the Neural Network algorithm output used for the identification of the b-quark jets, and on the simulation of $t \to Wq$ decays, where q=d or s.

We will first describe the data and MC samples used in the analysis, as well as the setup. Then we will describe the backgrounds and selection steps. In a third part we will detail the template method used to measure R_b. Finally, we will conclude and talk about the combination with the ℓ+jets channel.

This paper also includes an updated measurement of the dilepton cross section compared to the preliminary result on winter 2010 [2].

II. DATA SET AND EVENT SELECTION

1. Global Strategy

The largest background in the dilepton channels comes from $Z \to \ell\ell$ and WW processes with either two electrons, two muons and one electron and one muon in their final states. Other physical backgrounds come from WZ and ZZ processes. These physical backgrounds are evaluated from MC (see section III).

All sources of fake electron background which mainly has a poor electron likelihood [34] are evaluated using a fit on the electron likelihood distribution (see [3] and section III). With this strategy, the QCD background with one fake electron and one fake isolated muon in the electron-muon channel, the $W \to \mu\nu$ background with one fake electron as well as the background processes with γ faking electrons are all computed at the same time. The background contribution coming from fake isolated muons is computed by multiplying the number of events with a loose isolated muons by the muon isolation fake rate (as in [3]).

2. Selection Cuts

The general object selection used in the three channels is the following:

1. *Top_tight* electrons are used in electron-muon and dielectron final states. They are defined as follow:
   (a) Electron $|ID|$=10 or 11.
   (b) $|\eta_{calo}| < 2.5$ and exclusion of the ICD region ($|\eta_{calo}| < 1.1$ *or* $|\eta_{calo}| > 1.5$).
   (c) High energy fraction in the EM part of the calorimeter: $f_{EM} > 0.9$.
   (d) Isolated EM cluster: $f_{iso} < 0.15$.
   (e) Shower shape cut: $\chi^2_{hmx7} < 50$.
   (f) $p_T > 15$ GeV (for MC, this corresponds to the smeared electron p_T according to the data / MC difference in energy resolution).

(g) One track matched with E/p requiring $p_{\chi^2_{\text{trk EOP}}} > 0$ and track $p_T > 5$ GeV.

(h) Electron likelihood $\mathcal{L}_e > 0.85$.

(i) For MC events, the electron selection efficiency is corrected for the *Top_tight* electron data / MC efficiency difference using standard EM ID correction factors [25]. We are using scale factors dependent on the electron detector η and ϕ.

2. Following muon selection is used for electron-muon and dimuon final states:

   (a) Muon quality definition is *Loose v2*.

      i. *Loose* muon quality.

      ii. $|\eta_{det}| < 2$.

      iii. Timing cuts against cosmic muons background .

   (b) Muon is required to match to a central track with *loose v2* quality.

      i. Quality criteria on the matched track: $|DCA| < 0.04$ cm for tracks with SMT hits and $|DCA| < 0.2$ cm for tracks without SMT hits.

   (c) $p_T > 15$ GeV (for MC, this corresponds to the smeared muon p_T according to the data / MC difference in muon momentum resolution).

   (d) Muon isolation is *TopScaledMedium*.

      i. Calorimeter isolation divided by the muon p_T is: $etHaloScaled < 0.15$.

      ii. Tracker isolation divided by the muon p_T is: $etTrkConeScaledMin < 0.15$.

   (e) For MC events, the muon selection efficiency is corrected for the *Loose* muon as well as for the *loose* track and *TopScaledMedium* data / MC efficiency differences using standard muon ID correction factors [27]. We are using scale factors parametrized with the muon ϕ and detector η for the muon quality part and parametrized with z and CFT η and luminosity for the track part and parametrized with CFT η, distance from the jets, muon p_T and luminosity for the isolation part.

3. Jets for all three final states are selected as follows:

   (a) Correct jet p_T with jet energy scale (JES) including muon corrections. Muons identified with the criteria 2 are excluded from the list of muons used for JES correction.

   (b) For simulated jets, the following corrections are applied:

      i. Jet p_T is smeared using SSR procedure.

      ii. Jet with JES corrected $p_T < 15$ GeV are removed (no muon correction applied to JES for this cut).

      iii. SSR "shifting" correction applied to all MC samples except $t\bar{t}$ one.

      iv. Jet reconstruction "plateau" efficiency correction using the jet ID group procedure [28].

   (c) Jet p_T are greater than 20 GeV.

   (d) The absolute value of the jet detector η is less than 2.5.

   (e) EM jet fraction f_{EM} is below 0.95 and above a minimum f_{EM} depending on η_{det} as described in [29].

   (f) The jet coarse hadronic fraction is below an η_{det} dependent cut optimized to reject fake coarse hadronic energy clustered with small random seeds from the inner layers [29].

   (g) The reconstructed jet must be confirmed by the L1 trigger readout.

   (h) The $dR = \sqrt{d\eta_{det}^2 + d\phi^2}$ between the jet and the electrons selected with the criteria 1 is larger than 0.5. If not the jet is rejected.

   (i) Vertex confirmation is applied to all jets, which consists in requiring at least two tracks coming from the primary vertex to be present in the jet (only for p20).

Given the above standard object selections, the list of cuts used to select signal events depending on the dilepton channel considered is the following:

1. Luminosity block selection i.e. removal of "bad" LBN.

2. The calorimeter event quality variables described in the note [9] were required to be good both in data and MC samples. In MC this selection is taken into account in the efficiency calculation and no correction due to this cut is applied.

3. Luminosity [38] and vertex reweightings [19].
4. Vertex selection:
   (a) $|z_{PV}| < 60$ cm.
   (b) Number of tracks associated with the primary vertex greater or equal to 3.
5. Exactly one (electron-muon channel) or two or more (dielectron channel) electrons identified as above.
6. No electrons identified with a selection above are allowed in dimuon channels.
7. One or more (electron-muon channel) or two or more (dimuon channel) loose muons identified as above.
8. In the electron-muon channel: remove events with $dR(e, \mu) < 0.3$ between electron and muon tracks. This selection significantly suppresses the bremsstrahlung background (a photon emission by the muon, where photon takes the same track as the muon).
9. Choose the two leptons to have opposite charges. If more than one lepton pair is found, choose the lepton pair for which the p_T scalar sum is maximum.
10. Distance in Z between the two selected lepton tracks $|z_{\ lepton\ 1} - z_{\ lepton\ 2}|$ is less than 2 cm.
11. Trigger selection in the dielectron and dimuon channels:
    (a) Data sample:
        i. Global trigger selection (single electron or single muon "OR")
        ii. The offline muon, electron and tracks are asked to be matched with the corresponding L1, L2 and L3 objects to be consistent with the trigger efficiency calculation in data.
    (b) For MC, events are weighted according to the calculated trigger efficiency measured in data [11–13] using caf_trigger package.
12. At least 2 jets satisfying the standard selection above are required. In the $e\mu$ channel, events with only 1 jet are also considered.
13. Final topological selection:
    (a) In the electron-muon channel with two jets required, $H_T > 110$ GeV where $H_T = p_T(leading\ lepton) + p_T(2\ leading\ jets)$, where "jets" mean jets satisfying selection criteria above;
    (b) In the electron-muon channel with only one jet required, $H_T > 105$ GeV;
    (c) In the dielectron channel, cut on the $\not\!\!E_T$ significance: $\sigma_{\not\!\!E_T} > 5$;
    (d) In the dimuon channel, cut on $\not\!\!E_T$ and $\not\!\!E_T$ significance: $\not\!\!E_T > 40$ GeV and $\sigma_{\not\!\!E_T} > 5$.

III. BACKGROUND ESTIMATION

The physcical backgrounds (WW, WZ, ZZ and $Z \to \ell\ell$) have been evaluated using MC.

The WW, WZ, ZZ backgrounds have been generated using Pythia and normalised to the next-to-leading order (NLO) cross section which is about 40 % higher than the LO calculation as performed with the package MCFM [36]. We take a 7% uncertainty on these cross sections.

The $Z \to \ell\ell$ background have been studied using samples generated by Alpgen+Pythia. We are then scaling the $Z \to \ell\ell$ sample to the next-to-next-to-leading order (NNLO) cross-section [37]. As the Z boson p_T is not properly described in Alpgen, we reweighted the Z p_T distribution inclusively using the standard tool in *caf_mc_util*.

The "fake" backgrounds have been evaluated as described in [3].

"Fake electron" refers to a jet misidentified as an electron as well as to real electrons produced by jets, e.g. in the case of b quark semileptonic decay. These second types of "fake electrons" indeed are real electrons. Mostly these electrons are not isolated and tend to have a low likelihood value. This background is mainly composed of multijet events (QCD) including light or heavy flavor jets. In order to separate the background from the signal, we use the 7-variable electron likelihood distribution [34]. Using the shape of the electron likelihood distribution measured with a sample of real electrons ($Z \to ee$ sample) and the shape for "fake electrons" measured in a sample dominated by

multijet background (low MET with anti-isolated muons EMU sample), one can fit the electron likelihood distribution for the selected events to determine the number of signal and background events.

The fake muon background comes from events with at least one fake isolated muon coming mainly from heavy flavor quark decays. Because the fake muon isolation rate is low especially when requiring two jets, this background is low. In order to estimate this background, we first estimate the fake muon rate in data using $b\bar{b}$ events and then estimate the number of fake muon background using a same sign selection with loose isolation requirements ($etHaloScaled < 0.5$ and $etTrkConeScaledMin < 0.5$) in our signal sample. To measure the muon isolation fake rate f_μ i.e. the rate at which a muon appears isolated in events where it should not, we select dimuon events with one tag non isolated matched muon ($etHaloScaled > 0.15$, $etTrkConeScaledMin > 0.15$, near a jet : $dR(\mu, jet) < 0.5$) with $p_T > 15$ GeV and a probe matched muon with $p_T > 15$ GeV and loose isolation requirements ($etHaloScaled < 0.5$ and $etTrkConeScaledMin < 0.5$). We then count the number of probe muons that appears tightly isolated ($etHaloScaled > 0.15$, $etTrkConeScaledMin > 0.15$).

The results are shown in Table 1 corresponding to the measured fake muon isolation rate derived for the full dataset.

	0 jet exclusive	1 jet exclusive	2 jets inclusive
f_μ	27.90 ± 1.21 %	20.73 ± 1.25 %	21.62 ± 2.01 %

TABLE 1: Fake muon isolation rate for different number of jet requirement (the errors quoted are statistical only).

The number of events in our selection coming from fake muon isolation background is then estimated as the number of events in the selection identical to the signal selection except that we require a loose isolation for the muon ($etHaloScaled < 0.5$ and $etTrkConeScaledMin < 0.5$) but we ask for the muon and the other lepton to be same sign to prevent contamination from physics background ("same sign loose isolation" selection) times the fake muon isolation rate computed above. The kinematics in this loose isolated sample is expected to be closer to the one in the signal sample than a sample without any muon isolation.

IV. EVENT YIELDS

The number of events expected for the different MC samples and observed in data are presented in Tables 2 to 9.

TABLE 2: The measured and predicted event yield in $t\bar{t} \to ee$ process for RunIIa. The errors shown include all systematic uncertainties (except the one from the luminosity).

	$Z \to \ell\ell$	$Z \to \ell\ell$+HF	Dibosons	$tt \to \ell\ell jj$, $\sigma_{t\bar{t}}$ =7.454 pb m_t =172 GeV	Expected N of events	N of events	$\frac{Data}{MC}$
Inclusive selection	$54280.9^{+11099.3}_{-8373.9}$	$1463.8^{+299.3}_{-225.9}$	$81.5^{+10.6}_{-9.8}$	$23.7^{+2.0}_{-2.0}$	$55849.9^{+11406.3}_{-8606.0}$	56990	1.02
N jets ≥ 1	$7336.8^{+1500.3}_{-1132.0}$	$594.3^{+121.6}_{-91.7}$	$37.3^{+4.9}_{-4.5}$	$23.1^{+2.0}_{-2.0}$	$7991.6^{+1625.9}_{-1227.1}$	7888	0.99
N jets ≥ 2	$865.0^{+176.9}_{-133.5}$	$155.1^{+31.8}_{-24.0}$	$17.6^{+2.3}_{-2.1}$	$17.0^{+1.5}_{-1.4}$	$1054.8^{+210.9}_{-159.4}$	1154	1.09
MET significance > 4.8	$3.4^{+0.7}_{-0.6}$	$1.1^{+0.3}_{-0.2}$	$0.9^{+0.1}_{-0.1}$	$12.2^{+1.0}_{-1.0}$	$17.6^{+1.8}_{-1.6}$	23	1.31
MET significance > 5	$3.1^{+0.7}_{-0.5}$	$0.9^{+0.2}_{-0.2}$	$0.9^{+0.1}_{-0.1}$	$12.0^{+1.0}_{-1.0}$	$16.9^{+1.7}_{-1.6}$	23	1.36

TABLE 3: The measured and predicted event yield in $t\bar{t} \to ee$ process for RunIIb. The errors shown include all systematic uncertainties (except the one from the luminosity).

	$Z \to \ell\ell$	$Z \to \ell\ell$+HF	Dibosons	$t\bar{t} \to \ell\ell jj$, $\sigma_{t\bar{t}}$ =7.454 pb m_t =172 GeV	Expected N of events	N of events	$\frac{Data}{MC}$
Inclusive selection	$162084.2^{+22198.2}_{-21067.7}$	$4259.7^{+583.8}_{-554.1}$	$260.1^{+33.6}_{-33.5}$	$77.6^{+7.3}_{-7.3}$	$166681.6^{+22809.2}_{-21649.5}$	165769	0.99
N jets ≥ 1	$18928.1^{+2592.9}_{-2461.0}$	$1610.4^{+221.1}_{-209.9}$	$109.7^{+14.2}_{-14.1}$	$75.2^{+7.1}_{-7.1}$	$20723.4^{+2828.0}_{-2685.1}$	19729	0.95
N jets ≥ 2	$1923.3^{+264.1}_{-250.7}$	$385.2^{+53.2}_{-50.5}$	$46.0^{+6.0}_{-5.9}$	$53.0^{+5.0}_{-5.0}$	$2407.5^{+324.4}_{-308.5}$	2563	1.06
MET significance > 4.8	$6.6^{+1.2}_{-1.2}$	$3.5^{+0.9}_{-0.9}$	$2.2^{+0.3}_{-0.3}$	$34.3^{+3.2}_{-3.2}$	$46.6^{+4.7}_{-4.7}$	51	1.09
MET significance > 5	$5.7^{+1.1}_{-1.1}$	$2.8^{+0.7}_{-0.7}$	$2.1^{+0.3}_{-0.3}$	$33.6^{+3.2}_{-3.2}$	$44.2^{+4.4}_{-4.4}$	51	1.15

The estimation of the systematic uncertainties is described in section VI.

TABLE 4: The measured and predicted event yield in $t\bar{t} \to e\mu$ process for RunIIa. The errors shown include all systematic uncertainties (except the one from the luminosity).

	$Z \to \ell\ell$	$Z \to \ell\ell$+HF	Dibosons	Fake electron events	Fake muon events	$tt \to \ell\ell jj$, $\sigma_{t\bar{t}}$ =7.454 pb m_t =172 GeV	Expected N of events	N of events	$\frac{Data}{MC}$
Inclusive selection	$763.7^{+95.3}_{-95.3}$	$19.1^{+2.4}_{-2.4}$	$107.4^{+9.7}_{-9.7}$	$116.4^{+53.8}_{-53.8}$	-	$63.3^{+4.5}_{-4.5}$	$1070.0^{+115.8}_{-115.8}$	1232	1.15
N jets ≥ 1	$131.1^{+31.0}_{-19.6}$	$8.4^{+1.5}_{-1.2}$	$19.9^{+4.7}_{-2.2}$	$50.5^{+24.5}_{-24.5}$	$3.1^{+1.6}_{-1.4}$	$62.4^{+4.4}_{-4.4}$	$275.5^{+38.9}_{-33.0}$	320	1.16
N jets ≥ 2	$17.3^{+7.5}_{-3.2}$	$2.8^{+0.8}_{-0.6}$	$3.6^{+1.0}_{-0.6}$	$12.8^{+6.0}_{-6.0}$	$1.0^{+0.9}_{-0.8}$	$47.9^{+3.7}_{-3.6}$	$85.3^{+10.6}_{-8.4}$	94	1.10
$H_T \geq 110\ GeV$	$9.0^{+1.7}_{-1.5}$	$1.6^{+0.4}_{-0.3}$	$2.5^{+0.6}_{-0.4}$	$7.8^{+3.7}_{-3.7}$	$1.7^{+0.8}_{-0.7}$	$46.3^{+3.6}_{-3.5}$	$69.0^{+6.0}_{-5.8}$	69	1.00

TABLE 5: The measured and predicted event yield in $t\bar{t} \to e\mu$ process for RunIIb. The errors shown include all systematic uncertainties (except the one from the luminosity).

	$Z \to \ell\ell$	$Z \to \ell\ell$+HF	Dibosons	Fake electron events	Fake muon events	$tt \to \ell\ell jj$, $\sigma_{t\bar{t}}$ =7.454 pb m_t =172 GeV	Expected N of events	N of events	$\frac{Data}{MC}$
Inclusive selection	$2268.1^{+204.0}_{-204.0}$	$59.3^{+5.8}_{-5.6}$	$352.6^{+31.1}_{-31.1}$	$296.8^{+134.5}_{-134.5}$	-	$211.8^{+14.4}_{-14.3}$	$3188.6^{+266.7}_{-266.7}$	3279	1.03
N jets ≥ 1	$284.7^{+38.6}_{-35.0}$	$24.4^{+3.1}_{-2.8}$	$54.9^{+6.8}_{-6.1}$	$92.7^{+43.8}_{-43.8}$	$11.1^{+2.5}_{-2.3}$	$206.4^{+14.5}_{-14.4}$	$674.4^{+64.3}_{-62.5}$	713	1.06
N jets ≥ 2	$31.3^{+6.6}_{-5.8}$	$5.9^{+1.6}_{-1.4}$	$8.1^{+1.4}_{-1.3}$	$19.3^{+8.9}_{-8.9}$	$1.6^{+1.2}_{-1.1}$	$149.8^{+14.5}_{-14.5}$	$215.9^{+19.4}_{-19.0}$	244	1.13
$H_T \geq 110\ GeV$	$16.2^{+2.9}_{-3.1}$	$3.4^{+1.1}_{-0.8}$	$6.0^{+1.0}_{-0.9}$	$10.5^{+5.0}_{-5.0}$	$2.5^{+1.1}_{-1.0}$	$145.2^{+14.2}_{-14.0}$	$183.9^{+15.3}_{-15.2}$	212	1.15

TABLE 6: The measured and predicted event yield in $t\bar{t} \to e\mu$ process for RunIIa in the one jet bin. The errors shown include all systematic uncertainties (except the one from the luminosity).

	$Z \to \ell\ell$	$Z \to \ell\ell$+HF	Dibosons	Fake electron events	Fake muon events	$tt \to \ell\ell jj$, $\sigma_{t\bar{t}}$ =7.454 pb m_t =172 GeV	Expected N of events	N of events	$\frac{Data}{MC}$
Inclusive selection	$763.7^{+95.3}_{-95.3}$	$19.1^{+2.4}_{-2.4}$	$107.4^{+9.7}_{-9.7}$	$116.4^{+53.8}_{-53.8}$	-	$63.3^{+9.9}_{-9.9}$	$1070.0^{+116.1}_{-116.1}$	1232	1.15
N jets == 1	$113.7^{+23.9}_{-16.6}$	$5.6^{+0.8}_{-0.8}$	$16.4^{+3.8}_{-1.8}$	$37.8^{+18.8}_{-18.7}$	$2.1^{+1.3}_{-1.2}$	$14.5^{+2.7}_{-2.5}$	$190.1^{+29.1}_{-25.4}$	226	1.19
$H_T \geq 105\ GeV$	$10.3^{+1.6}_{-1.4}$	$0.6^{+0.2}_{-0.2}$	$5.0^{+0.6}_{-0.6}$	$6.2^{+3.4}_{-3.4}$	$2.7^{+0.7}_{-0.6}$	$10.7^{+1.9}_{-1.8}$	$35.6^{+4.4}_{-4.3}$	37	1.04

TABLE 7: The measured and predicted event yield in $t\bar{t} \to e\mu$ process for RunIIb in the one jet bin. The errors shown include all systematic uncertainties (except the one from the luminosity).

	$Z \to \ell\ell$	$Z \to \ell\ell$+HF	Dibosons	Fake electron events	Fake muon events	$tt \to \ell\ell jj$, $\sigma_{t\bar{t}}$ =7.454 pb m_t =172 GeV	Expected N of events	N of events	$\frac{Data}{MC}$
Inclusive selection	$2268.1^{+204.0}_{-204.0}$	$59.3^{+5.8}_{-5.6}$	$352.6^{+31.1}_{-31.1}$	$296.8^{+134.5}_{-134.5}$	-	$211.8^{+33.0}_{-32.9}$	$3188.6^{+268.3}_{-268.3}$	3279	1.03
N jets == 1	$253.4^{+32.7}_{-29.9}$	$18.5^{+2.2}_{-2.1}$	$46.8^{+5.6}_{-4.9}$	$73.5^{+35.3}_{-35.3}$	$9.6^{+2.2}_{-2.1}$	$56.7^{+11.6}_{-11.6}$	$458.5^{+49.0}_{-47.8}$	469	1.02
$H_T \geq 105\ GeV$	$27.5^{+3.5}_{-3.4}$	$2.4^{+0.4}_{-0.4}$	$15.6^{+1.7}_{-1.7}$	$15.2^{+7.3}_{-7.2}$	$5.8^{+1.1}_{-1.0}$	$41.5^{+8.2}_{-8.1}$	$108.1^{+11.3}_{-11.2}$	113	1.05

V. METHOD FOR THE MEASUREMENT OF RB

A. Template method

The R_b measurement is based on a variable that has a discriminating power between $t\bar{t} \to$ bb, bq and qq events. The main difference between these three types of events is the number of b-quarks generated. To use this difference, we implemented the b-tagging in the selection and the variable used for the measurement comes from the output of the b-tagging neural network. In Monte-Carlo simulations, templates for the three different kinds of events are built

TABLE 8: The measured and predicted event yield in $t\bar{t} \to \mu\mu$ process for RunIIa. The errors shown include all systematic uncertainties (except the one from the luminosity).

	$Z \to \ell\ell$	$Z \to \ell\ell$+HF	Dibosons	Fake muon events	$tt \to \ell\ell jj$, $\sigma_{t\bar{t}}$ =7.454 pb m_t =172 GeV	Expected N of events	N of events	$\frac{Data}{MC}$
Inclusive selection	$85364.1^{+18606.2}_{-12521.2}$	$2384.7^{+519.8}_{-349.8}$	$126.7^{+15.0}_{-13.3}$	-	$35.5^{+2.8}_{-2.8}$	$87911.1^{+19136.7}_{-12878.5}$	87326	0.99
N jets ≥ 1	$13059.8^{+2846.6}_{-1915.7}$	$989.8^{+215.8}_{-145.2}$	$62.7^{+7.4}_{-6.6}$	$28.1^{+2.5}_{-2.4}$	$35.1^{+2.8}_{-2.8}$	$14175.5^{+3068.3}_{-2065.3}$	14060	0.99
N jets ≥ 2	$1655.2^{+360.8}_{-242.9}$	$281.8^{+61.5}_{-41.4}$	$31.1^{+3.7}_{-3.3}$	$11.1^{+1.6}_{-1.5}$	$28.0^{+2.2}_{-2.2}$	$2007.3^{+425.6}_{-286.8}$	2199	1.10
MET significance > 4.8	$23.6^{+5.2}_{-3.5}$	$4.4^{+1.0}_{-0.7}$	$1.9^{+0.3}_{-0.2}$	$3.2^{+0.8}_{-0.7}$	$16.9^{+1.4}_{-1.3}$	$50.0^{+7.1}_{-5.1}$	60	1.20
MET significance > 5	$22.1^{+4.9}_{-3.3}$	$4.1^{+0.9}_{-0.6}$	$1.8^{+0.2}_{-0.2}$	$3.1^{+0.8}_{-0.7}$	$16.5^{+1.3}_{-1.3}$	$47.5^{+6.7}_{-4.8}$	58	1.22

TABLE 9: The measured and predicted event yield in $t\bar{t} \to \mu\mu$ process for RunIIb. The errors shown include all systematic uncertainties (except the one from the luminosity).

	$Z \to \ell\ell$	$Z \to \ell\ell$+HF	Dibosons	Fake muon events	$t\bar{t} \to \ell\ell jj$, $\sigma_{t\bar{t}}$ =7.454 pb m_t =172 GeV	Expected N of events	N of events	$\frac{Data}{MC}$
Inclusive selection	$257556.5^{+32866.0}_{-31519.5}$	$6228.8^{+795.4}_{-762.9}$	$380.5^{+43.8}_{-43.1}$	-	$107.0^{+9.7}_{-9.6}$	$264272.8^{+33694.8}_{-32314.9}$	261329	0.99
N jets ≥ 1	$32552.0^{+4154.6}_{-3984.4}$	$2365.8^{+302.3}_{-290.0}$	$169.2^{+19.5}_{-19.2}$	$58.8^{+4.1}_{-4.0}$	$104.6^{+9.5}_{-9.4}$	$35250.3^{+4475.1}_{-4292.3}$	32200	0.91
N jets ≥ 2	$3458.3^{+442.2}_{-424.1}$	$614.6^{+78.8}_{-75.6}$	$75.4^{+8.7}_{-8.6}$	$18.4^{+2.2}_{-2.1}$	$79.0^{+7.1}_{-7.1}$	$4245.6^{+530.9}_{-509.5}$	4415	1.04
MET significance > 4.8	$36.5^{+5.3}_{-5.2}$	$8.3^{+1.7}_{-1.7}$	$3.5^{+0.4}_{-0.4}$	$4.8^{+1.0}_{-0.9}$	$44.9^{+4.1}_{-4.0}$	$98.0^{+9.8}_{-9.6}$	92	0.94
MET significance > 5	$33.4^{+4.9}_{-4.8}$	$7.8^{+1.7}_{-1.7}$	$3.2^{+0.4}_{-0.4}$	$4.5^{+1.0}_{-0.9}$	$43.4^{+3.9}_{-3.9}$	$92.3^{+9.2}_{-9.0}$	86	0.93

with this variable distributions. In data, we plot that same distribution and fit it to the templates, the free parameter being R_b.

We note:

- f_i the fraction of events in the bin i of the template;
- N_i the number of events in the bin i of the template;
- $\mathcal{L}$ the luminosity;
- ϵ the selection efficiency.

The distribution in data is fitted with a binned likelihood to the templates, so that in each bin of the distribution:

$$\begin{aligned} N_i^{data} &= R^2 N_i^{t\bar{t}\to bb} + 2R(1-R)N_i^{t\bar{t}\to bq} + (1-R)^2 N_i^{t\bar{t}\to qq} + N_i^{bkg} \\ &= R^2 \epsilon^{bb}\mathcal{L}\sigma B^2 f_i^{t\bar{t}\to bb} + 2R(1-R)\epsilon^{bq}\mathcal{L}\sigma B^2 f_i^{t\bar{t}\to bq} \\ &\quad + (1-R)^2\epsilon^{qq}\mathcal{L}\sigma B^2 f_i^{t\bar{t}\to qq} + \epsilon^{bkg}\mathcal{L}\sigma^{bkg} f_i^{bkg} \end{aligned} \tag{2}$$

The fit can be done in two different ways: we can fit only R_b if we don't take into account the overall number of events, or we can fit simultaneously R_b and σB^2 by varying the number of Monte-Carlo events.

B. Choice of the discriminating variable

The b-tagging algorithm is described in [20]. It is implemented after all the object corrections and before the selection on the number of jets.

We use the neural network tagger which for each jet in the event gives an output between 0 and 1, with b-like jet outputs peaking at 1. Twelve operating points are defined in this range, from 0.1 ("L6") to 0.925 ("MegaTight"), and the distributions are rebinned to match these working points. The jets with an output below 0.1 are said "non-tagged". The non-taggable jets are attributed an output of -1. In our analysis we don't apply any cut on the b-tagging output

to keep the maximum of information in our distributions. Thus, the non-taggable and non-tagged bins are also part of the fit.

Several distributions could be used as templates: the neural network output for the two leading jets (ie two entries per event), the maximum or minimum output of the two leading jets or the output for the leading (or next-to leading) jet. Figures 1, 2 and 3 show some of these distributions for $t\bar{t} \rightarrow$ bb, bq and qq samples, in the emu channel, for RunIIb1 and 2.

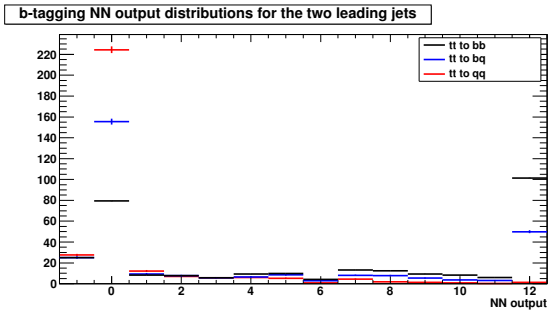

FIG. 1: NN Output Templates for $t\bar{t} \rightarrow bb$, $t\bar{t} \rightarrow bq$ and $t\bar{t} \rightarrow qq$ using the two leading jets

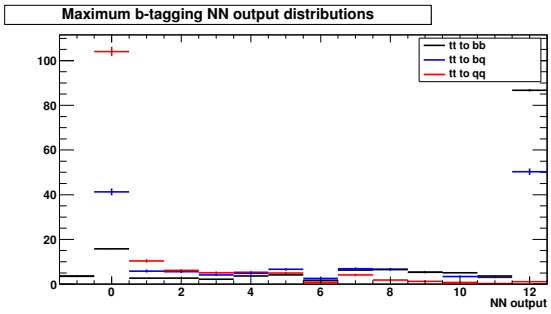

FIG. 2: NN Output Templates for $t\bar{t} \rightarrow bb$, $t\bar{t} \rightarrow bq$ and $t\bar{t} \rightarrow qq$ using the maximum jet NN ouput

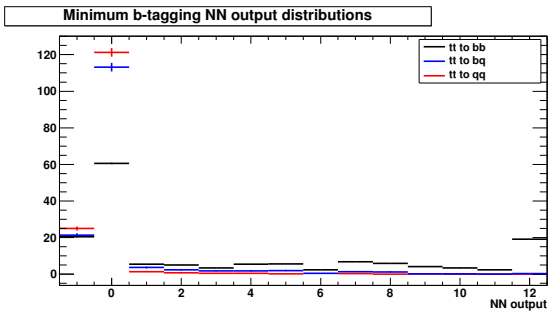

FIG. 3: NN Output Templates for $t\bar{t} \rightarrow bb$, $t\bar{t} \rightarrow bq$ and $t\bar{t} \rightarrow qq$ using the minimum jet NN ouput

Ensemble testing was performed to decide which distribution to use, the selection criterion being the expected statistical error on the measurement of R_b. Ensembles of 10000 events are created for ten different "true" values of R_b, and a fit is performed to obtain a "measured value" of R_b. A large number of pseudo-experiments are done for each "true" value, and the "measured value" distributions give the estimated statistical uncertainty. Figure 4 shows the expected uncertainties for the different choice of templates.

We can see that at large values of R_b, the most precise measurement is obtained with the minimum output template. In that case, the discrimination between $t\bar{t} \rightarrow$ bq and qq events is very small (see Figure 3), but the discrimination between $t\bar{t} \rightarrow$ bb and the rest is the biggest, which explains that result. Figures 5–6 show these distributions in data and MC for all final states after final selections. Figures 7 and 8 show the same distributions for the background dominated samples (selection after one jet requirement).

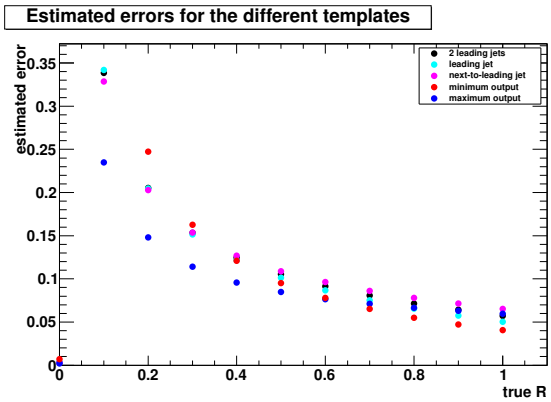

FIG. 4: Expected statistical uncertainties for different choice of templates

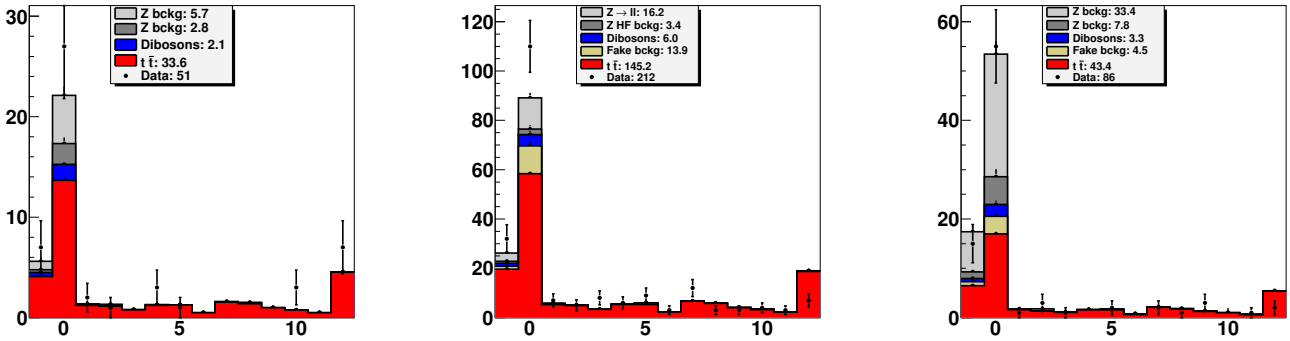

(a) Di-electron final state (b) Electron-muon final state (c) Di-muon final state

FIG. 5: B-tagging minimum output distribution in RunIIb data. Final selection.

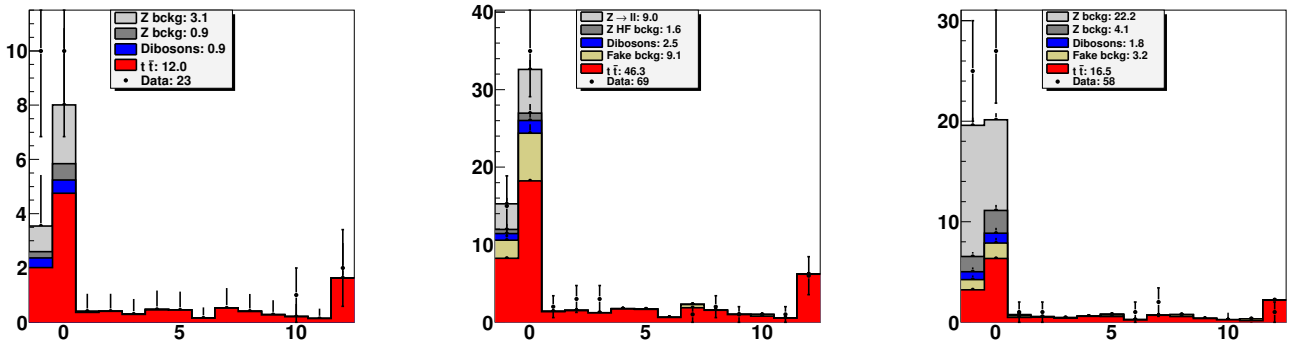

(a) Di-electron final state (b) Electron-muon final state (c) Di-muon final state

FIG. 6: B-tagging minimum output distribution in RunIIa data. Final Selection.

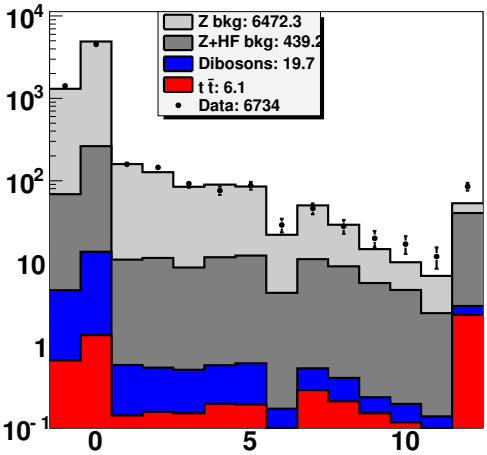

(a) Di-electron final state (RunIIa), logarithmic scale

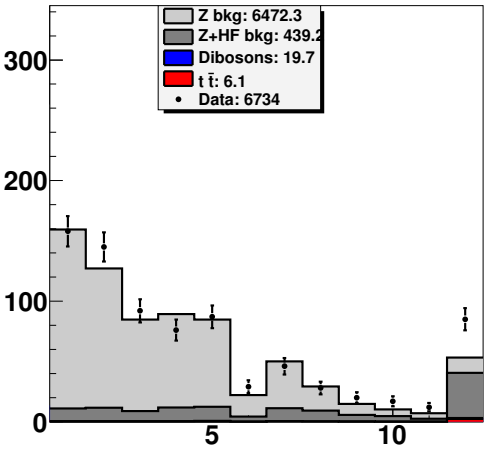

(b) Di-electron final state (RunIIa), linear scale for the highest NN bins

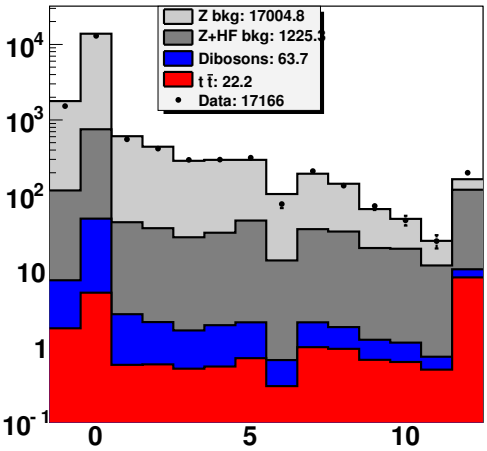

(c) Dielectron final state (RunIIb), logarithmic scale

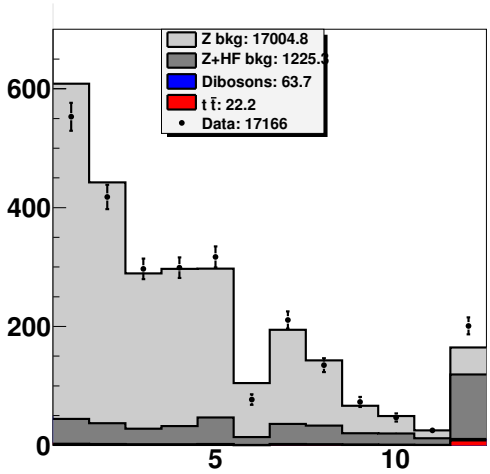

(d) Dielectron final state (RunIIb), linear scale for the highest NN bins

FIG. 7: B-tagging minimum output distributions for the dielectron final state in RunIIa (top) and RunIIb data (bottom). Selection after 1 jet requirement.

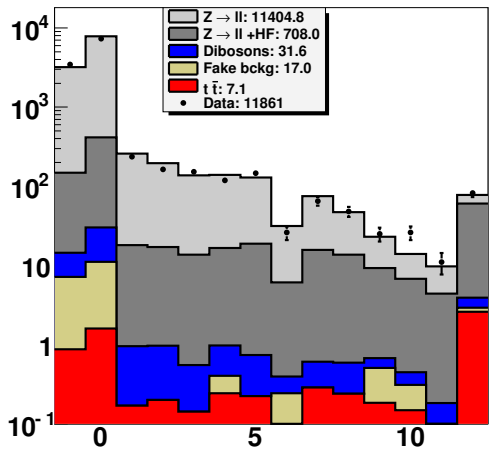

(a) Dimuon final state (RunIIa), logarithmic scale

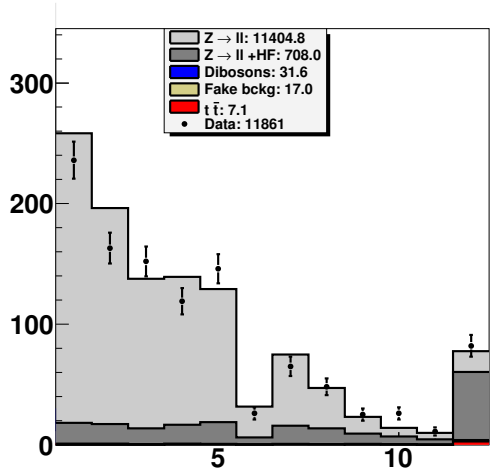

(b) Dimuon final state (RunIIa), linear scale for the highest NN bins

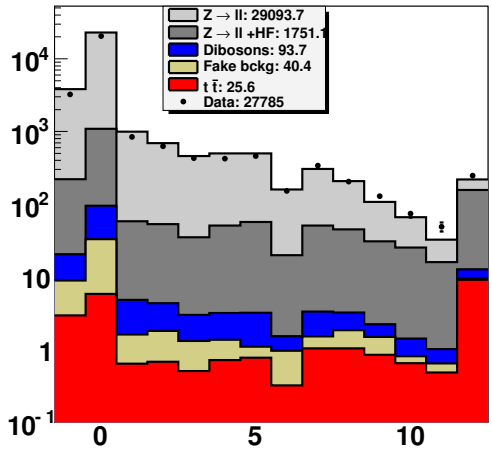

(c) Dimuon final state (RunIIb), logarithmic scale

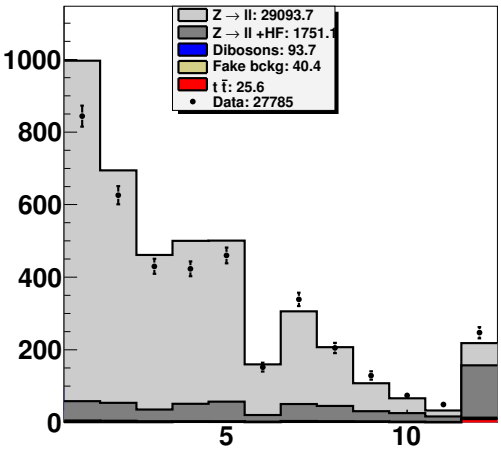

(d) Dimuon final state (RunIIb), linear scale for the highest NN bins

FIG. 8: B-tagging minimum output distributions for the dimuon final state in RunIIa (top) and RunIIb data (bottom). Selection after 1 jet requirement.

VI. SYSTEMATICS

We discuss here the systematic uncertainties related to our measurements.

- **Luminosity uncertainty**. The luminosity uncertainty is known to be 6.1% [52]. To obtain the luminosity error on the cross section we apply this uncertainty both on MC $t\bar{t}$ signal samples and on the background evaluated from MC in a correlated way.

- **Systematics due to the MC statistics**. This systematic error originates from the statistical error on the selection efficiencies.

- **Systematics due to the $W \to l$ branching ratio error**. This systematic error is computed by propagating the error on the W to lepton branching ratio assuming lepton universality [16].

- **Data quality flag systematics**. The systematic uncertainty on the measured data quality flag efficiency was estimated to be 0.5% [18].

- **Higher order effects and hadronization**. This uncertainty is evaluated by comparing Alpgen+Pythia with MC@NLO. For more details see [53]. This uncertainty has been evaluated in the electron-muon channel and ported in the dielectron and dimuon channels.

- **Color reconnection systematics**. This uncertainty is evaluated by comparing Pythia tune Apro with Pythia tune ACRpro. For more details see [53]. This uncertainty has been evaluated in the electron-muon channel and ported in the dielectron and dimuon channels.

- **ISR/FSR systematics**. This uncertainty is evaluated by comparing Pythia with the varied ISR/FSR parameters. The range of variation has been determined by CDF. For more details see [53]. This uncertainty has been evaluated in the electron-muon channel and ported in the dielectron and dimuon channels.

- **PDF uncertainties**. The standard *caf_pdfreweight* package is used for this estimation. The systematic uncertainty due to the choice of PDF is estimated by varying the 20 CTEQ6.1M PDF within their errors in the $t\bar{t}$ signal MC [46]. As our MC samples are generated using CTEQ6.1L, we have to consider the reweight efficiency from CTEQ6.1L to CTEQ6.1M as central value for this uncertainty determination.

- **b-quark fragmentation uncertainty**. This error is estimated using the standard procedure described in [47] by reweighting the $t\bar{t}$ events using different fragmentation functions.

- **Muon ID**. We quote under this systematics the uncertainties on the muon identification efficiency, the track scale factor and the isolation, and we use the numbers provided by the muon ID group [27].

- **Trigger systematics**. To estimate the uncertainty on the single electron and single muon "OR" triggers in the dielectron and dimuon channels, we estimate the trigger efficiencies both in data and MC. In the standard analysis, both leptons are allowed to fire the trigger. Alternatively, we can select one random electron or muon before applying the trigger turn-ons. We then compare the numbers of data and MC events in the two cases. If we suppose that the trigger efficiencies on both leptons can be factorized, the ratio of data events in both cases provides an estimation of the efficiency (and similarly in the MC). We note $\epsilon_D^{(1)}$ the trigger efficiency on one lepton, $\epsilon_D^{(2)}$ the efficiency on both leptons, and $\epsilon_{MC}^{(1)}$ and $\epsilon_{MC}^{(2)}$ in MC. $N_D^{(1)}$ (resp. $N_{MC}^{(1)}$) is the number of events in data (resp. MC) when only one lepton is allowed to fire the trigger, and $N_D^{(2)}$ (resp. $N_{MC}^{(2)}$) when the two leptons can fire the trigger. We set:

$$\begin{aligned} R_D &= \frac{N_D^{(2)}}{N_D^{(1)}} = \frac{\epsilon_D^{(2)}}{\epsilon_D^{(1)}} \\ R_{MC} &= \frac{N_{MC}^{(2)}}{N_{MC}^{(1)}} = \frac{\epsilon_{MC}^{(2)}}{\epsilon_{MC}^{(1)}}. \end{aligned} \tag{3}$$

We can then write:

$$\begin{aligned} \epsilon_D^{(2)} &= 1 - (1 - \epsilon_D^{(1)})^2 \\ &= \epsilon_D^{(1)}(2 - \epsilon_D^{(1)}) \\ \frac{\epsilon_D^{(2)}}{\epsilon_D^{(1)}} &= 2 - \epsilon_D^{(1)} = R_D \end{aligned} \tag{4}$$

and similarly for MC. R_D and R_{MC} allow then to extract $\epsilon_D^{(1)}$ and $\epsilon_{MC}^{(1)}$.

We find that the difference in efficiencies on data and MC for the single electron "OR" trigger is negligible and we don't apply any trigger uncertainty in the dielectron channel. In the dimuon channel, we apply an uncertainty of 6% being the difference in efficiency on data and MC computing in the way described above.

In the electron-muon channel we compare data and MC after applying the single electron "OR" trigger requirement or the single muon "OR" requirement. The data/MC ratio changes by 3.9% in RunIIa and 3.6% in RunIIb for the single electron "OR" and by 8% for the single muon "OR". We choose to use the single electron trigger "OR" result to assign the systematics, as this trigger OR is more efficient and known to be better measured than single muon "OR".

- **Opposite charge requirement systematics**. The electron charge misidentification fraction is not the same in data and in MC. To evaluate the systematic uncertainty on the opposite sign requirement, we have to evaluate these fractions, both for MC and data, in the CC and the EC. We use the $Z \to ee$ MC samples, and require successively opposite and same sign events. Before applying cuts on the jet multiplicity, we fit the invariant mass distributions to keep only events in the Z peak, and compute the misID fraction for one electron in the EC and the CC. They are presented in Table 10.

	Data	MC
CC	0.28	0.07
EC	6.7	2.9

TABLE 10: Electron charge misidentification fraction (in %)

The obtained results are consistent with those of the EMID group [45]. We then compute the probability to have same sign events in the background and signal samples in MC and data. We assign the difference of these probabilities as the systematic uncertainty on the opposite sign requirement. The method is applied separately for RunIIa and RunIIb1 and 2, and the uncertainties obtained are very close. We have studied this misidentification fraction in $Z \to \mu\mu$ events and found it negligible.

- **Uncertainty from the dZ cut**. Our selection requires a maximal distance of 2 cm along the beam axis between the two lepton tracks. We want to estimate the difference of efficiency for this cut in data and MC. The method is similar to the one used for the opposite charge requirement systematics. We run the selection with and without the cut and we count the number of events in the Z peak. We compute the efficiency difference between data and MC and apply this difference as uncertainty. This study is done separately in the dielectron and dimuon channels, and for RunIIa and RunIIb1 and 2. We apply the highest uncertainty in the electron-muon channel.

- **Z vertex distribution difference between data and MC**. The Z vertex distribution simulated in MC events is quite different from the data. In order to correct for this difference the reweighting from the *caf_mc_util* package is applied. This reweighting is based on the study from the note [19]. In order to estimate the systematics for this correction, an alternative parametrization for the beam shape could be used. The difference in the event selection efficiency between default and alternative parametrization is quoted as a systematic uncertainty.

- **Electron ID scale factor systematics**. We apply the same uncertainties as we did for the previous cross section measurement [2], which takes into account the error given by the EMID group on the certification procedure and the efficiency parametrization.

- **Electron momentum scale and smearing systematics**. Corrections are applied to simulated electrons to take into account the difference in momentum scale and resolution between data and MC. The uncertainties due to these corrections are derived separately by varying the momentum scale and smearing parameters applied in the EMresolution package. They are found to be very small, and we did not include them in the systematic tables for the cross section.

- **Muon momentum scale and resolution systematics**. In standard analyses, additional corrections are applied to MC muon to take into account the difference of momentum scale and resolution between data and MC. The systematic uncertainty due to these corrections are evaluated simultaneously by shifting the corresponding parameters by their uncertainties [51].

- **Jet ID systematics**. The standard procedure defined by the jet ID group has been used which consists of varying the jet ID efficiency by its uncertainty.

- **Jet resolution systematics**. The JSSR procedure applies additional smearing to the MC jets, in order to account for the different jet p_T resolution in data and MC. To compute the systematic uncertainty on the jet resolution, the width of the gaussian used to smear the jet energy should be varied by the size of the uncertainty on the jet energy resolution parameters in MC.

- **Vertex confirmation systematics**. The uncertainty on the jet vertex confirmation efficiency is evaluated by the jet ID group and implement in the caf_eff_util package. We estimated this uncertainty by varying the vertex confirmation efficiency scale factor by one standard deviation.

- **Jet energy scale systematics**. This systematic error has been evaluated by shifting the JES corrections by -1σ or $+1\sigma$ where σ has been measured in the JSSR procedure [32].

- **b-quark JES**. This error takes into account the difference between the nominal inclusive JES and the JES for b-hadrons. This later JES has been evaluated to be 1.8 % smaller [48]. This systematic error is obtained by shifting down by 1.8 % the nominal JES.

- **Uncertainties on the diboson cross section.** These uncertainties have been discussed in section III.

- **Z background uncertainty.** We know that the Z p_T spectrum is not well described in MC, especially in the one and two inclusive jet multiplicity bins. The uncertainty on the inclusive Z p_T reweighting was computed but does not explain the full difference between data and MC yields after the 2 jet cut. We decided to take the difference of the data to MC events ratios between the inclusive and the two jet cut as uncertainty. These differences are evaluated separately for RunII and RunIIb1 and 2, in the three different channels. The largest difference for each period is applied.

- **Likelihood fit statistics**. This error comes from the uncertainty of the electron likelihood fit determined in [2].

- **Likelihood fit systematics for the fake electron background**. This systematics comes from the uncertainty on the parameters used for the electron likelihood fit. The procedure is described in [2]. We assigned a 50% uncertainty on the number of fake electron background in CC and 100% uncertainty on the number of fake electron background in EC.

- **Fake muon systematic uncertainties.** An uncertainty due to the statistical error on the fake muon rate determination and on the statistical error of the non isolated muon sample have been assigned to the fake muon background estimation.

- **Cross-section dependence with the top mass (to be done)**.

The total systematic errors for the different MC samples are summarized in the tables 11 to 18 including all systematic errors except the error on the top mass. We call the variations of the systematics uncertainties "up", if it shifts the $t\bar{t}$ efficiency to the larger values. Usually it corresponds to the negative shift on the cross-section and hence to to the "down" variation of total cross section.

TABLE 11: Relative systematics for the different MC samples in the dielectron channel (RunIIa).

	$t\bar{t} \to \ell\ell jj$, %		$Z \to \ell\ell$, %		$Z \to \ell\ell$+HF, %		Dibosons, %		Total, pb	
	up	down	up	down	up	down	up	down	down	up
MC statistics	0.70	-0.70	7.46	-7.46	9.01	-9.01	8.83	-8.83	-0.18	0.18
Jet energy scale	1.78	-1.66	7.72	-6.35	7.72	-6.35	4.22	-3.55	-0.42	0.37
Jet resolution	1.51	-0.18	13.20	-3.66	13.20	-3.66	4.67	-1.05	-0.53	0.12
b quark JES	0.72	-0.72							-0.08	0.08
Jet ID	1.13	-1.13	1.35	-1.35	1.35	-1.35	1.22	-1.22	-0.17	0.17
Vertex Z distribution	0.70	-0.70	0.70	-0.70	0.70	-0.70	0.75	-0.75	-0.10	0.10
Electron ID	7.05	-7.05	7.58	-7.58	7.58	-7.58	8.68	-8.68	-1.03	1.03
dZ(leptons)	0.05	-0.05	0.05	-0.05	0.05	-0.05	0.05	-0.05	-0.01	0.01
Opposite charge	1.80	-1.80	1.80	-1.80	1.80	-1.80	1.80	-1.80	-0.26	0.26
b quark modeling	2.35	-2.35							-0.26	0.26
Higher order and hadronization	2.80	-2.80							-0.31	0.31
Color reconnection	1.30	-1.30							-0.15	0.15
ISR/FSR	0.70	-0.70							-0.08	0.08
W branching ratio	1.70	-1.70							-0.19	0.19
DQ event selection	0.50	-0.50	0.50	-0.50	0.50	-0.50	0.50	-0.50	-0.07	0.07
PDF	0.23	-0.29	2.56	-1.95	2.22	-2.04	0.82	-0.81	-0.12	0.12
Z normalization			11.00	-11.00	11.00	-11.00			-0.28	0.28
Diboson cross section							7.00	-7.00	-0.04	0.04
Total:	8.94	-8.80	24.86	-26.06	22.68	-18.21	15.77	-14.93	1.41	-1.30

TABLE 12: Relative systematics for the different MC samples in the dielectron channel (RunIIb1 and 2).

	$t\bar{t} \to \ell\ell jj$, %		$Z \to \ell\ell$, %		$Z \to \ell\ell$+HF, %		Dibosons, %		Total, pb	
	up	down	up	down	up	down	up	down	down	up
MC statistics	0.82	-0.82	13.21	-13.21	22.43	-22.43	5.57	-5.57	-0.23	0.23
Jet energy scale	1.13	-1.10	3.68	-3.27	3.68	-3.27	1.87	-1.81	-0.18	0.17
Jet resolution	0.54	-0.65	5.28	-3.48	5.28	-3.48	1.42	-0.99	-0.15	0.13
b quark JES	0.50	-0.50							-0.04	0.04
Jet ID	0.50	-0.50	0.42	-0.42	0.42	-0.42	0.60	-0.60	-0.06	0.06
Vertex confirmation	4.51	-4.51	5.95	-5.95	5.95	-5.95	5.71	-5.71	-0.54	0.54
Vertex Z distribution	0.53	-0.53	0.45	-0.45	0.45	-0.45	0.53	-0.53	-0.06	0.06
Electron ID	7.05	-7.05	7.58	-7.58	7.58	-7.58	8.68	-8.68	-0.82	0.82
dZ(leptons)	0.16	-0.16	0.16	-0.16	0.16	-0.16	0.16	-0.16	-0.02	0.02
Opposite charge	1.90	-1.90	1.90	-1.90	1.90	-1.90	1.90	-1.90	-0.22	0.22
b quark modeling	2.65	-2.65							-0.24	0.24
Higher order and hadronization	2.80	-2.80							-0.25	0.25
Color reconnection	1.30	-1.30							-0.12	0.12
ISR/FSR	0.70	-0.70							-0.06	0.06
W branching ratio	1.70	-1.70							-0.15	0.15
DQ event selection	0.50	-0.50	0.50	-0.50	0.50	-0.50	0.50	-0.50	-0.06	0.06
PDF	0.32	-0.46	3.05	-2.39	2.01	-1.87	0.59	-0.49	-0.11	0.13
Z normalization			7.00	-7.00	7.00	-7.00			-0.13	0.13
Diboson cross section							7.00	-7.00	-0.03	0.03
Total:	9.85	-9.87	20.03	-23.87	26.51	-26.13	14.09	-14.04	1.15	-1.15

TABLE 13: Relative systematics for the different MC samples in the electron-muon channel (RunIIa).

	$t\bar{t} \to \ell\ell jj$, %		$Z \to \ell\ell$, %		$Z \to \ell\ell$+HF, %		Dibosons, %		Fake EM, %		Fake Mu, %		Total, pb	
	up	down	up	down	up	down	up	down	up	down	up	down	down	up
MC statistics	0.41	-0.41	4.87	-4.87	9.34	-9.34	7.09	-7.09					-0.09	0.09
DQ event selection	0.50	-0.50	0.50	-0.50	0.50	-0.50	0.50	-0.50					-0.05	0.05
W branching ratio	1.70	-1.70											-0.13	0.13
Trigger	3.90	-3.90	3.90	-3.90	3.90	-3.90	3.90	-3.90					-0.37	0.37
Electron ID	3.50	-3.50	3.81	-3.81	3.81	-3.81	3.42	-3.42					-0.34	0.34
Muon ID	1.44	-1.44	1.44	-1.44	1.44	-1.44	1.44	-1.44					-0.14	0.14
dZ(leptons)	0.25	-0.25	0.25	-0.25	0.25	-0.25	0.25	-0.25					-0.02	0.02
Opposite charge	0.90	-0.90	0.90	-0.90	0.90	-0.90	0.90	-0.90					-0.09	0.09
Higher order and hadronization	2.80	-2.80											-0.21	0.21
Color reconnection	1.30	-1.30											-0.10	0.10
ISR/FSR	0.70	-0.70											-0.05	0.05
Jet energy scale	1.54	-1.54	4.53	-5.69	6.97	-6.21	4.59	-4.95					-0.33	0.35
Jet resolution	1.38	-0.06	8.53	-3.40	5.20	-2.81	12.84	-6.78					-0.39	0.09
b quark JES	0.77	-0.77											-0.06	0.06
Jet ID	1.00	-1.00	1.49	-1.49	2.05	-2.05	1.25	-1.25					-0.18	0.18
Vertex Z distribution	-0.83	0.83	-0.89	0.89	-0.59	0.59	-0.74	0.74					0.14	-0.14
Muon resolution	-0.10	0.00	0.34	0.00	2.81	0.14	0.87	0.00					-0.00	-0.00
b quark modeling	1.67	-1.67	-0.00	0.00	1.50	-1.50	-1.23	1.23					-0.25	0.25
PDF	0.23	-0.37	5.07	-3.80	7.33	-4.57	0.66	-0.96					-0.13	0.13
Z normalization			11.00	-11.00	11.00	-11.00							-0.19	0.19
Diboson cross section							7.00	-7.00					-0.03	0.03
Fit statistical error									14.71	-13.18	52.54	-40.60	-0.23	0.20
Fit systematics									44.84	-44.84			-0.57	0.57
Fake muon rate											7.29	-7.29	-0.02	0.02
Total:	7.87	-7.64	20.54	-17.33	25.95	-21.54	22.61	-16.72	47.19	-46.74	53.04	-41.24	1.08	-1.01

TABLE 14: Relative systematics for the different MC samples in the electron-muon channel (RunIIb1 and 2).

	$t\bar{t} \to \ell\ell jj$, %		$Z \to \ell\ell$, %		$Z \to \ell\ell$+HF, %		Dibosons, %		Fake EM, %		Fake Mu, %		Total, pb	
	up	down	up	down	up	down	up	down	up	down	up	down	down	up
MC statistics	0.43	-0.43	9.11	-9.11	12.08	-12.08	3.84	-3.84					-0.09	0.09
DQ event selection	0.50	-0.50	0.50	-0.50	0.50	-0.50	0.50	-0.50					-0.05	0.05
W branching ratio	1.70	-1.70											-0.15	0.15
Trigger	3.60	-3.60	3.60	-3.60	3.60	-3.60	3.60	-3.60					-0.37	0.37
Electron ID	3.50	-3.50	3.81	-3.81	3.81	-3.81	3.42	-3.42					-0.36	0.36
Muon ID	1.44	-1.44	1.44	-1.44	1.44	-1.44	1.44	-1.44					-0.15	0.15
dZ(leptons)	0.17	-0.17	0.17	-0.17	0.17	-0.17	0.17	-0.17					-0.02	0.02
Opposite charge	0.90	-0.90	0.90	-0.90	0.90	-0.90	0.90	-0.90					-0.09	0.09
Higher order and hadronization	2.80	-2.80											-0.25	0.25
Color reconnection	1.30	-1.30											-0.12	0.12
ISR/FSR	0.70	-0.70											-0.06	0.06
Jet energy scale	1.57	-1.47	6.45	-7.58	7.32	-4.08	6.64	-5.24					-0.37	0.35
Jet resolution	0.69	-0.43	2.96	-3.98	10.30	0.69	3.09	-3.54					-0.17	0.12
b quark JES	0.63	-0.63											-0.06	0.06
Jet ID	0.42	-0.42	-0.00	0.00	0.47	-0.47	0.44	-0.44					-0.08	0.08
Vertex confirmation	4.43	-4.43	4.91	-4.91	9.45	-9.45	5.68	-5.68					-0.86	0.86
Vertex Z distribution	0.51	-0.51	0.59	-0.59	0.48	-0.48	0.70	-0.70					-0.10	0.10
b quark modeling	1.78	-1.78	-0.00	0.00	3.56	-3.56	-0.09	0.09					-0.32	0.32
Muon resolution	-0.59	0.05	0.46	0.00	1.69	0.45	0.10	0.00					0.10	-0.01
PDF	0.28	-0.42	6.43	-4.98	5.50	-3.92	0.81	-0.61					-0.12	0.12
Z normalization			7.00	-7.00	7.00	-7.00							-0.07	0.07
Diboson cross section							7.00	-7.00					-0.02	0.02
Fit statistical error									13.68	-12.43	46.43	-34.35	-0.10	0.08
Fit systematics									45.79	-45.79			-0.25	0.25
Fake muon rate											6.70	-6.70	-0.01	0.01
Total:	9.75	-9.67	19.89	-20.19	33.34	-25.12	16.32	-15.44	47.79	-47.45	46.91	-35.00	1.24	-1.22

TABLE 15: Relative systematics for the different MC samples in the electron-muon 1jet channel (RunIIa).

	$t\bar{t} \to \ell\ell jj$, %		$Z \to \ell\ell$, %		$Z \to \ell\ell$+HF, %		Dibosons, %		Fake EM, %		Fake Mu, %		Total, pb	
	up	down	up	down	up	down	up	down	up	down	up	down	down	up
MC statistics	0.86	-0.86	5.55	-5.55	13.74	-13.74	4.77	-4.77					-0.44	0.44
DQ event selection	0.50	-0.50	0.50	-0.50	0.50	-0.50	0.50	-0.50					-0.10	0.10
W branching ratio	1.70	-1.70											-0.14	0.14
Trigger	3.90	-3.90	3.90	-3.90	3.90	-3.90	3.90	-3.90					-0.75	0.75
Electron ID	3.50	-3.50	3.81	-3.81	3.81	-3.81	3.42	-3.42					-0.69	0.69
Muon ID	1.44	-1.44	1.44	-1.44	1.44	-1.44	1.44	-1.44					-0.28	0.28
dZ(leptons)	0.25	-0.25	0.25	-0.25	0.25	-0.25	0.25	-0.25					-0.05	0.05
Opposite charge	0.90	-0.90	0.90	-0.90	0.90	-0.90	0.90	-0.90					-0.17	0.17
Higher order and hadronization	12.10	-12.10											-0.97	0.97
Color reconnection	0.14	-0.14											-0.01	0.01
ISR/FSR	7.70	-7.70											-0.62	0.62
Jet energy scale	-2.18	2.63	1.41	-2.25	-0.77	-11.49	2.48	-4.29					0.16	-0.06
Jet resolution	-4.81	0.45	-2.48	1.27	-9.21	3.80	3.03	0.68					0.88	-0.20
b quark JES	-0.45	0.45											0.04	-0.04
Jet ID	-2.63	2.63	0.52	-0.52	-0.49	0.49	0.56	-0.56					0.37	-0.37
Vertex Z distribution	-0.45	0.45	-0.78	0.78	-0.07	0.07	-0.62	0.62					0.15	-0.15
Muon resolution	0.00	0.00	4.12	0.16	1.48	0.00	-0.06	-0.06					-0.30	-0.01
b quark modeling	1.45	-1.45	-0.00	0.00	1.98	-1.98	0.62	-0.62					-0.26	0.26
PDF	0.89	-1.29	3.16	-2.50	2.62	-2.82	0.74	-0.70					-0.41	0.42
Z normalization			11.00	-11.00	11.00	-11.00							-0.84	0.84
Diboson cross section							7.00	-7.00					-0.25	0.25
Fit statistical error									14.04	-12.42			-0.61	0.54
Fit systematics									52.40	-52.40			-2.29	2.29
Statistical error on SS											24.01	-19.77	-0.57	0.47
Fake muon rate											3.80	-3.80	-0.09	0.09
Total:	17.77	-16.62	16.02	-14.57	25.27	-28.60	11.65	-11.95	54.25	-53.85	24.31	-20.13	3.27	-3.11

TABLE 16: Relative systematics for the different MC samples in the electron-muon 1jet channel (RunIIb1 and 2).

	$t\bar{t} \to \ell\ell jj$, %		$Z \to \ell\ell$, %		$Z \to \ell\ell$+HF, %		Dibosons, %		Fake EM, %		Fake Mu, %		Total, pb	
	up	down	up	down	up	down	up	down	up	down	up	down	down	up
MC statistics	0.80	-0.80	6.80	-6.80	13.51	-13.51	2.60	-2.60					-0.36	0.36
DQ event selection	0.50	-0.50	0.50	-0.50	0.50	-0.50	0.50	-0.50					-0.08	0.08
W branching ratio	1.70	-1.70											-0.14	0.14
Trigger	3.60	-3.60	3.60	-3.60	3.60	-3.60	3.60	-3.60					-0.58	0.58
Electron ID	3.50	-3.50	3.81	-3.81	3.81	-3.81	3.42	-3.42					-0.58	0.58
Muon ID	1.44	-1.44	1.44	-1.44	1.44	-1.44	1.44	-1.44					-0.23	0.23
dZ(leptons)	0.17	-0.17	0.17	-0.17	0.17	-0.17	0.17	-0.17					-0.03	0.03
Opposite charge	0.90	-0.90	0.90	-0.90	0.90	-0.90	0.90	-0.90					-0.15	0.15
Higher order and hadronization	12.10	-12.10											-0.96	0.96
Color reconnection	0.14	-0.14											-0.01	0.01
ISR/FSR	7.70	-7.70											-0.61	0.61
Jet energy scale	-2.26	1.87	2.51	-2.16	0.46	0.73	2.18	-2.59					0.17	-0.12
Jet resolution	-2.26	1.51	0.52	-0.18	-0.67	-1.75	0.82	-1.43					0.31	-0.18
b quark JES	0.18	-0.18											-0.01	0.01
Jet ID	-0.83	0.83	0.01	-0.01	-0.00	0.00	0.17	-0.17					0.13	-0.13
Vertex confirmation	-7.98	7.98	2.60	-2.60	-0.07	0.07	3.29	-3.29					1.05	-1.05
Vertex Z distribution	0.54	-0.54	0.52	-0.52	0.48	-0.48	0.48	-0.48					-0.13	0.13
b quark modeling	0.50	-0.50	-0.00	0.00	-2.38	2.38	0.27	-0.27					-0.08	0.08
Muon resolution	-0.72	0.00	2.12	0.06	0.44	0.00	0.72	0.10					-0.01	-0.01
PDF	0.28	-0.55	4.15	-3.33	2.48	-2.63	0.86	-0.58					-0.28	0.28
Z normalization			7.00	-7.00	7.00	-7.00							-0.38	0.38
Diboson cross section							7.00	-7.00					-0.20	0.20
Fit statistical error									8.96	-8.30			-0.24	0.23
Fit systematics									47.00	-47.00			-1.28	1.28
Statistical error on SS											15.24	-13.37	-0.22	0.19
Fake muon rate											3.57	-3.57	-0.05	0.05
Total:	19.73	-19.49	14.02	-13.10	17.35	-17.65	10.92	-11.14	47.84	-47.72	15.65	-13.84	2.34	-2.32

TABLE 17: Relative systematics for the different MC samples in the dimuon channel (RunIIa).

	$t\bar{t} \to \ell\ell jj$, %		$Z \to \ell\ell$, %		$Z \to \ell\ell$+HF, %		Dibosons, %		Fake Mu, %		Total, pb	
	up	down	up	down	up	down	up	down	up	down	down	up
MC statistics	0.59	-0.59	3.25	-3.25	5.46	-5.46	6.55	-6.55			-0.35	0.35
Jet energy scale	1.65	-1.54	11.02	-5.98	11.02	-5.98	3.72	-3.57			-1.54	0.93
Jet resolution	1.18	-0.09	13.65	-3.48	13.65	-3.48	5.45	-1.10			-1.81	0.43
b quark JES	0.59	-0.59									-0.07	0.07
Jet ID	1.02	-1.02	1.20	-1.20	1.20	-1.20	1.18	-1.18			-0.28	0.28
Vertex Z distribution	0.58	-0.58	0.47	-0.47	0.47	-0.47	0.65	-0.65			-0.13	0.13
Muon ID	2.88	-2.88	2.88	-2.88	2.88	-2.88	2.88	-2.88			-0.72	0.72
Muon resolution	-0.30	0.00	-0.19	-0.01	-0.19	-0.01	-0.24	0.06			0.06	0.00
dZ(leptons)	0.25	-0.25	0.25	-0.25	0.25	-0.25	0.25	-0.25			-0.06	0.06
b quark modeling	2.38	-2.38									-0.29	0.29
Higher order and hadronization	2.80	-2.80									-0.34	0.34
Color reconnection	1.30	-1.30									-0.16	0.16
ISR/FSR	0.70	-0.70									-0.09	0.09
Trigger	6.00	-6.00	6.00	-6.00	6.00	-6.00	6.00	-6.00			-1.49	1.49
W branching ratio	1.70	-1.70									-0.21	0.21
DQ event selection	0.50	-0.50	0.50	-0.50	0.50	-0.50	0.50	-0.50			-0.12	0.12
PDF	0.22	-0.30	1.23	-1.04	1.55	-1.45	0.38	-0.36			-0.21	0.21
Z normalization			11.00	-11.00	11.00	-11.00					-1.30	1.30
Diboson cross section							7.00	-7.00			-0.06	0.06
Statistical error on SS									24.73	-21.22	-0.34	0.29
Fake muon rate									7.29	-7.29	-0.10	0.10
Total:	8.34	-8.23	44.43	-45.08	23.36	-18.71	13.50	-12.35	25.78	-22.44	3.28	-2.48

TABLE 18: Relative systematics for the different MC samples in the dimuon channel (RunIIb1 and 2).

	$t\bar{t} \to \ell\ell jj$, %		$Z \to \ell\ell$, %		$Z \to \ell\ell$+HF, %		Dibosons, %		Fake Mu, %		Total, pb	
	up	down	up	down	up	down	up	down	up	down	down	up
MC statistics	0.72	-0.72	7.40	-7.40	17.36	-17.36	4.32	-4.32			-0.49	0.49
Jet energy scale	1.02	-0.98	3.52	-3.43	3.52	-3.43	2.07	-1.75			-0.33	0.31
Jet resolution	0.55	-0.58	4.86	-3.47	4.86	-3.47	1.64	-0.90			-0.39	0.29
b quark JES	0.49	-0.49									-0.03	0.03
Jet ID	0.37	-0.37	0.53	-0.53	0.53	-0.53	0.48	-0.48			-0.06	0.06
Vertex confirmation	4.56	-4.56	5.65	-5.65	5.65	-5.65	5.51	-5.51			-0.72	0.72
Vertex Z distribution	0.50	-0.50	0.41	-0.41	0.41	-0.41	0.48	-0.48			-0.06	0.06
Muon ID	2.88	-2.88	2.88	-2.88	2.88	-2.88	2.88	-2.88			-0.40	0.40
Muon resolution	-1.20	0.06	-0.93	-0.02	-0.93	-0.02	-0.92	0.08			0.15	-0.00
dZ(leptons)	0.17	-0.17	0.17	-0.17	0.17	-0.17	0.17	-0.17			-0.02	0.02
b quark modeling	2.10	-2.10									-0.13	0.13
Higher order and hadronization	2.80	-2.80									-0.18	0.18
Color reconnection	1.30	-1.30									-0.08	0.08
ISR/FSR	0.70	-0.70									-0.04	0.04
Trigger	6.00	-6.00	6.00	-6.00	6.00	-6.00	6.00	-6.00			-0.84	0.84
W branching ratio	1.70	-1.70									-0.11	0.11
DQ event selection	0.50	-0.50	0.50	-0.50	0.50	-0.50	0.50	-0.50			-0.07	0.07
PDF	0.28	-0.37	1.38	-1.21	1.77	-1.54	0.32	-0.33			-0.14	0.14
Z normalization			7.00	-7.00	7.00	-7.00					-0.50	0.50
Diboson cross section							7.00	-7.00			-0.04	0.04
Statistical error on SS									20.11	-17.72	-0.16	0.14
Fake muon rate									7.29	-7.29	-0.06	0.06
Total:	9.31	-9.24	23.08	-26.42	23.23	-24.68	12.29	-12.13	21.39	-19.16	1.51	-1.48

TABLE 19: Results for R_b only fit for different mass points

Top mass (GeV)	R_b (statistical errors only)
165	0.838 ± 0.042
170	0.867 ± 0.042
172.5	0.865 ± 0.042
175	0.890 ± 0.040
180	0.882 ± 0.039

VII. MASS DEPENDENCE

We use standard Alpgen+Pythia $t\bar{t}$ samples and Pythia samples with modified branching fractions generated for different mass points. R_b is fitted for each mass point without systematic uncertainties. The results are summarized in Table 19 and in Figure 9. As no significant mass dependence is observed, we are not quoting any systematic uncertainty associated with the top quark mass.

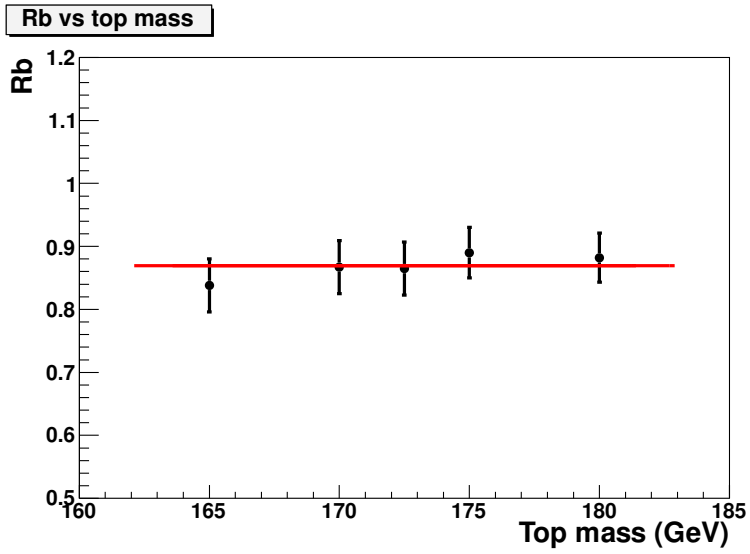

FIG. 9: Rb measurements for different top quark mass.

We plan to do the same test with systematics derived for the 172.5 GeV mass point, and extrapolated, and fit with the nuisance parameter method. That result will be added soon.

VIII. RB AND CROSS SECTION RESULTS

For our measurements, the treatments of uncertainties is done in two ways.

- With the standard derivation of the overall uncertainties, R_b and σ are recomputed for the variation of each systematic uncertainty, and the difference to the central value gives the error.
- With the nuisance method, each parameter is allowed to float within its systematic and statistical uncertainties, allowing to change the central value.

We will show the results obtained with both methods for R_b and the cross section measurements. The detailed systematics are only included for the nuisance method. For the standard method, they can be found in the Appendix A.

A. Measurement of $\sigma_{t\bar{t}}$

1. Separated channels

The $p\bar{p} \to t\bar{t}$ cross-section is found to be for the RunIIa:

$$\text{ee}: \quad \sigma_{t\bar{t}} = 11.23 \pm 2.99\,(\text{stat})\ \pm 1.32\,(\text{syst})\ \pm 0.86\,(\text{lumi})\ \text{pb}$$

$$e\mu\,(1jet): \quad \sigma_{t\bar{t}} = 8.02 \pm 4.26\,(\text{stat})\ \pm 3.16\,(\text{syst})\ \pm 1.17\,(\text{lumi})\ \text{pb}$$

$$e\mu\,(2jets): \quad \sigma_{t\bar{t}} = 7.45 \pm 1.33\,(\text{stat})\ \pm 1.04\,(\text{syst})\ \pm 0.58\,(\text{lumi})\ \text{pb}$$

$$\mu\mu: \quad \sigma_{t\bar{t}} = 12.19 \pm 3.45\,(\text{stat})\ \pm 2.86\,(\text{syst})\ \pm 1.36\,(\text{lumi})\ \text{pb}.$$

For RunIIb1 and 2 we find:

$$\text{ee}: \quad \sigma_{t\bar{t}} = 8.96 \pm 1.59\,(\text{stat})\ \pm 1.12\,(\text{syst})\ \pm 0.69\,(\text{lumi})\ \text{pb}$$

$$e\mu\,(1jet): \quad \sigma_{t\bar{t}} = 7.95 \pm 1.91\,(\text{stat})\ \pm 2.31\,(\text{syst})\ \pm 0.99\,(\text{lumi})\ \text{pb}$$

$$e\mu\,(2jets): \quad \sigma_{t\bar{t}} = 8.90 \pm 0.75\,(\text{stat})\ \pm 1.23\,(\text{syst})\ \pm 0.62\,(\text{lumi})\ \text{pb}$$

$$\mu\mu: \quad \sigma_{t\bar{t}} = 6.38 \pm 1.59\,(\text{stat})\ \pm 1.48\,(\text{syst})\ \pm 0.80\,(\text{lumi})\ \text{pb}.$$

2. RunIIa and RunIIb combinations

Using a counting method, we find for the combination of the four channels in the RunIIa:

$$\sigma_{t\bar{t}} = 8.71^{+1.16}_{-1.10}\,(\text{stat})\ \pm 1.38\,(\text{syst} + \text{lumi})\ \text{pb}.$$

For the RunIIb1 and 2:

$$\sigma_{t\bar{t}} = 8.51^{+0.60}_{-0.58}\,(\text{stat})\ ^{+1.22}_{-1.14}\,(\text{syst} + \text{lumi})\ \text{pb}.$$

3. Total combination

The combination of the four channels for RunIIa and RunIIb1 and 2, gives with a counting method:

$$\sigma_{t\bar{t}} = 8.55^{+0.53}_{-0.51}\,(\text{stat})\ ^{+1.16}_{-1.09}\,(\text{syst})\ \text{pb};$$

Using the likelihood fit method:

- for the standard method: $\sigma_{t\bar{t}} = 8.02^{+0.50}_{-0.48}\,(\text{stat})\ ^{+1.03}_{-0.94}\,(\text{syst})\ \text{pb}$;
- for the nuisance method: $\sigma_{t\bar{t}} = 7.29^{+0.90}_{-0.79}\,(\text{stat} + \text{syst})\ \text{pb}$.

Systematics errors on the cross section are summarized in Table 20 for the nuisance method.

TABLE 20: Systematics errors on the dilepton cross section combination (obtained with the nuisance method).

Source	Offset	$+\sigma$	$-\sigma$
Statistical only	+8.02	+0.50	-0.48
Event preselection	-0.01	+0.07	-0.06
Muon identification	-0.00	+0.13	-0.12
Muon resolution and scale	+0.01	+0.03	-0.03
Electron identification and smearing	-0.21	+0.28	-0.25
Electron scale	+0.00	+0.00	-0.00
Z pT reweighting	-0.18	+0.16	-0.15
signal modeling	+0.11	+0.31	-0.27
Color reconnection	-0.00	+0.10	-0.09
ISR/FSR variation	+0.04	+0.12	-0.11
Muon triggers	+0.02	+0.08	-0.07
Dilepton trigger	-0.09	+0.21	-0.19
Opposite charge requirement	-0.03	+0.10	-0.09
Jet energy scale	-0.16	+0.15	-0.14
Jet shifting	+0.00	+0.00	+0.00
Vertex confirmation	-0.13	+0.22	-0.20
b-Jet energy scale	+0.00	+0.05	-0.04
Jet energy resolution	-0.10	+0.10	-0.09
Jet reconstruction and identification	-0.01	+0.04	-0.03
Taggability in data	+0.01	+0.00	+0.00
b-tag TRF	+0.08	+0.07	-0.07
light tag TRF	-0.00	+0.00	+0.00
b fragmentation	-0.01	+0.15	-0.14
Monte Carlo background x-section	-0.02	+0.05	-0.05
Monte Carlo signal & bkg branching ratio	+0.00	+0.14	-0.13
Monte Carlo bkg scale factors	-0.13	+0.18	-0.17
Monte Carlo statistics	+0.00	+0.00	+0.00
Instrumental background	-0.02	+0.17	-0.17
PDF	+0.00	+0.00	+0.00
Luminosity	-0.60	+0.59	-0.51
Template statistics for template fits	+0.00	+0.00	+0.00
Total error (nuisance parameter fit)	7.29	+0.90	-0.79

B. Measurement of R_b

1. *Separated channels*

We show here the results obtained for the measurement of r_b alone with the standard method, in every channel separately. For RunIIa we have:

$$\text{ee}: \quad R_b = 0.715^{+0.225}_{-0.221}\,(\text{stat})\,^{+0.037}_{-0.032}\,(\text{syst})$$

$$e\mu\,(1jet): \quad R_b = 0.372^{+0.365}_{-0.270}\,(\text{stat})\,^{+0.120}_{-0.091}\,(\text{syst})$$

$$e\mu\,(2jets): \quad R_b = 0.925^{+0.108}_{-0.111}\,(\text{stat})\,^{+0.040}_{-0.037}\,(\text{syst})$$

$$\mu\mu: \quad R_b = 0.747^{+0.199}_{-0.198}\,(\text{stat})\,^{+0.062}_{-0.049}\,(\text{syst})$$

For RunIIb1 and 2 we find:

$$\text{ee}: \quad R_b = 0.942^{+0.111}_{-0.116}\,(\text{stat})\ \pm 0.036\,(\text{syst})$$

$$e\mu\,(1jet): \quad R_b = 0.766^{+0.174}_{-0.165}\,(\text{stat})\,^{+0.147}_{-0.091}\,(\text{syst})$$

$$e\mu\,(2jets): \quad R_b = 0.885^{+0.058}_{-0.060}\,(\text{stat})\ \pm 0.030\,(\text{syst})$$

$$\mu\mu: \quad R_b = 0.815^{+0.138}_{-0.137}\,(\text{stat})\ ^{+0.059}_{-0.057}\,(\text{syst})$$

2. RunIIa and RunIIb combinations

The measurement of R_b alone for all channels combined yields:

- for RunIIa:
  - for the standard method: $R_b = 0.831^{+0.087}_{-0.088}\,(\text{stat})\ ^{+0.043}_{-0.035}\,(\text{syst})$;
  - for the nuisance method: $R_b = 0.843 \pm 0.092\,(\text{stat} + \text{syst})$.
- for RunIIb1 and 2:
  - for the standard method: $R_b = 0.877^{+0.047}_{-0.048}\,(\text{stat})\ ^{+0.039}_{-0.034}\,(\text{syst})$;
  - for the nuisance method: $R_b = 0.876^{+0.054}_{-0.053}\,(\text{stat} + \text{syst})$.

3. Total combination

We obtain for all channels and the RunIIa and RunIIb1 and 2 combination:

- with the standard method: $R_b = 0.867 \pm 0.042\,(\text{stat})\ ^{+0.037}_{-0.032}\,(\text{syst})$;
- with the nuisance method: $R_b = 0.861^{+0.046}_{-0.045}\,(\text{stat} + \text{syst})$.

Systematics errors on the combination result are summarized in Table 21 for the nuisance method.

Using the value obtained with the nuisance method, we obtain the limits on R_b with the Feldman-Cousin method [56]:

- at 95% C.L., $0.739 < R_b < 0.952$;
- at 99% C.L., $0.704 < R_b < 0.983$.

We can also yield limits on V_{tb}:

- at 95% C.L., $0.859 < V_{tb} < 0.976$;
- at 99% C.L., $0.837 < V_{tb} < 0.989$.

If we don't assume the CKM matrix unitarity, we can only extract information on the ratio:

$$\frac{|V_{ts}|^2 + |V_{td}|^2}{|V_{tb}|^2} = \frac{1-R}{R}.$$

The limits obtained on that ratio are:

- at 95% C.L., $0.049 < \frac{1-R}{R} < 0.343$;
- at 99% C.L., $0.017 < \frac{1-R}{R} < 0.414$.

The figure 10 shows the limit bands, and the measured value with the nuisance method.

TABLE 21: Systematics errors on the dilepton R_b measurement (obtained with the nuisance method).

Source	Offset	$+\sigma$	$-\sigma$
Statistical only	+0.867	+0.042	-0.042
Event preselection	+0.000	+0.000	+0.000
Muon identification	+0.000	+0.000	+0.000
Muon resolution and scale	+0.000	+0.001	-0.001
Electron identification and smearing	+0.001	+0.000	+0.000
Electron scale	+0.000	+0.000	-0.000
Z pT reweighting	+0.007	+0.006	-0.006
signal modeling	-0.003	+0.005	-0.005
Color reconnection	-0.000	+0.002	+0.000
ISR/FSR variation	-0.001	+0.003	-0.003
Muon triggers	-0.000	+0.001	-0.000
Dilepton trigger	+0.000	+0.000	+0.000
Opposite charge requirement	+0.000	+0.000	+0.000
Jet energy scale	+0.005	+0.005	-0.005
Jet shifting	+0.000	+0.000	-0.000
Vertex confirmation	+0.002	+0.003	-0.003
b-Jet energy scale	-0.000	+0.000	+0.000
Jet energy resolution	+0.005	+0.006	-0.005
Jet reconstruction and identification	+0.000	+0.000	+0.000
Taggability in data	+0.001	+0.000	-0.001
b-tag TRF	+0.000	+0.000	+0.000
light tag TRF	-0.000	+0.000	+0.000
b fragmentation	-0.002	+0.000	+0.000
Monte Carlo background x-section	+0.001	+0.003	-0.002
Monte Carlo signal & bkg branching ratio	-0.001	+0.002	-0.002
Monte Carlo bkg scale factors	+0.003	+0.010	-0.009
Monte Carlo statistics	+0.000	+0.000	-0.000
Instrumental background	-0.002	+0.009	-0.008
ttbar xsection error	-0.008	+0.005	-0.004
PDF	-0.000	+0.001	-0.004
Luminosity	+0.001	+0.000	+0.000
Template statistics for template fits	+0.000	+0.000	-0.000
All systematics (nuisance parameter fit)	0.861	+0.046	-0.045

C. Simultaneous measurement of R_b and σ

Measuring simultaneously R_b and the $t\bar{t}$ dilepton cross section with the standard method leads to the results:

$$R_b = 0.853^{+0.041}_{-0.042}\,(\text{stat})\,^{+0.039}_{-0.036}\,(\text{syst})$$
$$\sigma_{t\bar{t}} = 8.38^{+0.51}_{-0.49}\,(\text{stat})\,^{+1.10}_{-0.02}\,(\text{syst})$$

With the nuisance parameter method we obtain:

$$R_b = 0.851^{+0.047}_{-0.046}\,(\text{stat}+\text{syst})$$
$$\sigma_{t\bar{t}} = 8.29^{+1.07}_{-0.93}\,(\text{stat}+\text{syst})$$

Figure 11 shows the $tt \to$ bb, bq and qq templates, and data and Monte-Carlo after the fit.
Systematics errors on the result are summarized in Table 22 for the R_b and Table 23 for the cross section.

IX. COMBINATION WITH THE ℓ+JETS CHANNEL

In this section we present the combination of the measurement of $\sigma_{t\bar{t}}$ and R_b in the lepton+jets and dilepton channel. The details of the measurement in the ℓ+jetschannel are presented elsewhere [57]. All channels are constructed to be orthogonal. The method to combine the channels is by performing by adding the logarithms of the likelihood functions and minimize the sum. Correlations between systematic uncertianties are taken into account between all channels by using the same nuisance parameter for each correlated source of systematic uncertainty.

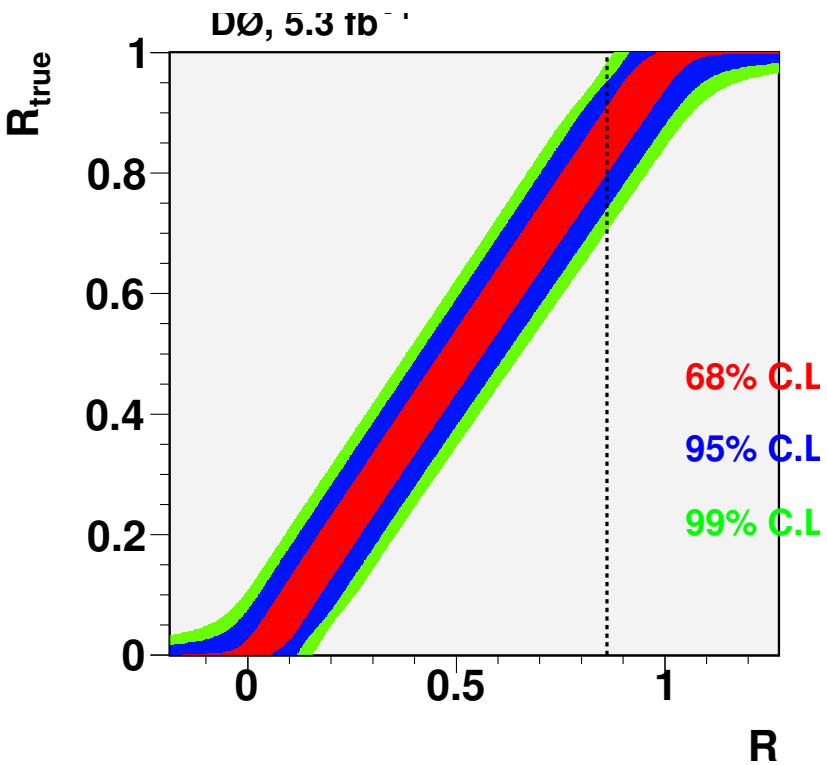

FIG. 10: Limit bands at one, two and three sigma obtained with the Feldman-Cousin method for the dilepton combination.

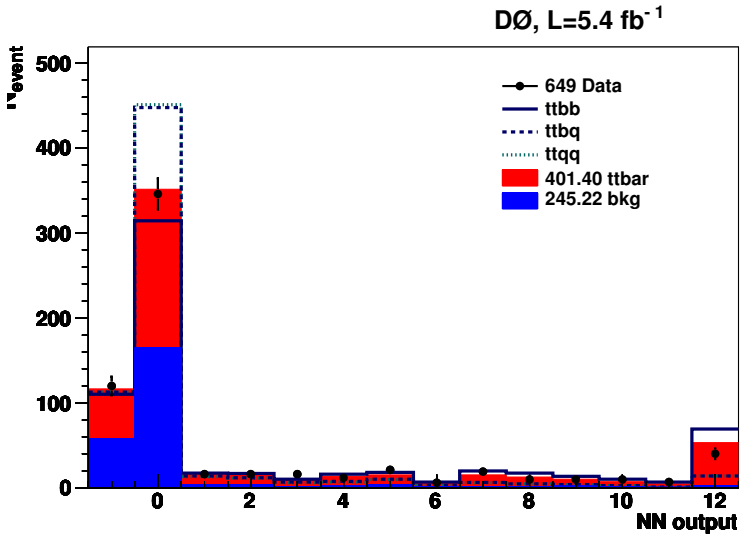

FIG. 11: The b-tagging NN output distribution for all analysis channels combined. In blue the sum of all backgrounds, in red the fitted top signal is shown. The dashed lines show the distribution for the $tt \to$ bb, bq and qq templates.

A. Cross section only fit

Fitting the cross section only, we find:

- using a counting method: $\sigma_{t\bar{t}} = 7.80^{+0.21}_{-0.20}(\text{stat})^{+0.86}_{-1.95}(\text{syst})pb$;
- using a template fit with the standard method: $\sigma_{t\bar{t}} = 7.72 \pm 0.20(\text{stat})^{+0.79}_{-0.72}(\text{syst})pb$;

TABLE 22: Systematics errors on R_b for the simultaneous measurement (obtained with the nuisance method).

Source	Offset	$+\sigma$	$-\sigma$
Statistical only	+0.853	+0.041	-0.042
Event preselection	+0.000	+0.001	-0.001
Muon identification	-0.000	+0.002	-0.002
Muon resolution and scale	+0.000	+0.000	-0.001
Electron identification and smearing	+0.002	+0.004	-0.004
Electron scale	+0.000	+0.000	-0.000
Z pT reweighting	+0.004	+0.009	-0.009
signal modeling	+0.000	+0.000	-0.001
Color reconnection	+0.000	+0.000	-0.000
ISR/FSR variation	+0.000	+0.000	-0.001
Muon triggers	-0.001	+0.001	-0.001
Dilepton trigger	+0.000	+0.003	-0.003
Opposite charge requirement	+0.000	+0.001	-0.001
Jet energy scale	+0.004	+0.007	-0.006
Jet shifting	+0.000	+0.000	-0.000
Vertex confirmation	-0.000	+0.007	-0.006
b-Jet energy scale	-0.000	+0.003	-0.004
Jet energy resolution	+0.005	+0.003	-0.003
Taggability in data	+0.001	+0.000	-0.000
b-tag TRF	+0.000	+0.000	+0.000
light tag TRF	+0.000	+0.000	+0.000
b fragmentation	+0.000	+0.000	-0.000
Monte Carlo background x-section	+0.000	+0.003	-0.003
Monte Carlo signal & bkg branching ratio	+0.000	+0.000	-0.001
Monte Carlo bkg scale factors	-0.006	+0.013	-0.012
Monte Carlo statistics	+0.000	+0.000	-0.000
Instrumental background	-0.012	+0.012	-0.010
PDF	+0.000	+0.000	-0.001
Luminosity	+0.002	+0.009	-0.009
Template statistics for template fits	+0.000	+0.000	-0.000
All systematics (nuisance parameter fit)	0.851	+0.047	-0.046

- using a template fit with the nuisance method: $\sigma_{t\bar{t}} = 7.55^{+0.64}_{-0.57}(\text{stat+syst})pb$.

B. R_b only fit

Fitting R_b only we find:

- with the standard method: $R_b = 0.984 \pm 0.021(\text{stat})^{+0.75}_{-0.71}(\text{syst})$;
- with the nuisance method: $R_b = 0.924^{+0.036}_{-0.035}(\text{stat+syst})$.

C. Simultaneous measurement

The results for the simultaneous measurement will be added soon.

TABLE 23: Systematics errors on the cross section for the simultaneous measurement (obtained with the nuisance method).

Source	Offset	$+\sigma$	$-\sigma$
Statistical only	+8.38	+0.51	-0.49
Event preselection	-0.00	+0.07	-0.07
Muon identification	+0.02	+0.13	-0.12
Muon resolution and scale	+0.00	+0.03	-0.03
Electron identification and smearing	-0.10	+0.29	-0.27
Electron scale	-0.00	+0.00	-0.00
Z pT reweighting	-0.08	+0.17	-0.16
signal modeling	+0.08	+0.31	-0.27
Color reconnection	-0.00	+0.10	-0.09
ISR/FSR variation	+0.02	+0.12	-0.11
Muon triggers	+0.04	+0.08	-0.08
Dilepton trigger	-0.03	+0.22	-0.20
Opposite charge requirement	-0.01	+0.10	-0.09
Jet energy scale	-0.08	+0.20	-0.16
Jet shifting	-0.00	+0.00	+0.00
Vertex confirmation	+0.01	+0.25	-0.23
b-Jet energy scale	+0.01	+0.13	-0.11
Jet energy resolution	-0.07	+0.08	-0.08
Jet reconstruction and identification	-0.00	+0.04	-0.04
Taggability in data	+0.00	+0.00	+0.00
b-tag TRF	+0.00	+0.00	+0.00
light tag TRF	-0.00	+0.00	+0.00
b fragmentation	-0.02	+0.19	-0.17
Monte Carlo background x-section	-0.00	+0.05	-0.05
Monte Carlo signal & bkg branching ratio	+0.00	+0.15	-0.13
Monte Carlo bkg scale factors	+0.09	+0.19	-0.18
Monte Carlo statistics	-0.00	+0.00	+0.00
Instrumental background	+0.22	+0.17	-0.17
PDF	+0.00	+0.04	-0.02
Luminosity	-0.14	+0.67	-0.58
Template statistics for template fits	-0.00	+0.00	+0.00
Total error (nuisance parameter fit)	8.29	+1.07	-0.93

[1] V. M. Abazov *et al.* [D0 Collaboration], "Measurement of the ttbar production cross section and top quark mass extraction using dilepton events in ppbar collisions," Phys. Lett. B **679**, 177 (2009) [arXiv:0901.2137 [hep-ex]].

[2] M. Besancon, S. Chevalier-Thery, A. Croc, F. Deliot, C. Deterre, A. Grohsjean, V. Sharyy, Y. Peters *Measurement of the ttbar Production Cross-Section in Dilepton Final State Using RunIIb1 and RunIIb2 Dataset for Winter 10 Conferences*, DØ Note 6027, February, 2010.

[3] M. Arthaud, M. Besançon, S. Chakrabarti, F. Déliot, E. Shabalina, V. Sharyy *Final Measurement of the ttbar Production Cross-section at sqrt(s)=1.96 TeV in Electron Muon Final States using p17 data set*, DØ Note 5580, February, 2008.

[4] B. Martin, Y. Arnoud, G. Sajot, E. Shabalina *Final Measurement of the ttbar production cross section at sqrt(s)= 1.96 TeV in the ee final state using p17 data set* DØ Note 5579, February, 2008.

[5] U. Bassler, J. P. Konrath, C. Schwanenberger, E. Shabalina *Final Measurement of the ttbar Production Cross-section at sqrt(s)=1.96 TeV in the Dimuon Final State Using p17 Data Set* DØ Note 5581, February, 2008.

[6] V. Sharyy, M. Besancon, F. Deliot *ttbar Event Selection in the Electron Muon Final State using p20 Dataset for Winter 09 Conferences* DØ Note 5864, February, 2009.

[7] M. Arthaud, M. Besancon, S. Chakrabarti, F. Deliot, V. Sharyy *ttbar Event Selection in the Electron Muon Final State using p20 Dataset*, DØ Note 5720, July, 2008.

[8] DQ web page *Infrastructure for physics analyses*, `http://www-d0.fnal.gov/computing/data_quality/d0_private/forusers.html`

[9] Laurent Duflot, *et al.*, *cal_event_quality package*, DØ Note 4614, September, 2004.

[10] F. Déliot, V. Shary, *Trigger Efficiency Measurement for the OR of Electron Muon Triggers*, DØ Note 5587, February 2008

[11] M. Owen and M. Hohlfeld, *Trigger Efficiencies for the OR of Single Electron Triggers in p17 Data*, DØ Note 5409, May, 2007

[12] Marc Hohlfeld, *Measurement of Single Electron Trigger Efficiencies for RunIIB*, DØ Note 5783, November 2008

[13] Philippe Calfayan, *ORing single muon triggers in p17 data*, DØ Note 5329, January, 2007

[14] Fabrice Couderc's talk at the summer 09 workshop:
`http://www-d0.hef.kun.nl//askArchive.php?base=agenda&categ=a09886&id=a09886s2t1/transparencies`

[15] `http://www-clued0.fnal.gov/~nunne/cross-sections/dy_cross-sections.html`

[16] C. Amsler *et al.* [Particle Data Group], Phys. Lett. B **667**, 1 (2008).

[17] J. Hays, J. Mitrevski, C. Schwanenberger, *The Program Package em_cert: Version p18-br-20*, DØ Note 5070, March 2006

[18] S.-J. Park, M. Begel, *Efficiency of the Data Quality Calorimeter Flags*, DØ Note 5324, January 2007.

[19] H. Schellman, *The longitudinal shape of the luminous region at DØ* , DØ Note 5142, June 2006.

[20] V. M. Abazov *et al.* [The D0 Collaboration], Nucl. Instrum. Meth. A **620** (2010) 490 [arXiv:1002.4224 [hep-ex]].

[21] A. Das and E. Varnes, *Measurement of the W Boson Helicity in Top Quark Decays Using 4 $fb1$ of RunII Data*, DØ Note 5947, June 2009.

[22] `http://hepforge.cedar.ac.uk/lhapdf`

[23] J. Hobbs, *et al.*, *Study of pp(bar) -¿ $Z/\gamma^* \rightarrow ee$ and mumu event yields as a luminosity cross check*, DØ Note 5268, October 2006.

[24] A. Schwartzman *Missing Et Significance Algorithm in RunII data*, DØ Note 4254, September 2003.

[25] J. Hays, J. Mitrevski, C. Schwanenberger, T. Toole, *ingle Electron Efficiencies in p17 Data and Monte-Carlo Using p18.05.00 d0correct*, DØ Note 5105, May 2006

[26] O. Atramentov, D. Bandurin, X. Bu, B. Calpas, E. Carrera, D. Duggan, A. Ferapontov, M. Takahashi, T. Uzbyakova, H. Yin, *Electron and Photon Identification with p20 data*, DØ Note 5761, August 2008.

[27] P. Calfayan, T. Gadfort, G. Hesketh, V. Lesne, M. Owen, R. Stroehmer, V. Sharyy, B. Tuchming, *Muon Identification Certification for p17 data*, DØ Note 5157, June 2006
O. Brandt, S.W. Cho, M. Cookc, M. Eads, D. Hedin, A. Santos, B. Tuchming, Y. Yatsunenko, S.W. Youn, *Muon Identication Certication for the Summer 2009 Extended Dataset (Run IIb-1 and -2)*, DØ Note 6025, January 2010.

[28] J. Kvita and A. Harel, *p20 Jet ID Efficiencies and Scale Factors*, DØ Note 5634, March 2008

[29] A. Harel *JetID Optimization* DØ Note 4919, September 2005.

[30] A. Harel *Capping the JES muon corrections* DØ Note 5563, January 2008.

[31] `http://www-d0.fnal.gov/phys_id/jes/d0_private/certified/certified_jes.html`

[32] Nicola Makovec and Jean-François Grivaz, *Shifting, Smearing and Removing Simulated Jets*, DØ Note 4914, November 2005
C. Ochando and J.-F. Grivaz, *SSR for p17*, DØ Note 5609, January 2008
C. Ochando, talk at the JES meeting
http://www-d0.hef.kun.nl//askArchive.php?base=agenda&categ=a08924&id=a08924s1t3/transparencies

[33] `http://www-d0.fnal.gov/phys_id/jets/jetid.html`

[34] J. Kozminski *et al.*, *The electron likelihood in p14*, DØ Note 4449, November 2003
A. Kumar, B. Choudhary, J. Kozminski, R. Kehoe, J. Hays, J. Stark, *Electron Likelihood Study*, DØ Note 4769, March 2005
L. Wang, J. Hays, J. Mitrevski, C. Schwanenberger *Electron Likelihood Efficiency in p17*, DØ Note 5114, May 2006.

[35] `http://www.thep.lu.se/~torbjorn/Pythia.html`
see also T. Sjöstrand, L. Lönnblad, S. Mrenna and P. Skands, hep-ph/0308153;

and T. Sjöstrand, P. Edén, C. Friberg, L. Lönnblad, G. Miu, S. Mrenna and E. Norrbin, Comp. Phys. Commun. **135** (2001) 238, hep-ph/0010017.

[36] J. Campbell and R.K. Ellis, MCFM - Monte Carlo for FeMtobarn processes, `http://mcfm.fnal.gov/`

[37] F. Deliot, C. Deterre, S. Shary, *$Z/\gamma^\star$ cross section computation at NNLO using the FEWZ code*, DØ Note 6050, April 2010

[38] V.Sharyy, *How to reweight MC according to the luminosity profile in data*, https://plone4.fnal.gov/P1/D0Wiki/comp/caf/caffaq/LumiReWeight

[39] M.L. Mangano, M. Moretti, F. Piccinini, R. Pittau, A. Polosa, ALPGEN, a generator for hard multiparton processes in hadronic collisions, JHEP **0307** (2003) 1, hep-ph/0206293; `http://mlm.home.cern.ch/mlm/alpgen/`

[40] R. J. Barlow, Nucl. Instrum. Meth. A **297**, 496 (1990).

[41] S. Moch and P. Uwer, JHEP 09, 127 (2008)
S. Moch and P. Uwer, Phys. Rev. D **78** (2008) 034003 [arXiv:0804.1476 [hep-ph]].

[42] T. Adams, *et al*, *Combination of the top quark pair production cross section, cross section ratios and top quark mass extraction*, DØ Note 5854, February 2009

[43] , T. Adams, *et al*, *Combination of the top quark pair production cross sections and search for charged Higgs boson*, DØ Note 5597, February 2008

[44] P. Sinervo, in *Proceedings of Statistical methods in Particle Physics, Astrophysics, and Cosmology*, edited by L. Lyons, R.P. Mount and R. Reitmeyer (SLAC, Standford, 2003), p 334.

[45] D. Bandurin and M. Takakhashi, *Electron charge misidentification for p17 and p20 data and Monte Carlo*, DØ Note 5927, May 2009.

[46] J. Pumplin, D.R. Stump, J.Huston, H.L. Lai, P. Nadolsky, W.K. Tung *New Generation of Parton Distributions with Uncertainties from Global QCD Analysis*, JHEP O207 (2002) 012, February, 2002.

[47] Y. Peters, M. Begel, K. Hamacher and D. Wicke, *Reweighting of the fragmentation function for the D0 Monte Carlo*, DØ Note 5325, January 2007.

[48] A. Harel, *Data over MC, b over light jet response corrections for RunIIa JES*, DØ Note 5654, April 2008.

[49] `https://plone4.fnal.gov/P1/D0Wiki/object-id/emid/emcert/Moriond2009/uncertainty_moriond09`

[50] EMid conveners, private communication.

[51] M. Arthaud, F. Deliot, B. Tuchming, V. Sharyy, D. Vilanova, *Muon Momentum Oversmearing for p20 Data*, DØ Note 5449 July 2007.

[52] T. Andeen et al., FERMILAB-TM-2365 (2007)

[53] F. Déliot, C. Schwanenberger, E. Shabalina, M. Wang, D. Wicke and Z. Ye, *Systematic Uncertainties in Top Quark Measurements*, DØ Note 6024, January 2010.

[54] M. Cacciari et al., JHEP **09** (2008) 127

[55] N. Kidonakis, R. Vogt, Phys. Rev. D **78** (2008) 074005.

[56] A. Harel, T. Kuhl, Y. Peters, C. Schwanenberger, E. Shabalina *Calculation of confidence regions with the cousins and Feldman method*, DØ Note 5526, October 2007.

[57] Y. Peters, F. Deliot, C. Schwanenberger, E. Shabalina *Simultaneous measurement of* $\mathbf{B(t \to Wb)/B(t \to Wq)}$ *and* $\sigma(\mathbf{p\bar{p} \to t\bar{t}}) \cdot \mathbf{B(t \to Wq)^2}$ *with 5.3fb^{-1} of data*, DØ Note 6148, January, 2011.

APPENDIX A: SYSTEMATIC TABLES

Here are shown the standard systematics tables for the main measurements. For the dilepton channel and the RunIIa-RunIIb1 and 2 combination, Table 24 shows the systematics on the cross section, and Table 25 on R_b. Tables 26 and 27 show these uncertainties in the case of the simultaneous measurement of $\sigma_{t\bar{t}}$ and R_b.

TABLE 24: Systematics errors on the dilepton cross section only fit (RunIIa-RunIIb1 and 2 combination).

Summary of systematics on cross section with standard method				
Source	$+\sigma$	$-\sigma$	$+\sigma$/central	$-\sigma$/central
Stat error only	0.000	-0.000	0.000	-0.000
Event preselection	0.065	-0.065	0.008	-0.008
Muon identification	0.125	-0.123	0.016	-0.015
Muon resolution and scale	0.031	-0.003	0.004	-0.000
Electron identification and smearing	0.295	-0.280	0.037	-0.035
Electron scale	0.002	-0.001	0.000	-0.000
Z pT reweighting	0.139	-0.156	0.017	-0.019
signal modeling	0.325	-0.304	0.041	-0.038
Color reconnection	0.094	-0.092	0.012	-0.011
ISR/FSR variation	0.125	-0.123	0.016	-0.015
Muon triggers	0.087	-0.086	0.011	-0.011
Dilepton trigger	0.213	-0.205	0.027	-0.026
Opposite charge requirement	0.093	-0.091	0.012	-0.011
Jet energy scale	0.129	-0.129	0.016	-0.016
Jet shifting	0.000	-0.000	0.000	-0.000
Vertex confirmation	0.259	-0.250	0.032	-0.031
b-Jet energy scale	0.047	-0.046	0.006	-0.006
Jet energy resolution	0.052	-0.079	0.007	-0.010
Jet reconstruction and identification	0.030	-0.030	0.004	-0.004
Taggability in data	0.016	-0.017	0.002	-0.002
b-tag TRF	0.116	-0.035	0.015	-0.004
light tag TRF	0.047	-0.000	0.006	-0.000
b fragmentation	0.149	-0.144	0.019	-0.018
Monte Carlo background x-section	0.098	-0.047	0.012	-0.006
Monte Carlo signal & bkg branching ratio	0.139	-0.134	0.017	-0.017
Monte Carlo bkg scale factors	0.235	-0.215	0.029	-0.027
Monte Carlo statistics	0.000	-0.000	0.000	-0.000
Instrumental background	0.257	-0.234	0.032	-0.029
PDF	0.036	-0.023	0.004	-0.003
Luminosity	0.685	-0.601	0.085	-0.075
Template statistics for template fits	0.029	-0.029	0.004	-0.004
Total systematic with ensembles	1.034	-0.944	0.129	-0.118

TABLE 25: Systematics errors on the dilepton Rb only fit (RunIIa-RunIIb1 and 2 combination).

Summary of systematics on B($t \to Wb$) with standard method		
Source	sigma+	sigma-
Stat error only	0.000	-0.000
Event preselection	0.000	-0.000
Muon identification	0.000	-0.000
Muon resolution and scale	0.001	-0.000
Electron identification and smearing	0.001	-0.001
Electron scale	0.000	-0.000
Z pT reweighting	0.008	-0.007
signal modeling	0.006	-0.006
Color reconnection	0.001	-0.001
ISR/FSR variation	0.003	-0.003
Muon triggers	0.000	-0.000
Dilepton trigger	0.000	-0.000
Opposite charge requirement	0.000	-0.000
Jet energy scale	0.006	-0.005
Jet shifting	0.000	-0.000
Vertex confirmation	0.005	-0.005
b-Jet energy scale	0.002	-0.001
Jet energy resolution	0.007	-0.005
Jet reconstruction and identification	0.000	-0.000
Taggability in data	0.001	-0.004
b-tag TRF	0.024	-0.017
light tag TRF	0.004	-0.000
b fragmentation	0.003	-0.002
Monte Carlo background x-section	0.003	-0.005
Monte Carlo signal & bkg branching ratio	0.002	-0.002
Monte Carlo bkg scale factors	0.013	-0.014
Monte Carlo statistics	0.000	-0.000
Instrumental background	0.012	-0.013
ttbar xsection error	0.013	-0.008
PDF	0.001	-0.000
Luminosity	0.001	-0.001
Template statistics for template fits	0.006	-0.006
Total systematic with ensembles	0.037	-0.032

TABLE 26: Systematics errors on the cross section measurement, for the simultaneous measurement in the dilepton channel (RunIIa-RunIIb1 and 2 combination).

Summary of systematics on cross section with standard method				
Source	$+\sigma$	$-\sigma$	$+\sigma$/central	$-\sigma$/central
Stat error only	0.000	-0.000	0.000	-0.000
Event preselection	0.069	-0.068	0.008	-0.008
Muon identification	0.132	-0.131	0.016	-0.016
Muon resolution and scale	0.027	-0.003	0.003	-0.000
Electron identification and smearing	0.312	-0.297	0.037	-0.035
Electron scale	0.005	-0.001	0.001	-0.000
Z pT reweighting	0.153	-0.173	0.018	-0.021
signal modeling	0.330	-0.310	0.039	-0.037
Color reconnection	0.099	-0.097	0.012	-0.012
ISR/FSR variation	0.123	-0.122	0.015	-0.015
Muon triggers	0.092	-0.092	0.011	-0.011
Dilepton trigger	0.225	-0.217	0.027	-0.026
Opposite charge requirement	0.098	-0.097	0.012	-0.012
Jet energy scale	0.155	-0.154	0.018	-0.018
Jet shifting	0.000	-0.000	0.000	-0.000
Vertex confirmation	0.300	-0.291	0.036	-0.035
b-Jet energy scale	0.117	-0.114	0.014	-0.014
Jet energy resolution	0.073	-0.110	0.009	-0.013
Jet reconstruction and identification	0.033	-0.033	0.004	-0.004
Taggability in data	0.015	-0.012	0.002	-0.001
b-tag TRF	0.050	-0.000	0.006	-0.000
light tag TRF	0.035	-0.000	0.004	-0.000
b fragmentation	0.185	-0.177	0.022	-0.021
Monte Carlo background x-section	0.108	-0.053	0.013	-0.006
Monte Carlo statistics	0.000	-0.000	0.000	-0.000
Instrumental background	0.274	-0.257	0.033	-0.031
PDF	0.037	-0.026	0.004	-0.003
Luminosity	0.725	-0.638	0.086	-0.076
Template statistics for template fits	0.029	-0.029	0.003	-0.003
Total systematic with ensembles	1.104	-1.022	0.132	-0.122

TABLE 27: Systematics errors on the R_b measurement, for the simultaneous measurement in the dilepton channel (RunIIa-RunIIb1 and 2 combination).

Summary of systematics on B($t \to Wb$) with standard method		
Source	sigma+	sigma-
Stat error only	0.000	-0.000
Event preselection	0.001	-0.001
Muon identification	0.002	-0.002
Muon resolution and scale	0.001	-0.000
Electron identification and smearing	0.005	-0.005
Electron scale	0.000	-0.000
Z pT reweighting	0.010	-0.009
signal modeling	0.002	-0.001
Color reconnection	0.000	-0.000
ISR/FSR variation	0.001	-0.001
Muon triggers	0.002	-0.001
Dilepton trigger	0.003	-0.003
Opposite charge requirement	0.001	-0.001
Jet energy scale	0.008	-0.007
Jet shifting	0.000	-0.000
Vertex confirmation	0.008	-0.008
b-Jet energy scale	0.003	-0.003
Jet energy resolution	0.009	-0.006
Jet reconstruction and identification	0.001	-0.001
Taggability in data	0.001	-0.003
b-tag TRF	0.023	-0.018
light tag TRF	0.003	-0.000
b fragmentation	0.001	-0.001
Monte Carlo background x-section	0.003	-0.006
Monte Carlo signal & bkg branching ratio	0.000	-0.000
Monte Carlo bkg scale factors	0.016	-0.016
Monte Carlo statistics	0.000	-0.000
Instrumental background	0.015	-0.015
PDF	0.000	-0.000
Luminosity	0.010	-0.010
Template statistics for template fits	0.005	-0.005
Total systematic with ensembles	0.039	-0.036

APPENDIX B: SANITY PLOTS

In this section data versus simulation comparisons are presented for 3 levels of selection:

a) inclusive selection: corresponding to events selected after cut 11 without any jet requirement;

b) 2 jet selection: corresponding to events selected after cut 11 with at least two jets (see jet selection in section II);

c) full selection: corresponding to events selected after all cuts.

The $t\bar{t}$ simulation is shown normalized to the theoretical $t\bar{t}$ cross-section. For all selections the number of "fake" background is normalized to the number given by the electron likelihood fit and/or by the muon fake rate while the shape of the distribution is taken from events where the leptons have the same sign.

1. Control plots for electron-muon channel in RunIIa

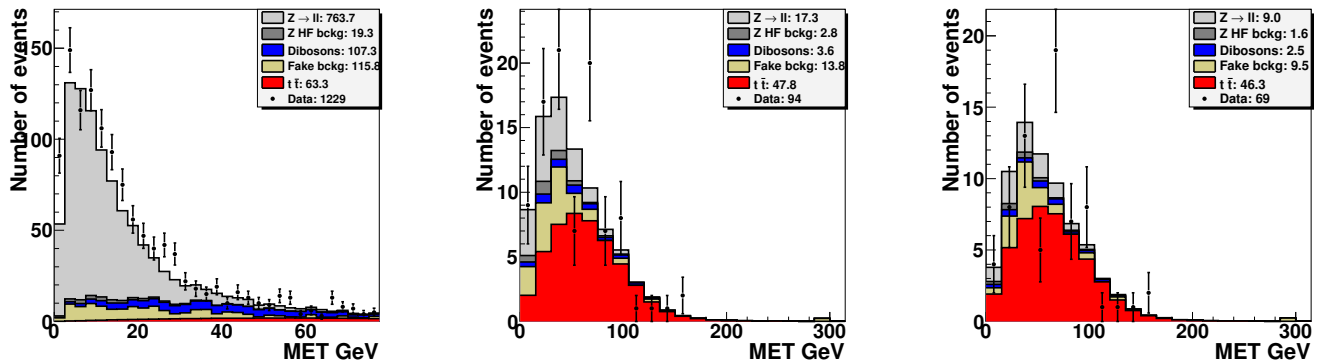

(a) Inclusive selection (b) 2 jet selection (c) Final selection.

FIG. 12: Transverse missing energy distributions in the eμ channel.

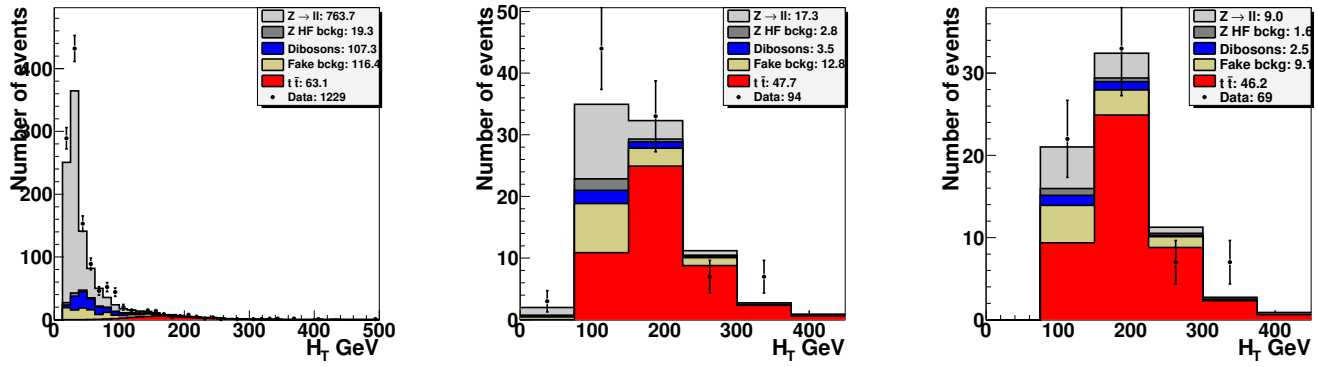

(a) Inclusive selection (b) 2 jet selection (c) Final selection.

FIG. 13: H_T distribution where H_T is the scalar sum of the leading lepton transverse momentum and transverse momentum of two leading jets in the eμ channel.

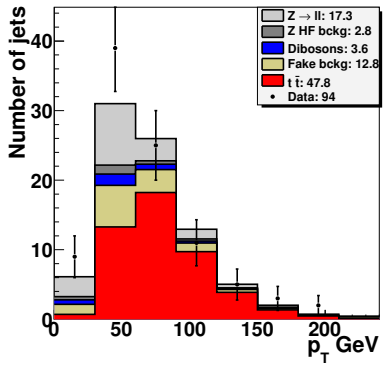

(a) 2 jet selection

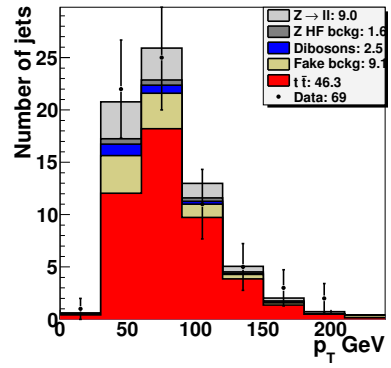

(b) Final selection

FIG. 14: Leading jet transverse momentum distribution in the eμ channel.

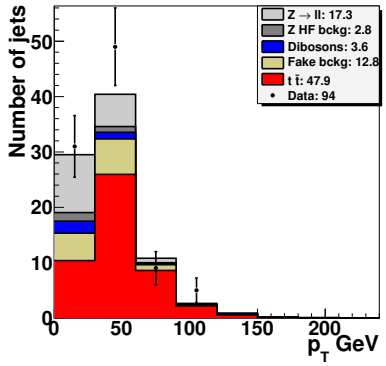

(a) 2 jet selection

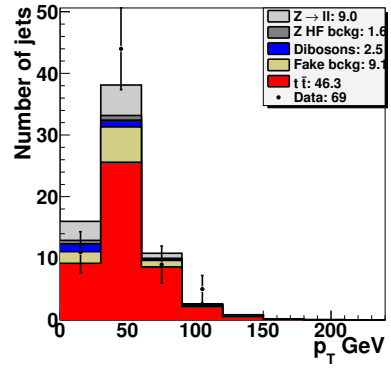

(b) Final selection

FIG. 15: Next to leading jet transverse momentum distribution in the eμ channel.

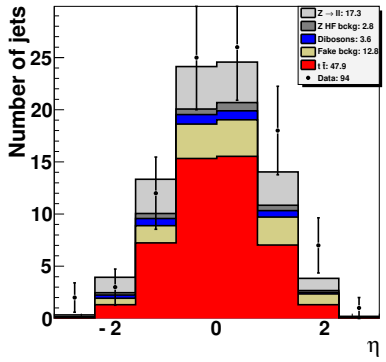

(a) 2 jet selection

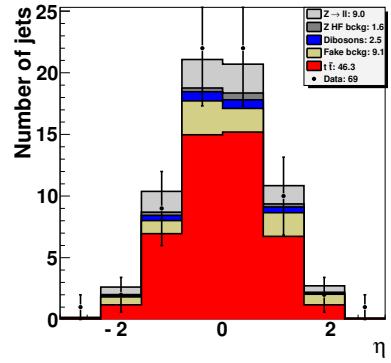

(b) Final selection. Leading jet

FIG. 16: Leading jet pseudo-rapidity distribution in the eμ channel.

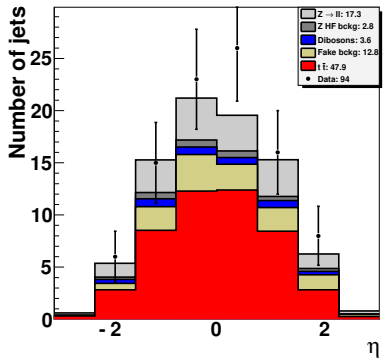

(a) 2 jet selection

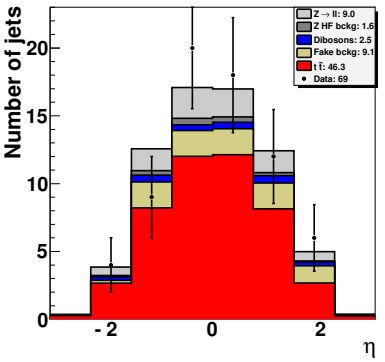

(b) Final selection

FIG. 17: Next to leading jet pseudo-rapidity distribution in the eμ channel.

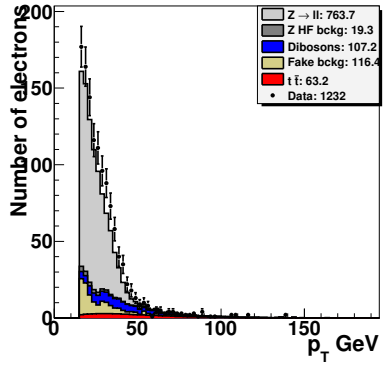

(a) Inclusive selection

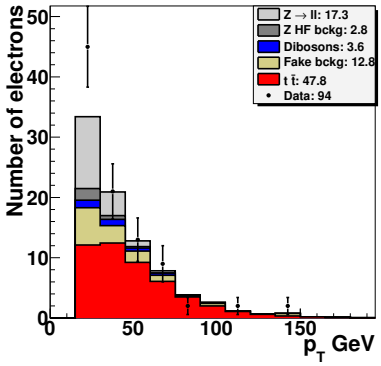

(b) 2 jet selection

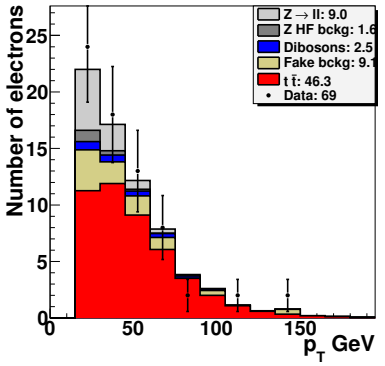

(c) Final selection.

FIG. 18: Electron transverse momentum distributions in the eμ channel.

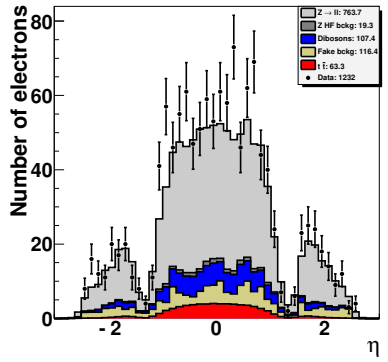

(a) Inclusive selection

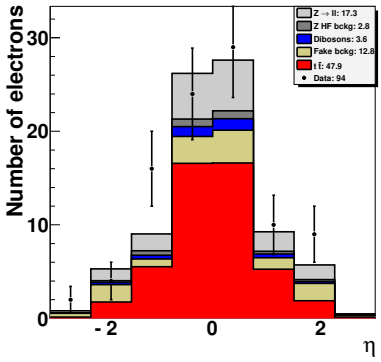

(b) 2 jet selection

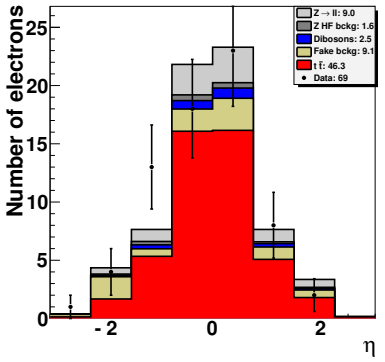

(c) Final selection.

FIG. 19: Electron η distributions in the eμ channel.

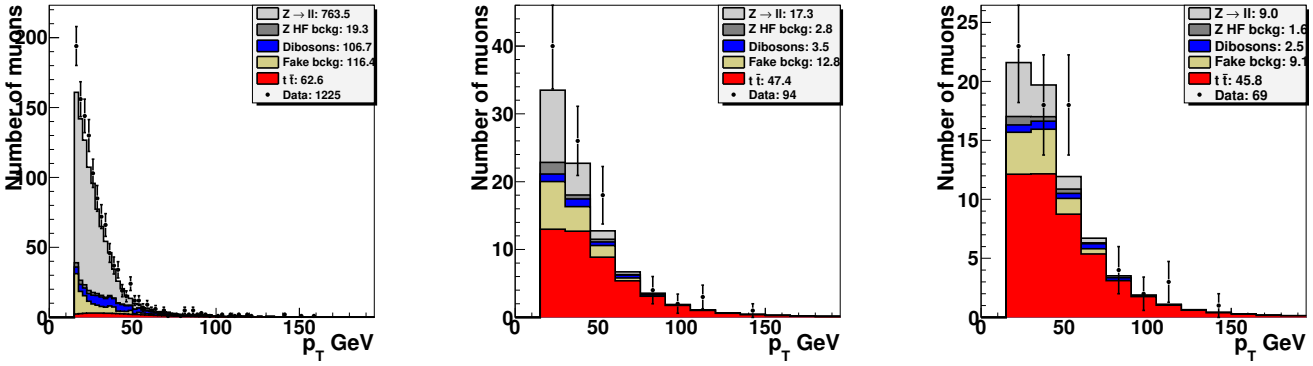

(a) Inclusive selection (b) 2 jet selection (c) Final selection.

FIG. 20: Muon transverse momentum distributions in the eμ channel.

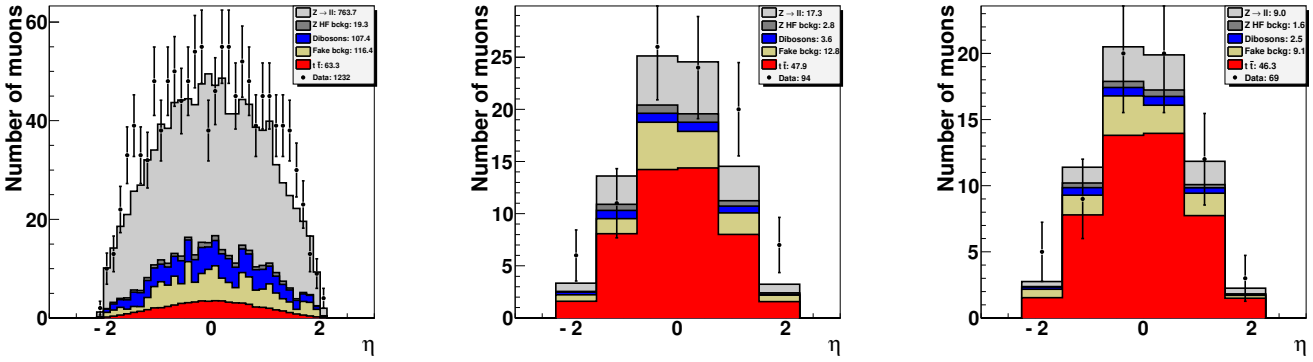

(a) Inclusive selection (b) 2 jet selection (c) Final selection.

FIG. 21: Muon η distributions in the eμ channel.

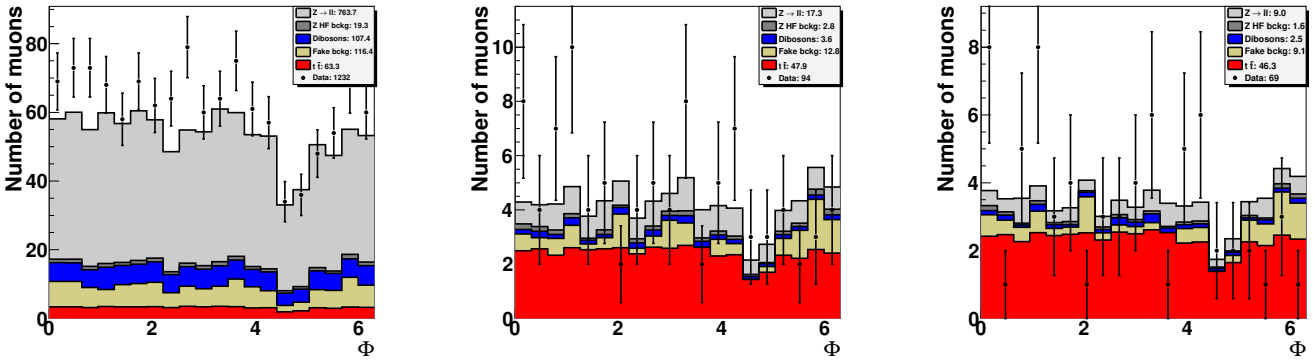

(a) Inclusive selection (b) 2 jet selection (c) Final selection.

FIG. 22: Muon ϕ distributions in the eμ channel.

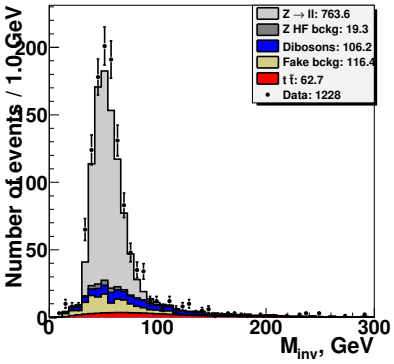

(a) Inclusive selection

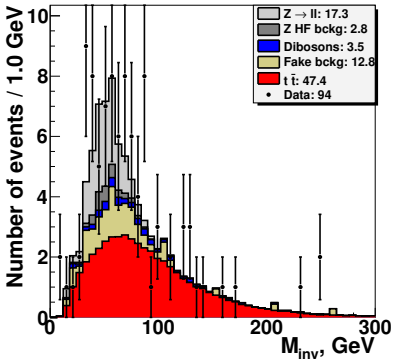

(b) 2 jet selection

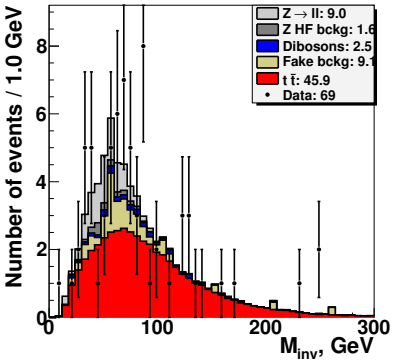

(c) Final selection.

FIG. 23: Electron - Muon Invariant Mass in the eμ channel.

2. Control plots for electron-muon channel in RunIIb

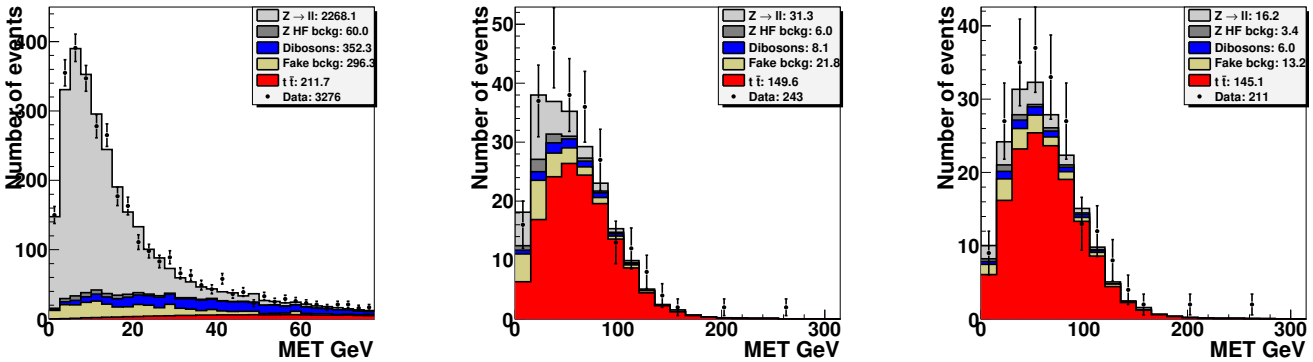

(a) Inclusive selection (b) 2 jet selection (c) Final selection.

FIG. 24: Transverse missing energy distributions in the eμ channel.

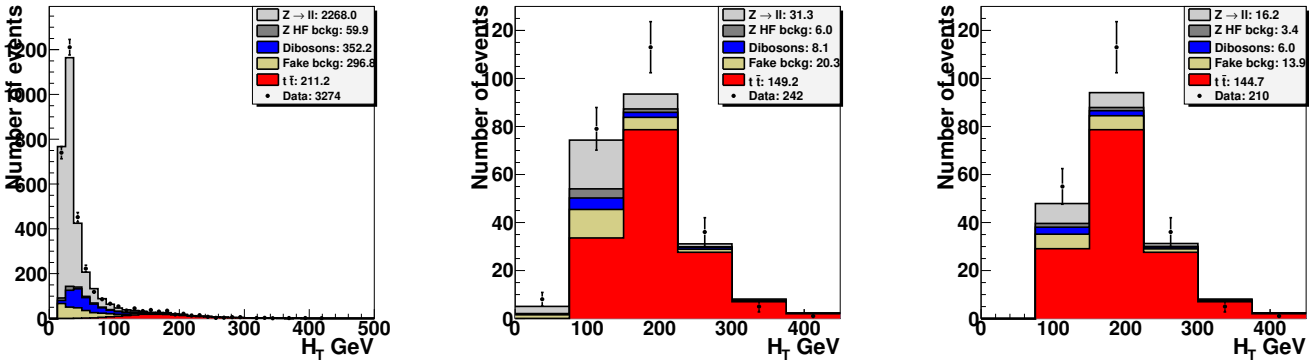

(a) Inclusive selection (b) 2 jet selection (c) Final selection.

FIG. 25: H_T distribution where H_T is the scalar sum of the leading lepton transverse momentum and transverse momentum of two leading jets in the eμ channel.

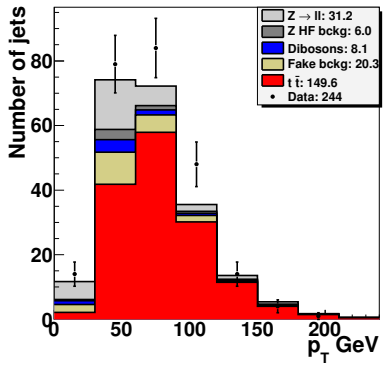

(a) 2 jet selection

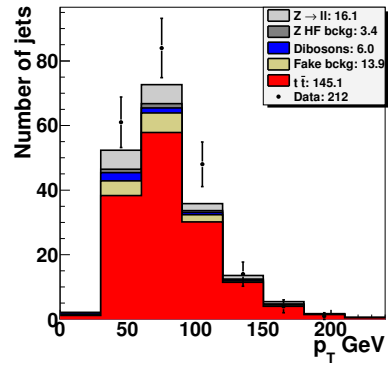

(b) Final selection

FIG. 26: Leading jet transverse momentum distribution in the eμ channel.

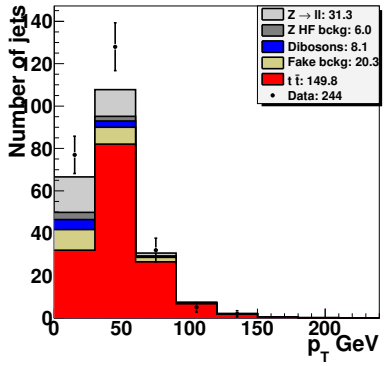

(a) 2 jet selection

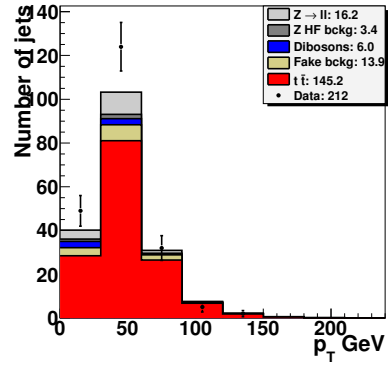

(b) Final selection

FIG. 27: Next to leading jet transverse momentum distribution in the eμ channel.

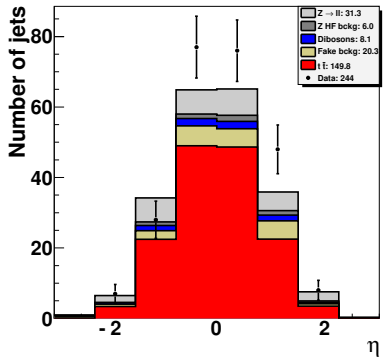

(a) 2 jet selection

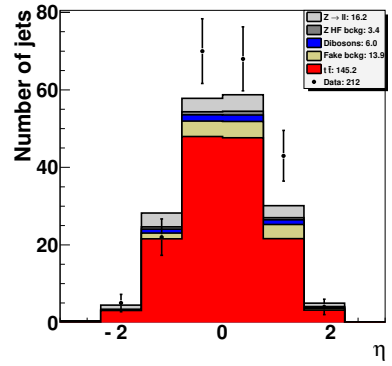

(b) Final selection. Leading jet

FIG. 28: Leading jet pseudo-rapidity distribution in the eμ channel.

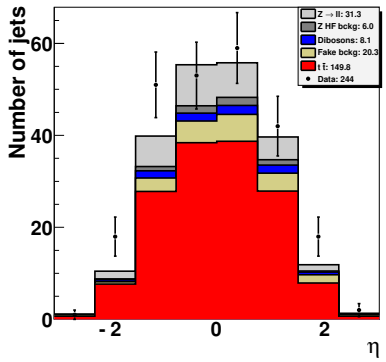

(a) 2 jet selection

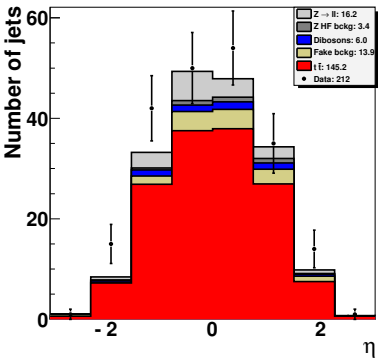

(b) Final selection

FIG. 29: Next to leading jet pseudo-rapidity distribution in the eμ channel.

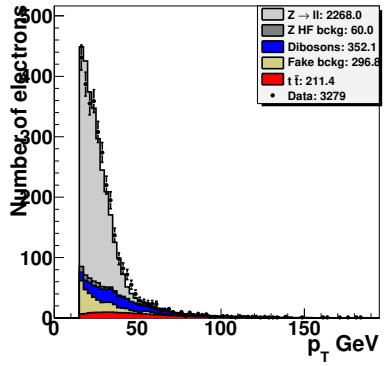

(a) Inclusive selection

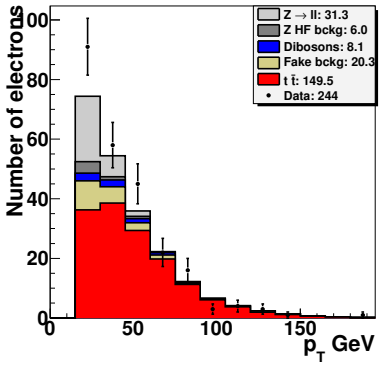

(b) 2 jet selection

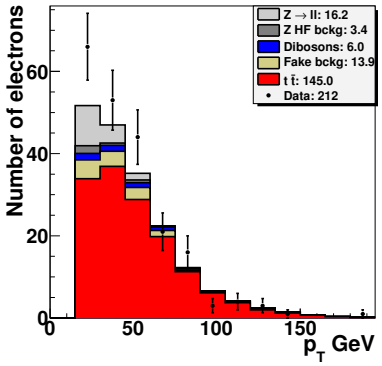

(c) Final selection.

FIG. 30: Electron transverse momentum distributions in the eμ channel.

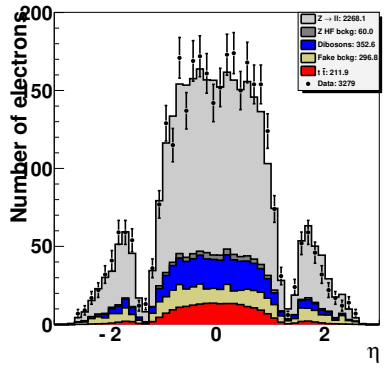

(a) Inclusive selection

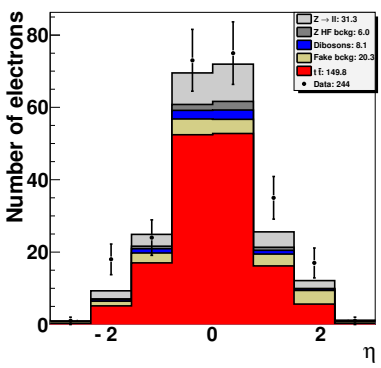

(b) 2 jet selection

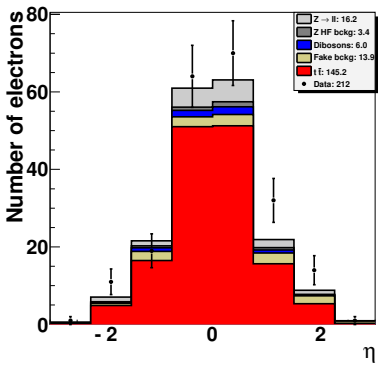

(c) Final selection.

FIG. 31: Electron η distributions in the eμ channel.

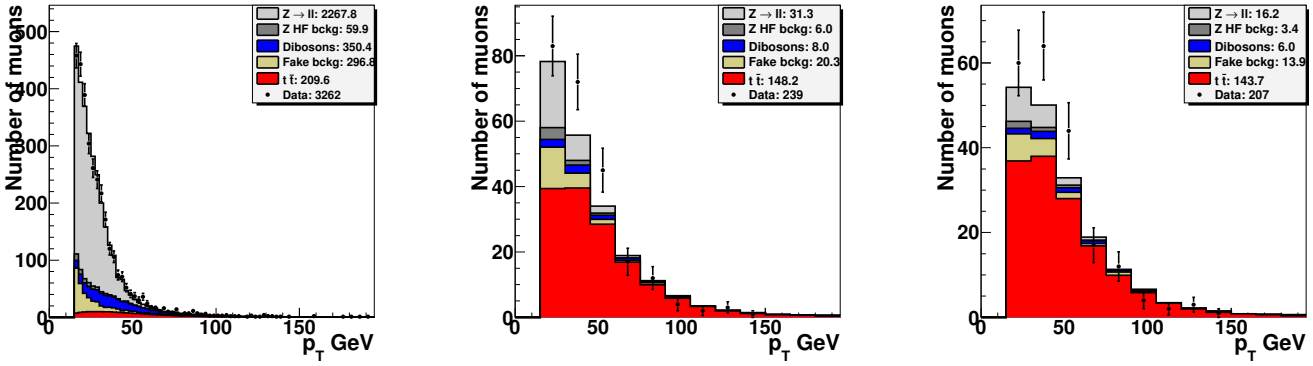

(a) Inclusive selection (b) 2 jet selection (c) Final selection.

FIG. 32: Muon transverse momentum distributions in the eμ channel.

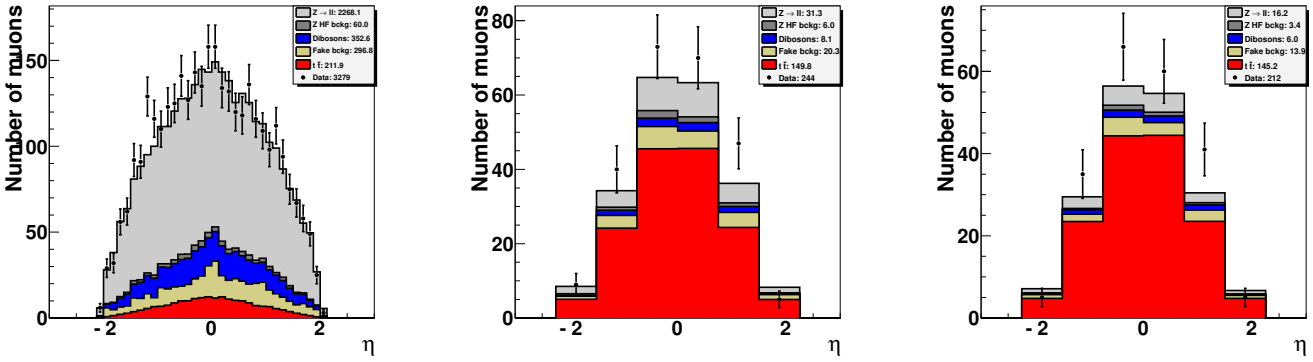

(a) Inclusive selection (b) 2 jet selection (c) Final selection.

FIG. 33: Muon η distributions in the eμ channel.

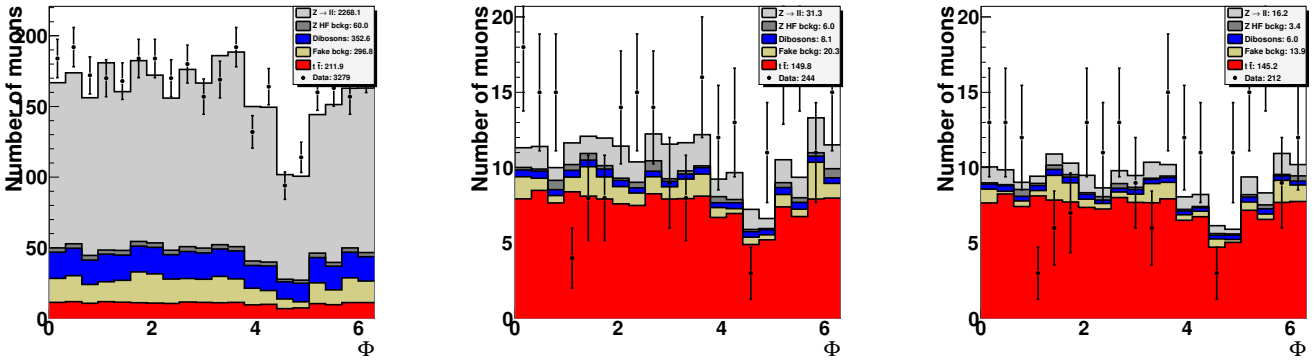

(a) Inclusive selection (b) 2 jet selection (c) Final selection.

FIG. 34: Muon ϕ distributions in the eμ channel.

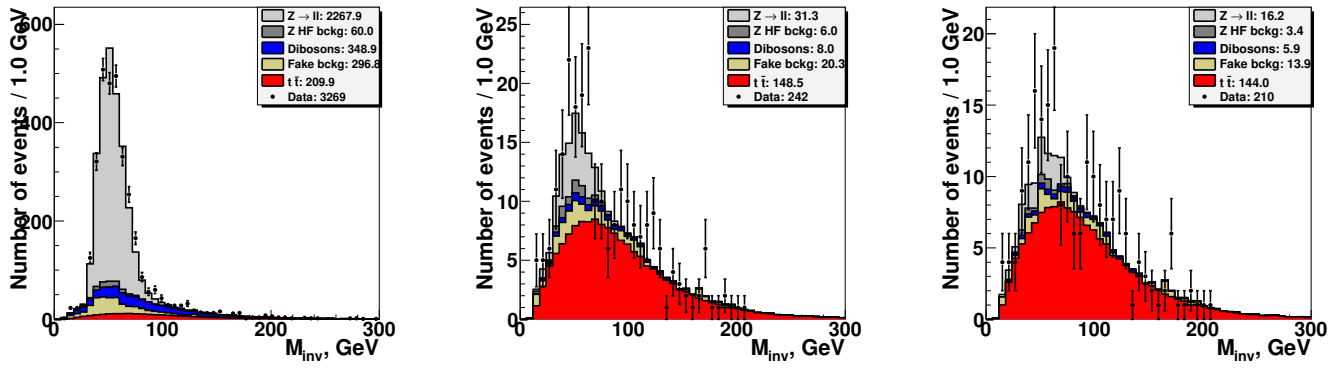

(a) Inclusive selection

(b) 2 jet selection

(c) Final selection.

FIG. 35: Electron - Muon Invariant Mass in the eμ channel.

3. Control plots for di-electron channel RunIIa

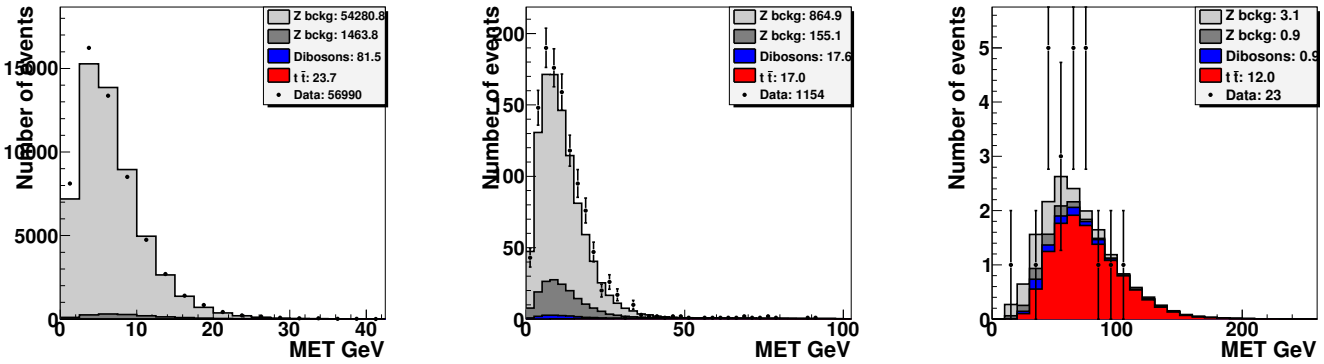

(a) Inclusive selection (b) 2 jet selection (c) Final selection.

FIG. 36: Transverse missing energy distributions in the ee channel.

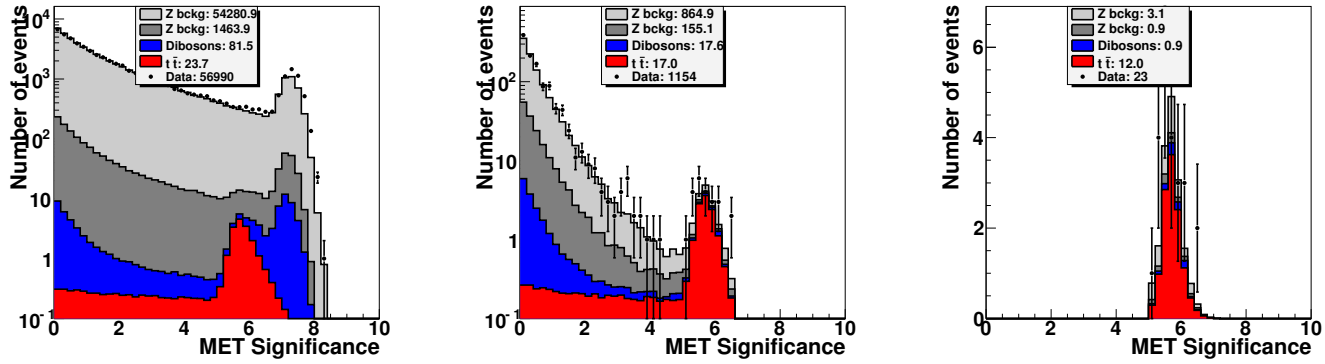

(a) Inclusive selection (b) 2 jet selection (c) Final selection.

FIG. 37: Missing energy significance in the ee channel.

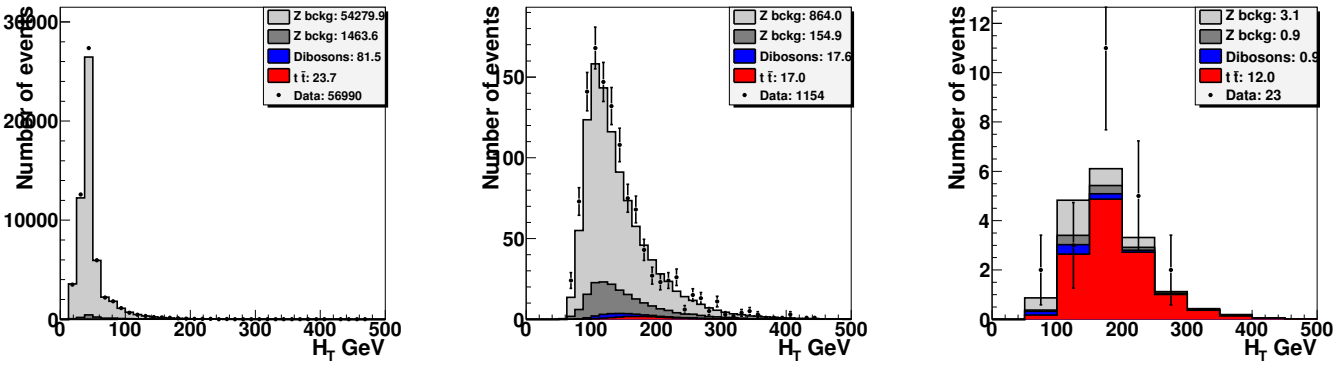

(a) Inclusive selection (b) 2 jet selection (c) Final selection.

FIG. 38: H_T distribution where H_T is the scalar sum of the leading lepton transverse momentum and transverse momentum of all jets in the ee channel.

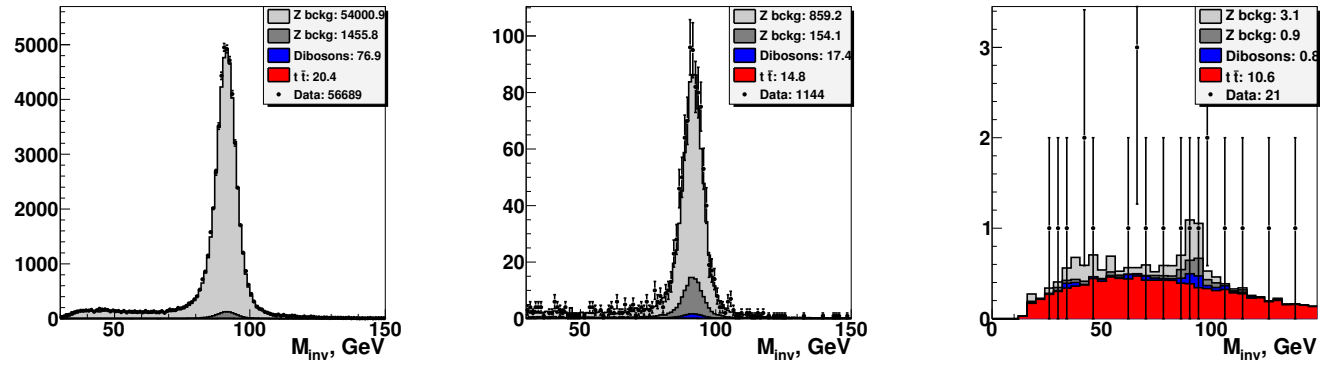

(a) Inclusive selection (b) 2 jet selection (c) Final selection.

FIG. 39: Dielectron invariant mass M_{ee} in the ee channel.

(a) 2 jet selection (b) Final selection

FIG. 40: Leading jet transverse momentum distribution in the ee channel.

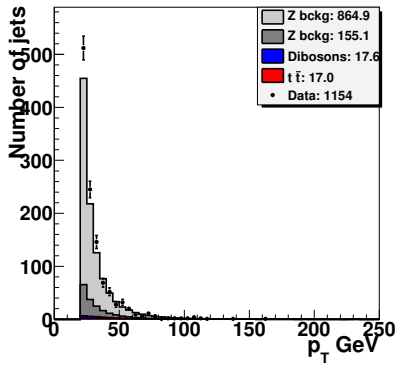

(a) 2 jet selection

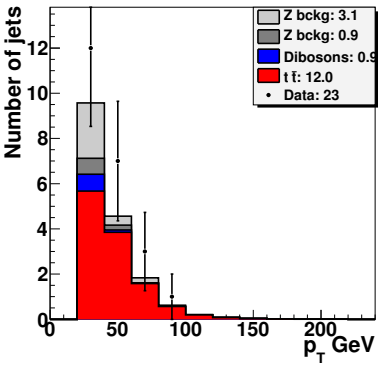

(b) Final selection

FIG. 41: Next to leading jet transverse momentum distribution in the ee channel.

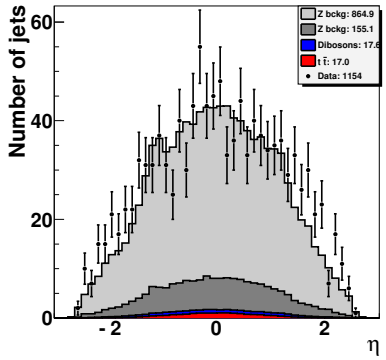

(a) 2 jet selection

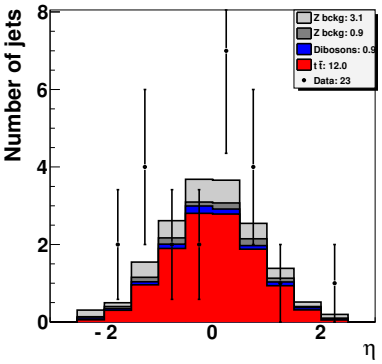

(b) Final selection

FIG. 42: Leading jet pseudo-rapidity distribution in the ee channel.

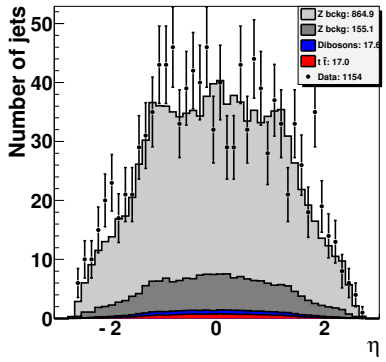

(a) 2 jet selection

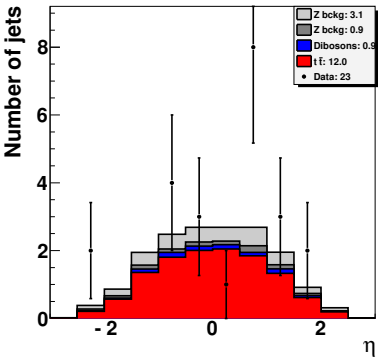

(b) Final selection

FIG. 43: Next to leading jet pseudo-rapidity distribution in the ee channel.

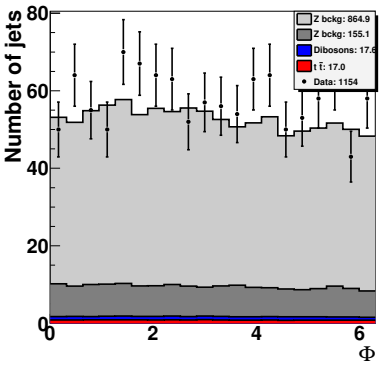

(a) 2 jet selection

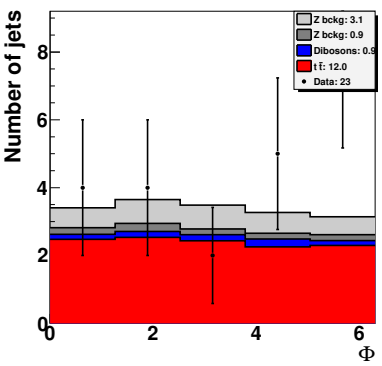

(b) Final selection

FIG. 44: Leading jet ϕ distributions in the ee channel.

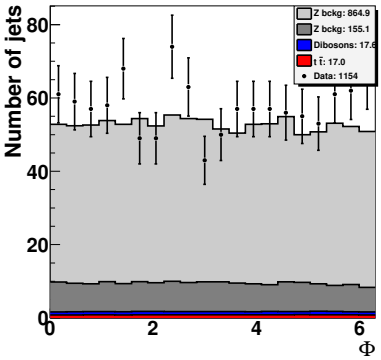

(a) 2 jet selection

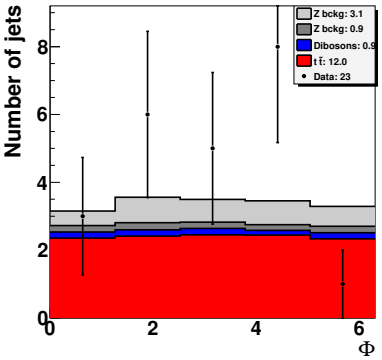

(b) Final selection

FIG. 45: Next to leading jet ϕ distributions in the ee channel.

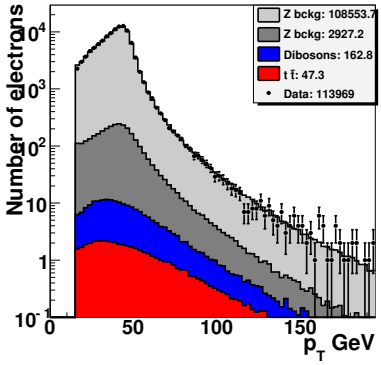

(a) Inclusive selection

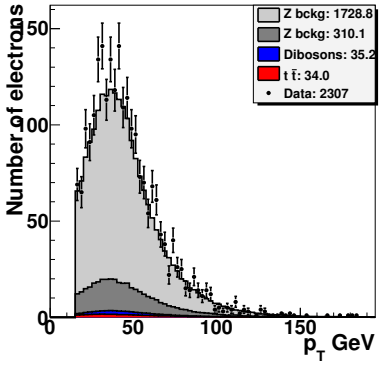

(b) 2 jet selection

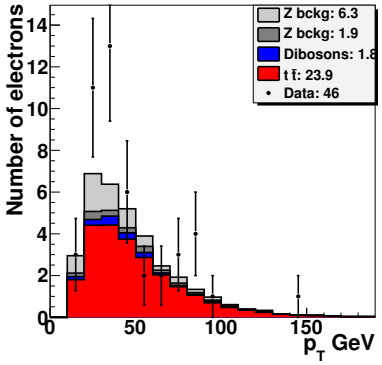

(c) Final selection.

FIG. 46: Electron transverse momentum distributions in the ee channel.

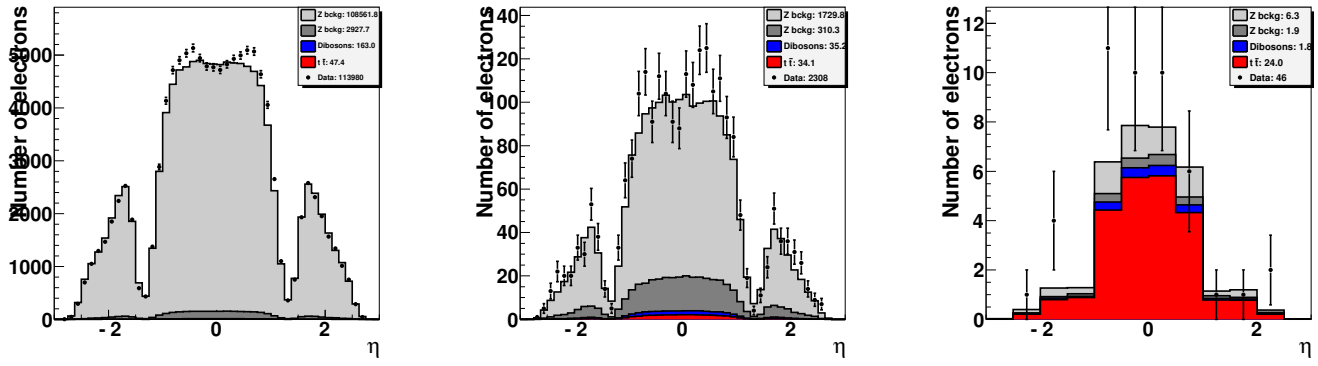

(a) Inclusive selection

(b) 2 jet selection

(c) Final selection.

FIG. 47: Electron η distributions in the ee channel.

4. Control plots for di-electron channel RunIIb

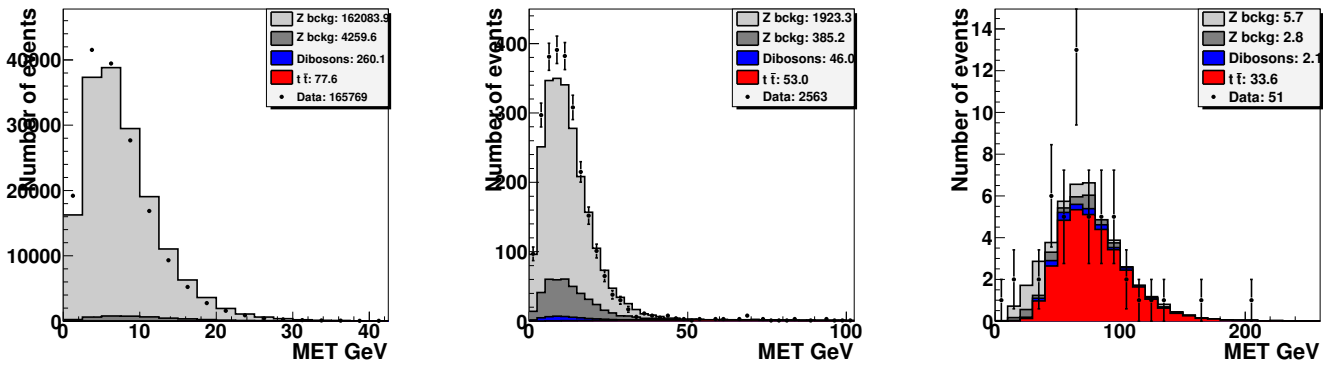

(a) Inclusive selection (b) 2 jet selection (c) Final selection.

FIG. 48: Transverse missing energy distributions in the ee channel.

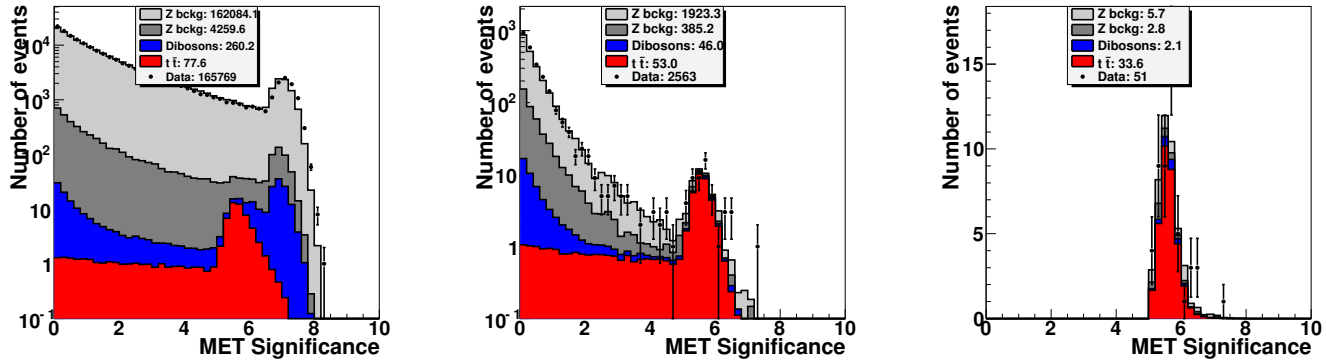

(a) Inclusive selection (b) 2 jet selection (c) Final selection.

FIG. 49: Missing energy significance in the ee channel.

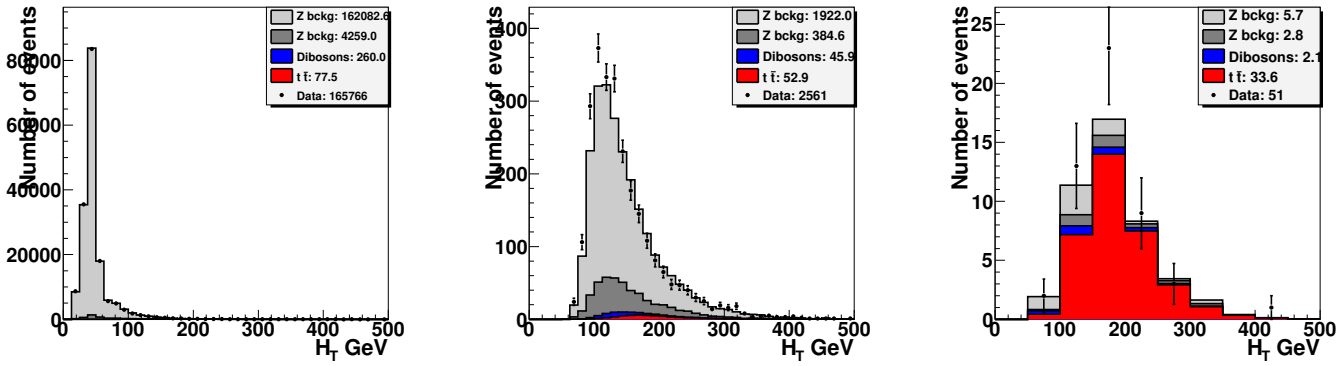

(a) Inclusive selection (b) 2 jet selection (c) Final selection.

FIG. 50: H_T distribution where H_T is the scalar sum of the leading lepton transverse momentum and transverse momentum of all jets in the ee channel.

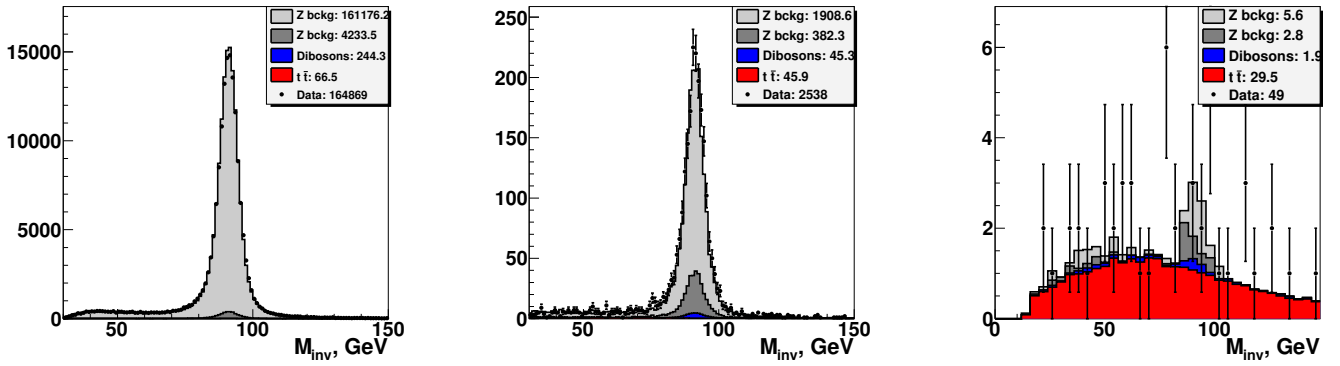

(a) Inclusive selection (b) 2 jet selection (c) Final selection.

FIG. 51: Dielectron invariant mass M_{ee} in the ee channel.

(a) 2 jet selection (b) Final selection

FIG. 52: Leading jet transverse momentum distribution in the ee channel.

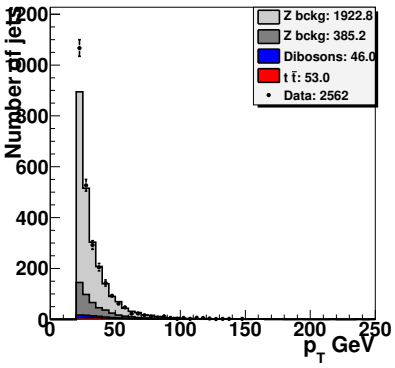

(a) 2 jet selection

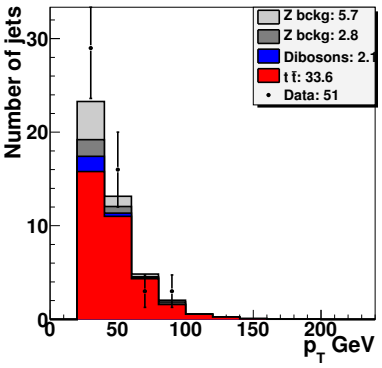

(b) Final selection

FIG. 53: Next to leading jet transverse momentum distribution in the ee channel.

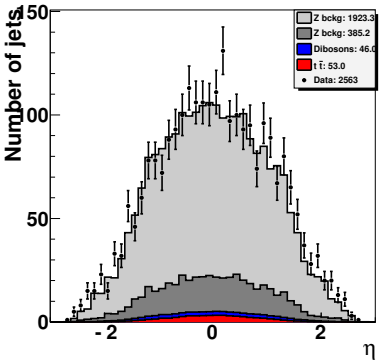

(a) 2 jet selection

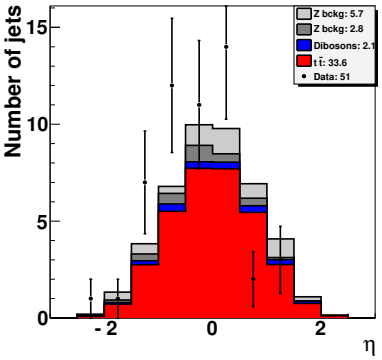

(b) Final selection

FIG. 54: Leading jet pseudo-rapidity distribution in the ee channel.

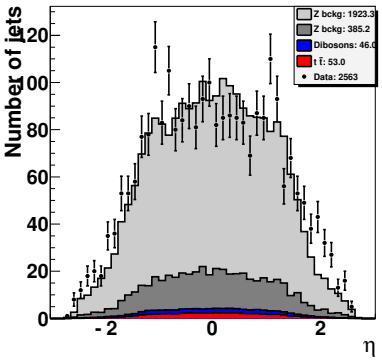

(a) 2 jet selection

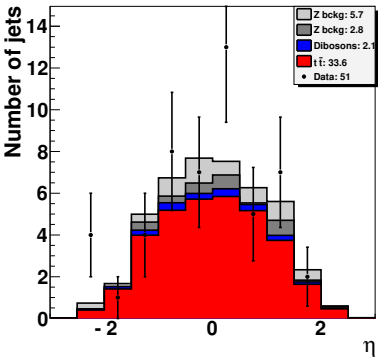

(b) Final selection

FIG. 55: Next to leading jet pseudo-rapidity distribution in the ee channel.

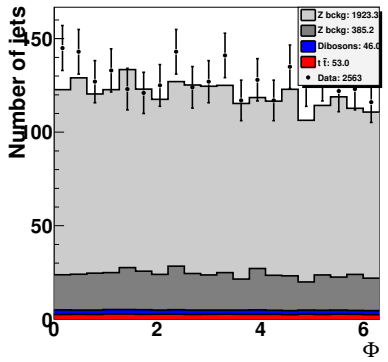

(a) 2 jet selection

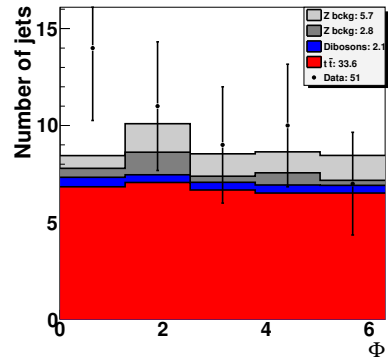

(b) Final selection

FIG. 56: Leading jet ϕ distributions in the ee channel.

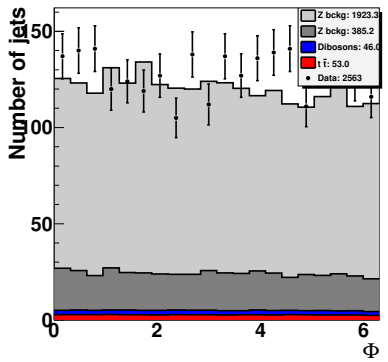

(a) 2 jet selection

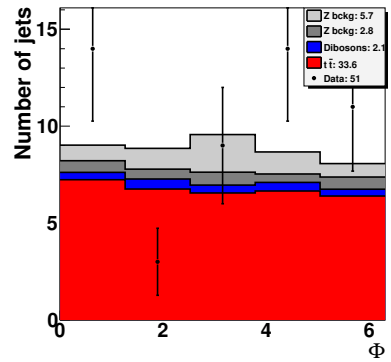

(b) Final selection

FIG. 57: Next to leading jet ϕ distributions in the ee channel.

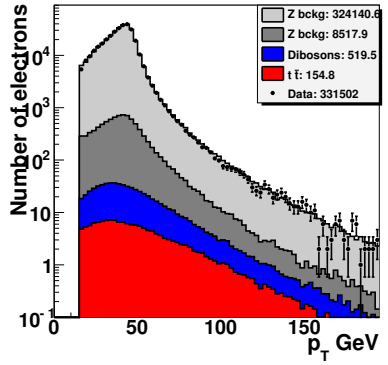

(a) Inclusive selection

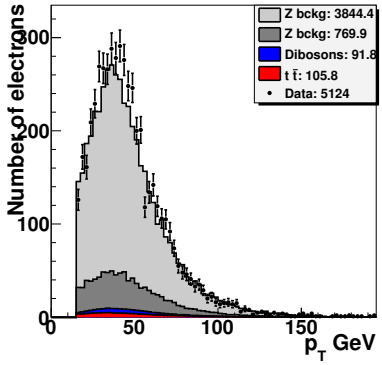

(b) 2 jet selection

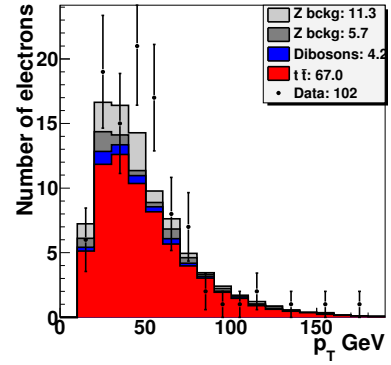

(c) Final selection.

FIG. 58: Electron transverse momentum distributions in the ee channel.

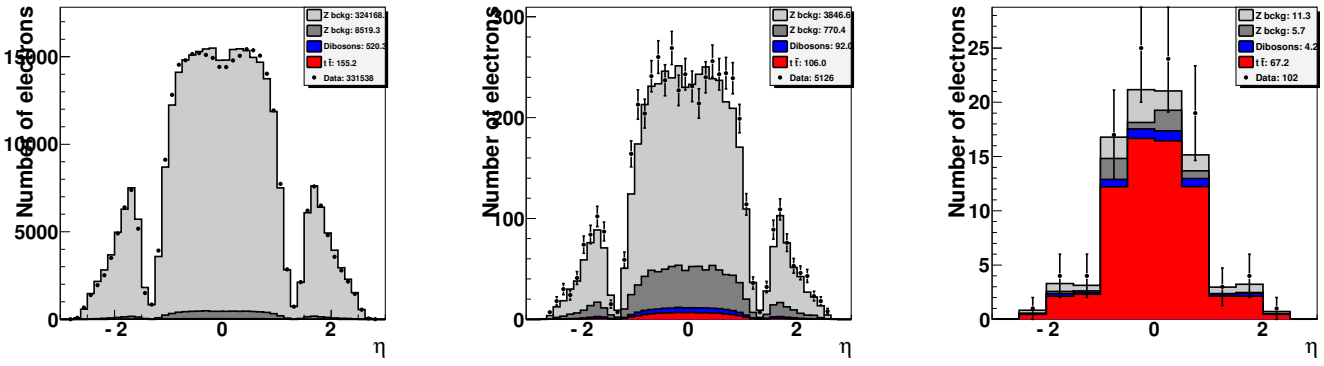

(a) Inclusive selection

(b) 2 jet selection

(c) Final selection.

FIG. 59: Electron η distributions in the ee channel.

5. Control plots for di-muon channel in RunIIa

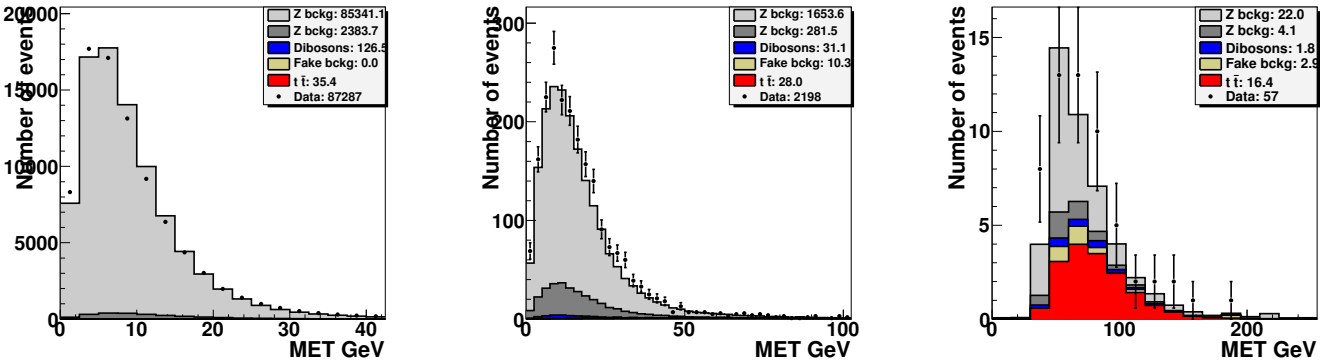

(a) Inclusive selection (b) 2 jet selection (c) Final selection.

FIG. 60: Transverse missing energy distributions in the $\mu\mu$ channel.

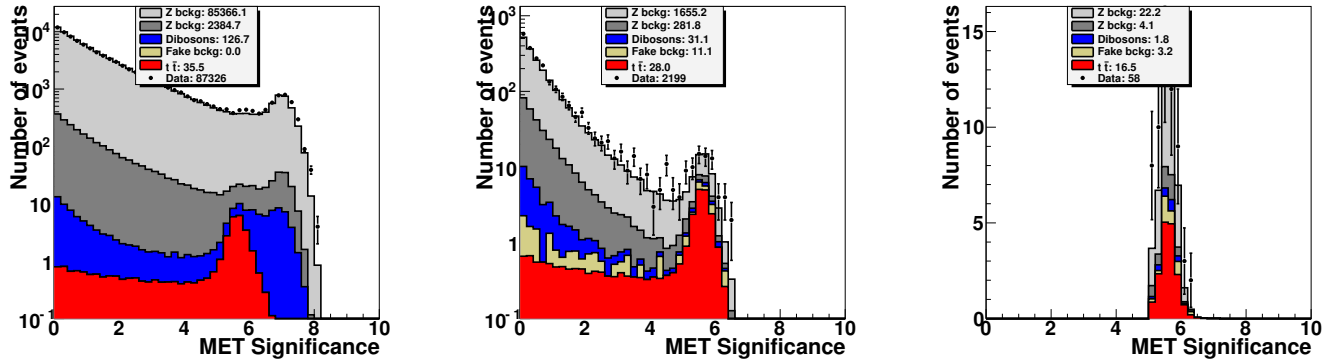

(a) Inclusive selection (b) 2 jet selection (c) Final selection.

FIG. 61: Missing energy significance in the $\mu\mu$ channel.

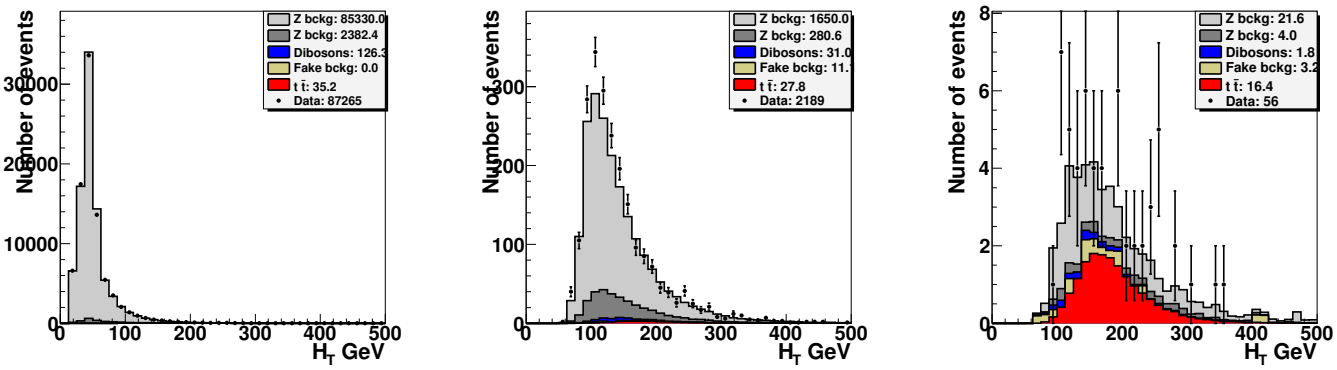

(a) Inclusive selection (b) 2 jet selection (c) Final selection.

FIG. 62: H_T distribution where H_T is the scalar sum of the leading lepton transverse momentum and transverse momentum of all jets in the $\mu\mu$ channel.

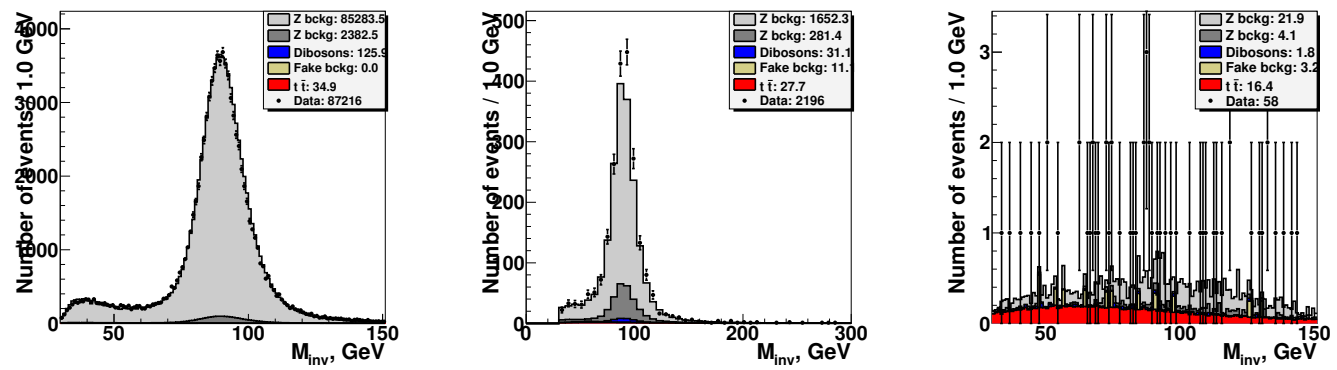

(a) Inclusive selection (b) 2 jet selection (c) Final selection.

FIG. 63: Dimuon invariant mass $M_{\mu\mu}$ in the $\mu\mu$ channel.

(a) 2 jet selection (b) Final selection

FIG. 64: Leading jet transverse momentum distribution in the $\mu\mu$ channel.

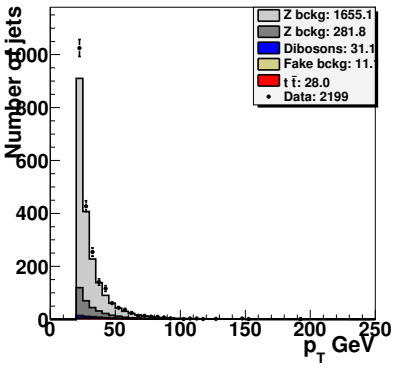

(a) 2 jet selection

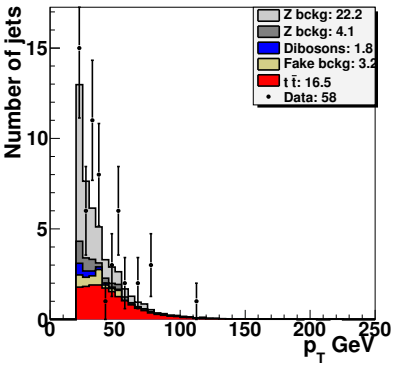

(b) Final selection

FIG. 65: Next to leading jet transverse momentum distribution in the $\mu\mu$ channel.

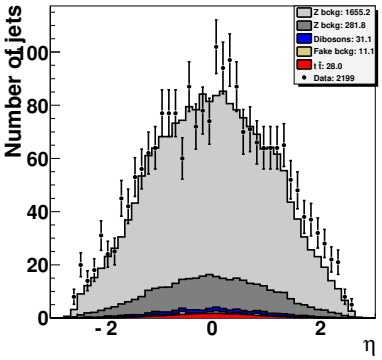

(a) 2 jet selection

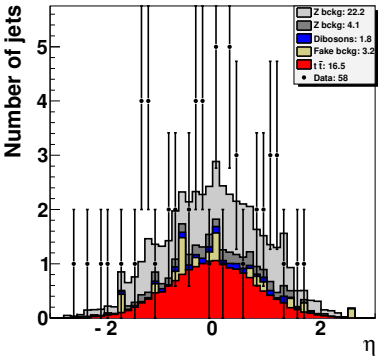

(b) Final selection

FIG. 66: Leading jet pseudo-rapidity distribution in the $\mu\mu$ channel.

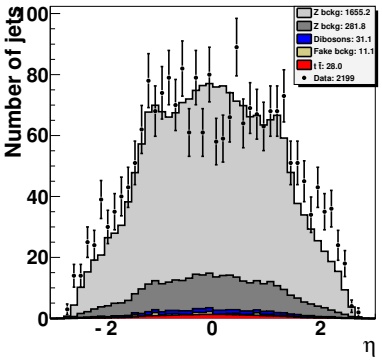

(a) 2 jet selection

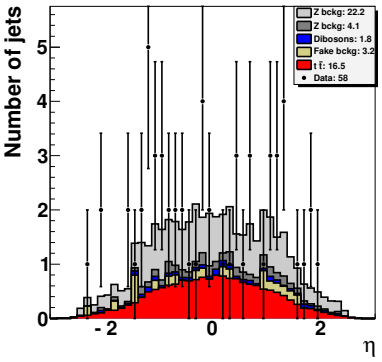

(b) Final selection

FIG. 67: Next to leading jet pseudo-rapidity distribution in the $\mu\mu$ channel.

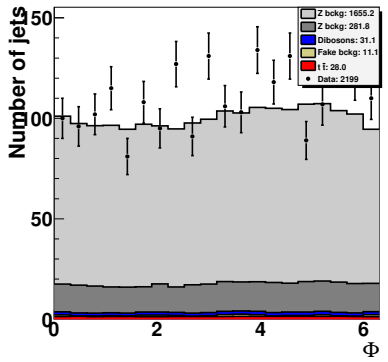

(a) 2 jet selection

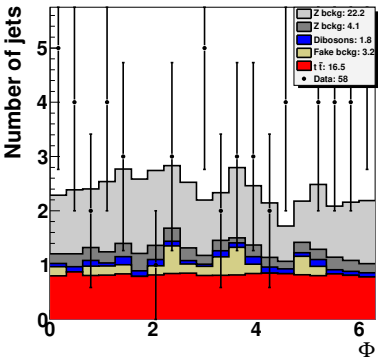

(b) Final selection

FIG. 68: Leading jet ϕ distributions in the $\mu\mu$ channel.

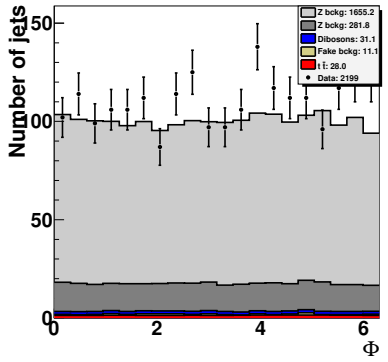

(a) 2 jet selection

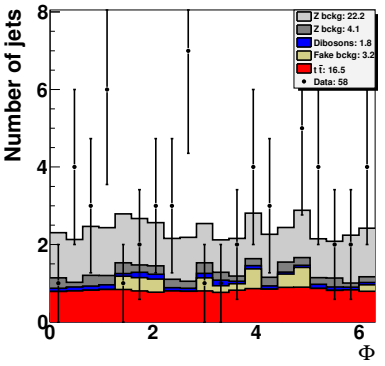

(b) Final selection

FIG. 69: Next to leading jet ϕ distributions in the $\mu\mu$ channel.

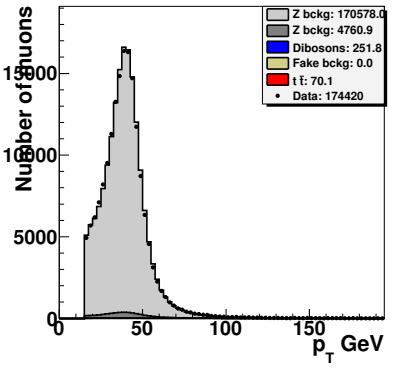

(a) Inclusive selection

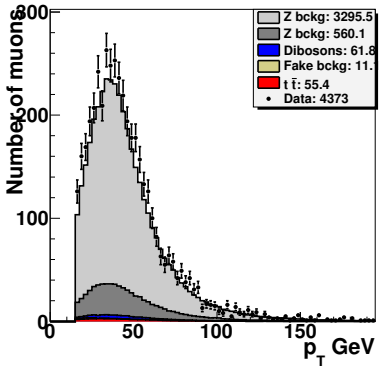

(b) 2 jet selection

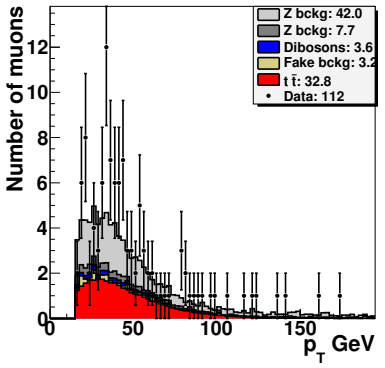

(c) Final selection.

FIG. 70: Muon transverse momentum distributions in the $\mu\mu$ channel.

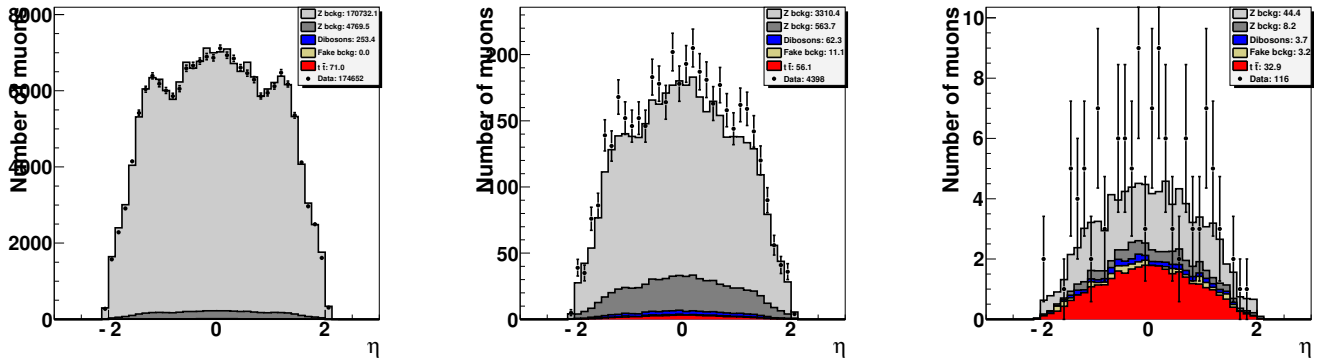

(a) Inclusive selection (b) 2 jet selection (c) Final selection.

FIG. 71: Muon η distributions in the $\mu\mu$ channel.

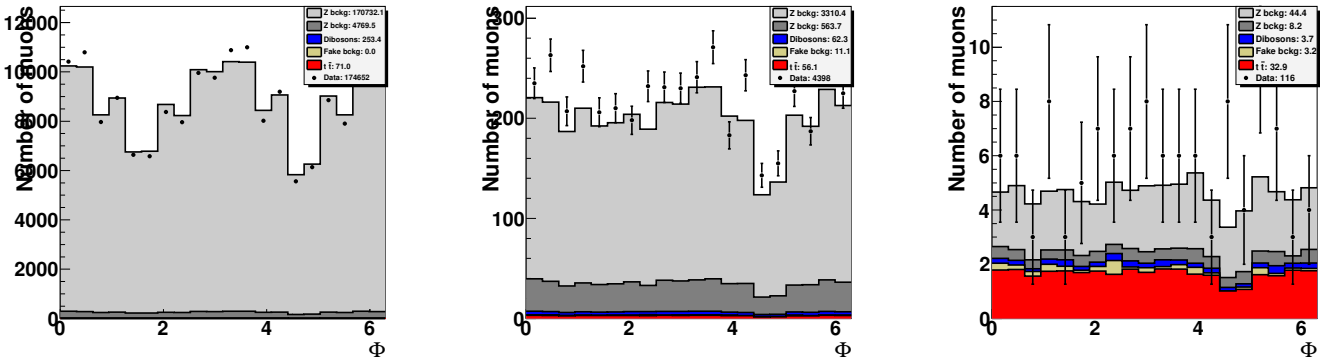

(a) Inclusive selection (b) 2 jet selection (c) Final selection.

FIG. 72: Muon ϕ distributions in the $\mu\mu$ channel.

6. Control plots for di-muon channel in RunIIb

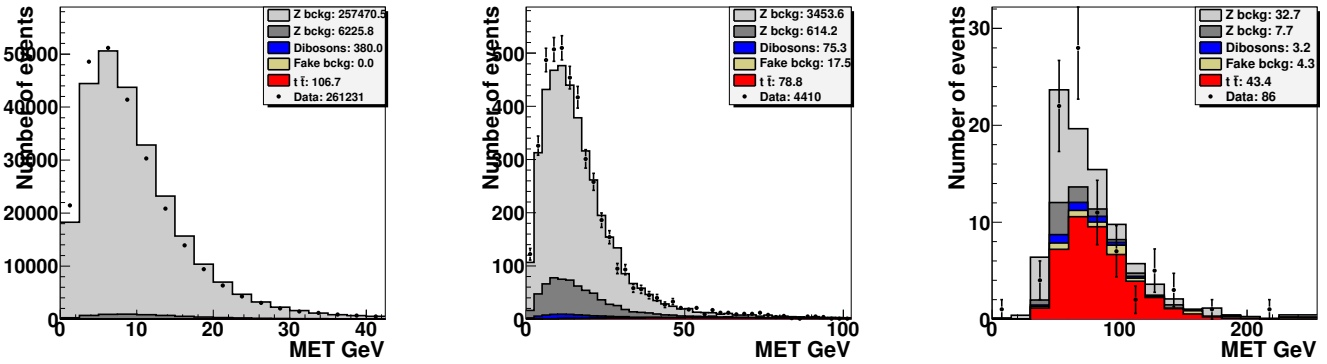

(a) Inclusive selection (b) 2 jet selection (c) Final selection.

FIG. 73: Transverse missing energy distributions in the $\mu\mu$ channel.

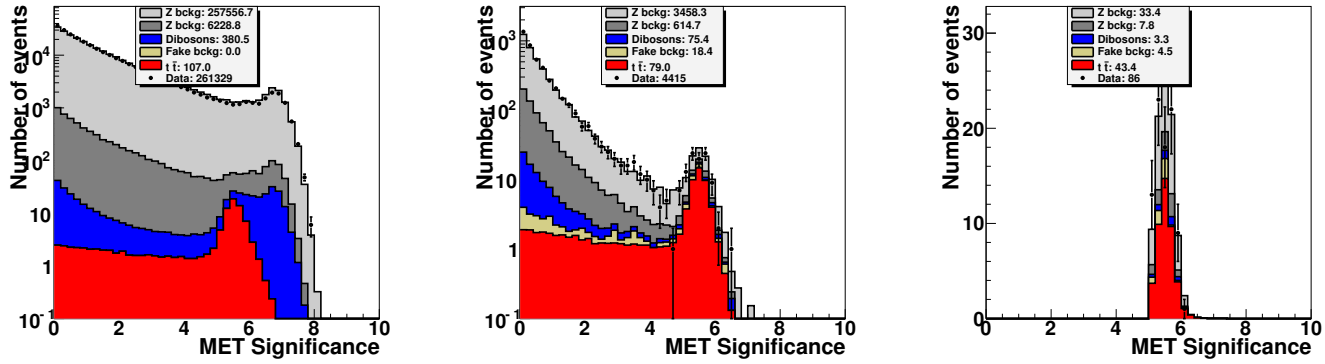

(a) Inclusive selection (b) 2 jet selection (c) Final selection.

FIG. 74: Missing energy significance in the $\mu\mu$ channel.

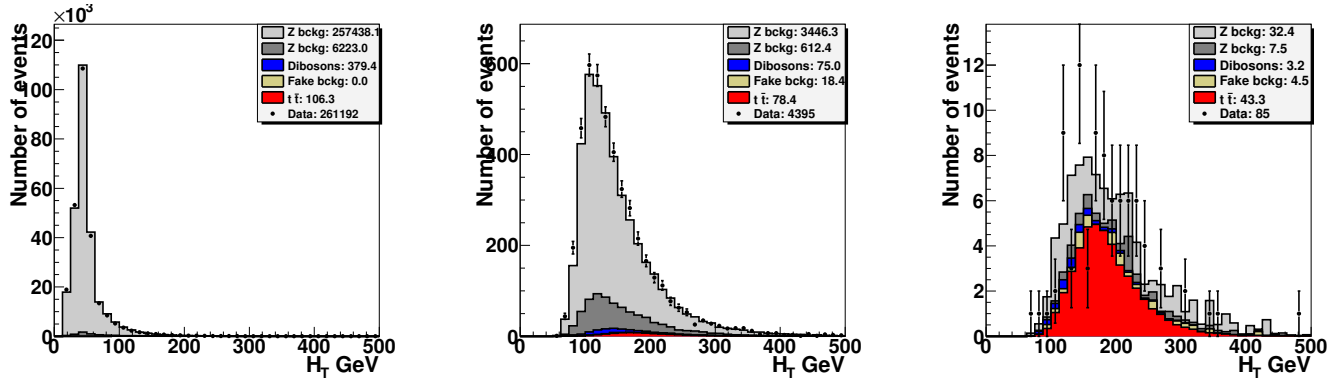

(a) Inclusive selection (b) 2 jet selection (c) Final selection.

FIG. 75: H_T distribution where H_T is the scalar sum of the leading lepton transverse momentum and transverse momentum of all jets in the $\mu\mu$ channel.

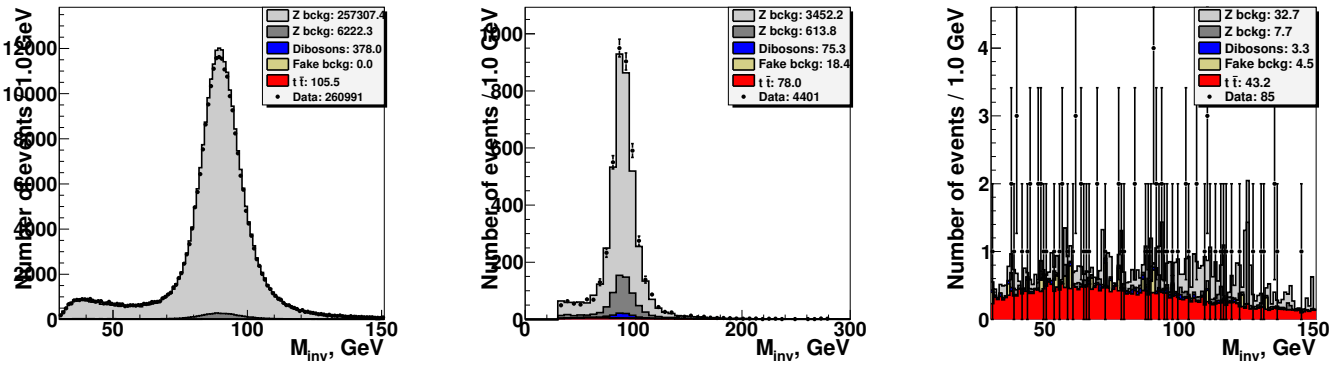

(a) Inclusive selection (b) 2 jet selection (c) Final selection.

FIG. 76: Dimuon invariant mass $M_{\mu\mu}$ in the $\mu\mu$ channel.

(a) 2 jet selection (b) Final selection

FIG. 77: Leading jet transverse momentum distribution in the $\mu\mu$ channel.

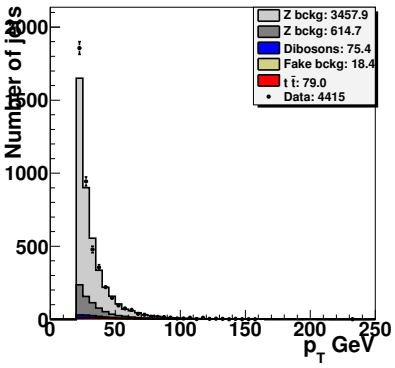

(a) 2 jet selection

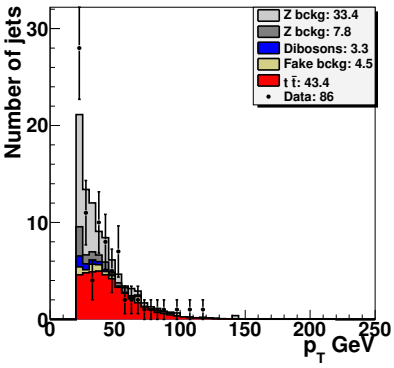

(b) Final selection

FIG. 78: Next to leading jet transverse momentum distribution in the $\mu\mu$ channel.

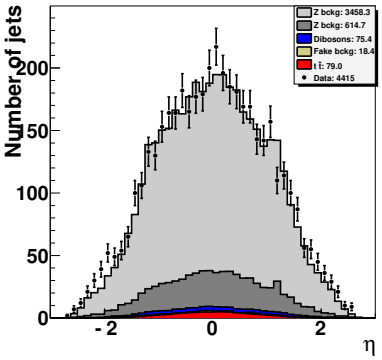

(a) 2 jet selection

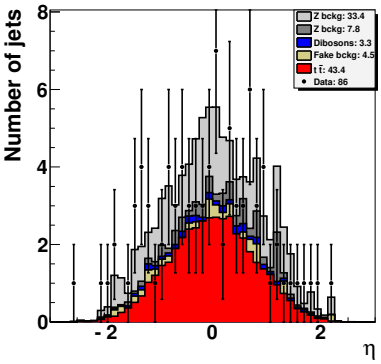

(b) Final selection

FIG. 79: Leading jet pseudo-rapidity distribution in the $\mu\mu$ channel.

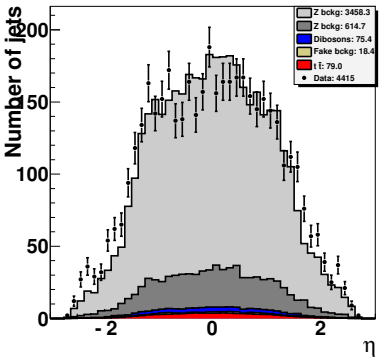

(a) 2 jet selection

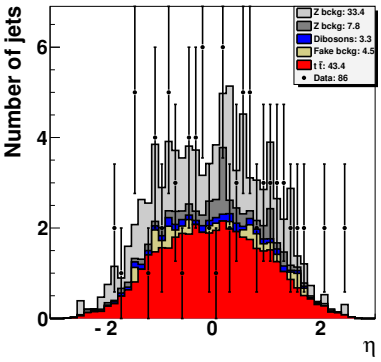

(b) Final selection

FIG. 80: Next to leading jet pseudo-rapidity distribution in the $\mu\mu$ channel.

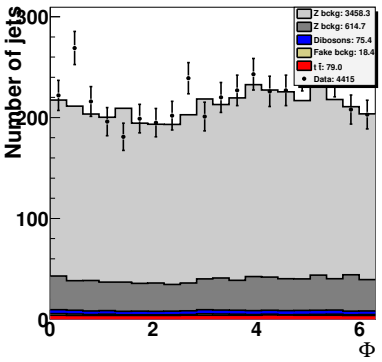

(a) 2 jet selection

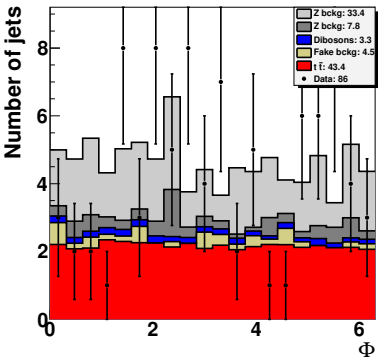

(b) Final selection

FIG. 81: Leading jet ϕ distributions in the $\mu\mu$ channel.

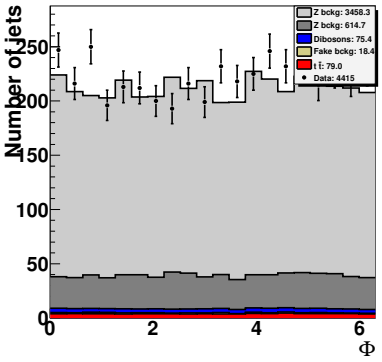

(a) 2 jet selection

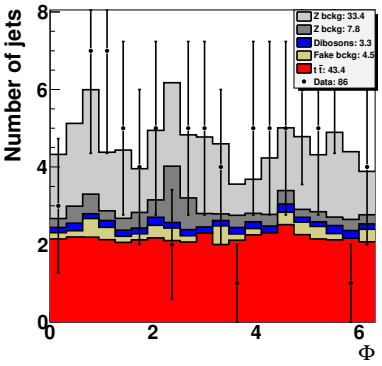

(b) Final selection

FIG. 82: Next to leading jet ϕ distributions in the $\mu\mu$ channel.

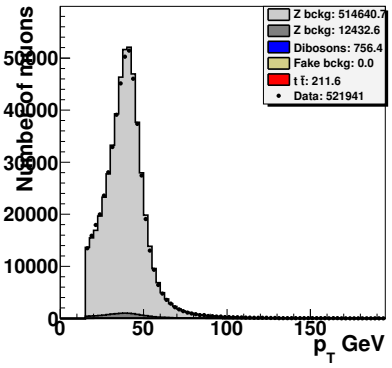

(a) Inclusive selection

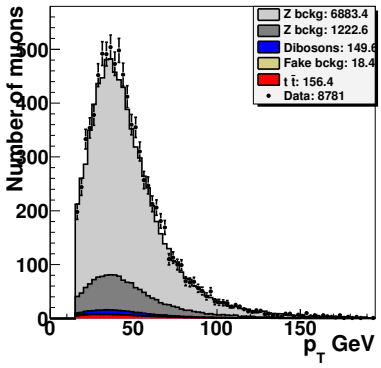

(b) 2 jet selection

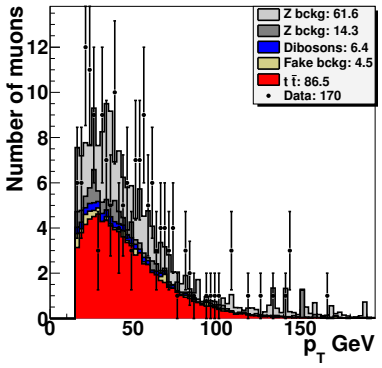

(c) Final selection.

FIG. 83: Muon transverse momentum distributions in the $\mu\mu$ channel.

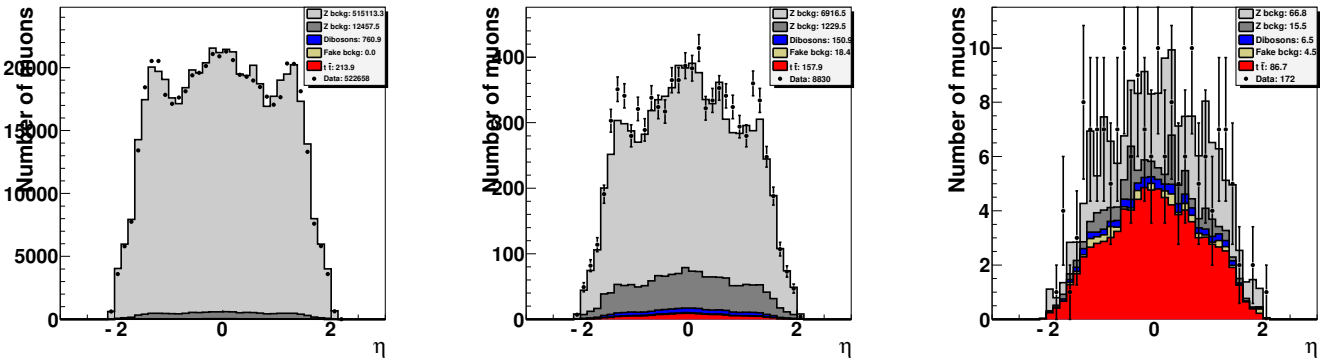

(a) Inclusive selection (b) 2 jet selection (c) Final selection.

FIG. 84: Muon η distributions in the $\mu\mu$ channel.

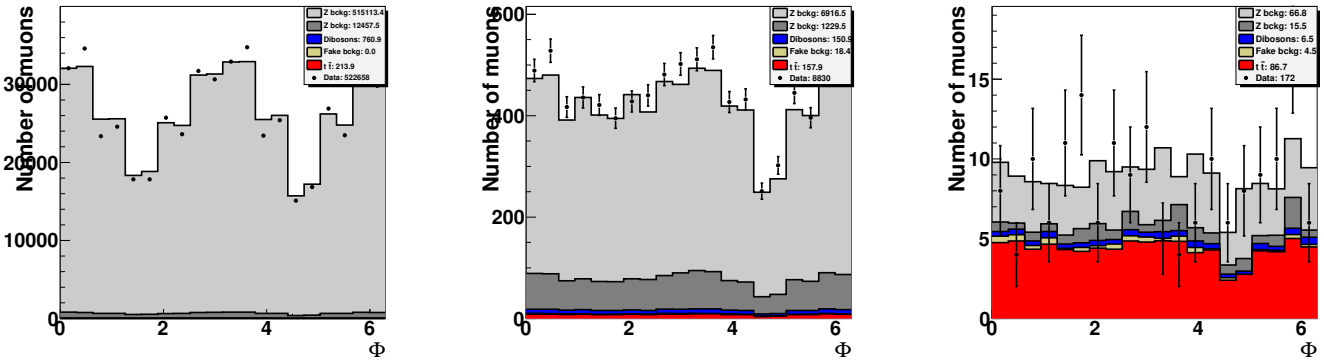

(a) Inclusive selection (b) 2 jet selection (c) Final selection.

FIG. 85: Muon ϕ distributions in the $\mu\mu$ channel.